NOAA Technical Memorandum ERL PMEL-87

EQUATORIAL OCEANIC RESPONSE TO FORCING ON TIME SCALES FROM DAYS TO MONTHS

Benjamin S. Giese

Joint Institute for the Study of Ocean and Atmosphere
University of Washington, Seattle Washington

Pacific Marine Environmental Laboratory
Seattle, Washington
April 1989

NOTICE

Mention of a commercial company or product does not constitute an endorsement by NOAA/ERL. Use of information from this publication concerning proprietary products or the tests of such products for publicity or advertising purposes is not authorized.

Contribution No. 1115 from NOAA/Pacific Marine Environmental Laboratory

For sale by the National Technical Information Service, 5285 Port Royal Road
Springfield, VA 22161

CONTENTS

LIST OF FIGURES

LIST OF TABLES

Equatorial Oceanic Response to Forcing on Time Scales from Days to Months

Benjamin S. Giese*

ABSTRACT. Episodes of westerly wind in the western Pacific may be an important source of sea surface temperature variability in the eastern Pacific on monthly, seasonal and interannual time scales. In this report we use a combination of data, linear theory and an ocean general circulation model to examine remote response to western Pacific wind forcing.

Characteristics of the wind anomaly are determined using daily averaged observations of wind from equatorial islands near the date line. In the model, wind anomalies generate a train of eastward propagating Kelvin pulses. When the wind anomaly is weak the Kelvin response agrees with predictions of linear theory. For more realistic strong forcing there are three important deviations from linear theory; the amplitude of low baroclinic modes increases, the amplitude of higher baroclinic modes decreases, and the phase speed increases. In the presence of realistic oceanic background conditions, response in the equatorial waveguide is complicated by the equatorial undercurrent, a sloping thermocline and instability waves. As Kelvin pulses propagate from western to eastern Pacific surface zonal velocity associated with the first mode decreases, whereas velocity associated with the second mode increases. These changes can be deduced by the principle of conservation of energy flux. In the central and eastern Pacific Kelvin pulses act to amplify and change the phase of existing instability waves. Thermal changes brought about by enlarged instability waves can be comparable in magnitude to changes brought about by zonal advection of the zonal temperature gradient by Kelvin pulses. At the coast of South America, model Kelvin pulses cause a warming of 2°C for 45 days.

Current observations made at 140°W and 110°W subsequent to a strong westerly wind event in May 1986 indicate passage of Kelvin-like pulses which agree in magnitude and timing with those modeled. At the coast of South America observations of sea surface temperature show a warm anomaly that lasts for almost two months, comparable in duration and magnitude to changes found in the model.

1. INTRODUCTION

Every few years the seasonal pattern of warming and cooling in the eastern tropical Pacific is greatly altered. An accentuated ocean warming known as El Niño occurs at intervals ranging from as short as two years to as long as a decade. The appearance of warm water in the eastern Pacific is not solely an oceanic phenomenon, but is coupled with changes in the atmosphere known as the Southern Oscillation (Bjerknes, 1969). Because the El Niño-Southern Oscillation (ENSO) has been linked to anomalous weather patterns both in the tropics and in mid-latitudes, it has become a subject of intense research.

Much of the research on ENSO has sought to define how the ocean and atmosphere are coupled, with particular emphasis on the tropical Pacific. Ever since Wyrtki (1975) suggested that onset of warming in the eastern Pacific results from a relaxation of tradewinds in the western and central Pacific, special attention has been paid to the possibility that warming is forced, not

* Joint Institute for the Study of Ocean and Atmosphere, University of Washington, AK-40, Seattle, WA, 98115.

by local winds, but remotely. Theoretical considerations (Lighthill, 1969; McCreary, 1976; Hurlburt *et al.*, 1976) predict that a sudden change in zonal wind stress will force equatorially-trapped Kelvin waves. In fact, observations in the tropical Pacific subsequent to a wind burst in April 1981 (Knox and Halpern, 1982) and May 1986 (Miller *et al.*, 1988; McPhaden *et al.*, 1988) indicate that a first baroclinic mode Kelvin wave forced in the western Pacific propagated all the way to the coast of South America. Because the Kelvin wave is non-dispersive and has a relatively fast phase speed (Moore and Philander, 1977), it can transmit changes in the atmosphere in the western Pacific to the ocean in the eastern Pacific with a time scale of months. Kelvin waves can cause anomalous warming either by a zonal advection of a horizontal temperature gradient (Philander, 1981; Gill, 1983; Harrison and Schopf, 1984) or by inhibition of vertical entrainment of cold water to the surface (McCreary, 1983). Numerical experiments (Kindle, 1979; Busalacchi and O'Brien, 1981) confirm that remote forcing by changes in wind stress in the western Pacific are important in seasonal changes in pycnocline depth in the eastern Pacific.

However, observations of wind stress taken from the western Pacific indicate that tradewinds do not relax broadly and over a long period of time, but through a series of strong westerly wind bursts of several days duration superposed on normal easterly tradewinds (Luther *et al.*, 1983). Philander and Pacanowski (1980) showed that in a model forced by periodic wind anomalies, response to fluctuations of short time scales is different than response to more slowly varying forcing. In the slowly varying case the ocean adjusts in equilibrium with the winds, whereas high frequency forcing creates oceanic fronts.

The purpose of this report is to examine the response of the eastern and central tropical Pacific to a single episode of intense westerly wind stress in the western Pacific. It has been suggested that onset of sea surface temperature warming in the eastern Pacific during an ENSO event could be triggered by such a burst of westerly wind (Keen, 1982). Using wind data from the western Pacific, an idealized episode of westerly wind can be formulated and incorporated into the model. Through a combination of linear theory and computer simulations of the tropical Pacific Ocean, dynamic and thermodynamic changes induced by a westerly wind burst will be elucidated. The role of episodes of westerly wind in sea surface temperature variability at the coast of South America on month, seasonal and interannual time scales is examined.

A general circulation model has two important properties that are important to the numerical study of westerly wind bursts. The first property is that the model includes several baroclinic modes of response. Theoretical calculations (Eriksen *et al.*, 1983) predict that forcing of the second vertical mode will be of comparable amplitude to the first mode in the western Pacific. In the eastern Pacific the second vertical mode is important both in observations of thermal structure (Gill, 1982) and sea level (Lukas *et al.*, 1984). Model experiments of Busalacchi and Cane (1985) show that timing and amplitude of sea level variability cannot be accurately reproduced with a single vertical mode. Harrison and Giese (1988) demonstrate that, although first and

second vertical modes are roughly equal in the western Pacific, changes in sea surface temperature along the coast of South America are dominated by the second mode. The second property is that the ocean model includes nonlinear terms. In a linear system the time-averaged response to high-frequency forcing is equal to the response to time-averaged forcing. However, for strong currents excited by the westerly wind bursts, nonlinear terms in the equation of motion become important. Thus, study of the ocean's response to impulsive wind forcing in the form of these westerly wind bursts is important in understanding and modeling of climate variability on much longer time scales.

Use of a general circulation model also allows nonlinear interaction of the Kelvin response with other forms of oceanic variability. The mean wind field over the equatorial Pacific consists of easterly tradewinds with zonal speeds of about 5 m sec^{-1}. Tradewinds force a barotropic pressure gradient up to the west, which is compensated for by a baroclinic pressure gradient which slopes up to the east (Colin *et al.*, 1971). A baroclinic pressure gradient drives an eastward flowing subsurface current, called the undercurrent. The undercurrent resembles a thin ribbon, about 200 m thick and extending from about 2°S to 2°N, that has maximum eastward speeds in excess of 100 cm sec^{-1}. The depth of the maximum speed of the undercurrent follows the thermal structure: in the west it is found at about 150 m, whereas in the eastern Pacific it shoals to about 50 m.

In the eastern Pacific, where tradewinds are strongest, Ekman pumping draws water up at the equator, cooling the surface. In the western Pacific tradewinds are much weaker and the thermocline is deeper, so that sea surface temperature can remain warm, exceeding 30°C for most of the year. Thus, for much of the year there is a zonal temperature gradient.

In this report an ocean general circulation model is used to examine evolution of the forced response in the context of this natural variability. The main body of the report includes three sections. Section 2 describes island wind data and characterization of westerly wind bursts. Section 3 deals with linear theory of wind-forced Kelvin waves and the expected oceanic response to a single episode of westerly wind. The effect of a shoaling thermocline on Kelvin waves is also examined. Section 4 includes a description of the model, model experiments and the model response to an idealized wind burst. Where data are available, a comparison with observed oceanic response to wind forcing is presented.

2. EPISODES OF WESTERLY STRESS

A. Introduction

Interannual variability of rainfall and air temperature in the tropics is linked to the Southern Oscillation, a large change in the atmospheric pressure gradient over the tropical Pacific (Walker, 1924). A measure of this pressure change is the Southern Oscillation Index (SOI), the pressure difference between the western and eastern Pacific (Walker and Blis, 1932). Coincident with this large scale pressure change is a relaxation of the Walker circulation. The surface manifestation of the Walker circulation, the easterly tradewinds, weaken and can even reverse during ENSO years. It has been known for over 20 years that El Niño occurs only during the negative phase of the Southern Oscillation, when pressure in the east is anomalously low and pressure in the west is anomalously high (Berlage, 1966). Because surface wind stress is the primary driving force of the equatorial waveguide, an understanding of the relaxation of the tradewinds will further our understanding of El Niño.

Recent work suggests that the tradewinds do not relax evenly and uniformly, but through a succession of energetic westerly wind bursts, each with a duration of two to ten days (Luther *et al.*, 1983). In the western tropical Pacific there is substantial zonal wind power at periods between 4 and 30 days (Luther and Harrison, 1984), inclusive of the period band characteristic of westerly wind bursts. Appearance of anomalous westerly winds prior to significant oceanic warming has been noted in all ENSO events between 1950 and 1978 except for the 1963 event (Luther *et al.*, 1983). Harrison (1987), using monthly mean surface wind anomalies, found that westerly wind anomalies, in the early stages of ENSO, tend to occur west of the date line and within 3° of the equator. In ensuing months, anomalies shift to near the date line and then south of the equator. The slow uniform relaxation may have been a consequence of averaging over large temporal and spatial regions.

There is some indication that episodes of westerly wind may be dynamically associated with tropical cyclone activity, particularly with formation of cyclone pairs (Keen, 1982). Revell and Goulter (1986) have shown that the formation region of tropical cyclones is correlated with the Southern Oscillation Index. In particular, during the positive phase of the Southern Oscillation (ENSO years), tropical cyclone formation in the Southern Hemisphere shifts northward and eastward.

In this section the temporal and spatial structures of westerly wind bursts in the western Pacific are considered briefly. Characteristics of an idealized westerly wind event are needed in later sections for the purposes of developing the linear oceanic response to a wind burst. The same idealization is used as a forcing function in an ocean general circulation model. Using surface wind data from several tropical islands near the date line, the seasonal and interannual distribution of wind bursts is investigated. The approach here is to examine island wind time series using both power spectra and an event analysis. A particularly energetic episode during

May 1986 is discussed. A full description of westerly wind variability in the island surface wind data is under preparation (Harrison and Giese, 1989)

B. Island Wind Data

For much of the tropical Pacific observations of surface wind stress are sparse. In many areas of the western Pacific the Ship of Opportunity Program makes as few as three observations per month for a 2° latitude by 10° longitude box. Ship observations also tend to include a fair weather bias (ships generally avoid the strongest wind events) which would tend to under-represent westerly wind bursts. Fortunately there is a network of islands in the western Pacific that have been used by the New Zealand Meteorological Service as observation posts. A site map of the western tropical Pacific with the location of stations is shown in Fig. 2.1. Data from these islands were collected by observers, rating winds on a Beaufort scale. Harrison and Luther (1989) discuss the island data and make a comparison with available ship winds.

Daily-averaged zonal winds from seven island stations near the date line for late 1964 to mid-1966 are shown in Fig. 2.2. These stations were chosen to demonstrate the meridional nature of the westerlies near the equator. Throughout this period, which includes the strong El Niño of 1965, the wind record is characterized by episodes of westerly wind. The duration of wind bursts varies from a few days to over a week, with peak anomalies exceeding 15 m sec^{-1}. During the period from November 1964 to February 1965 there are three energetic events at all stations except for Majuro, northernmost of these seven islands. Between wind bursts the wind relaxes to a normal easterly tradewind value, noticeably at Beru and Arorae, stations nearest to the equator. However, the other equatorial station, Ocean, does not fully recover to the normal tradewind value. Easterly wind bursts are not nearly as common in the records as westerly wind bursts; peak easterly wind anomalies are about 5 m sec^{-1}.

Arrows at the top of Fig. 2.2 denote the occurrence of a Northern Hemisphere cyclone which formed in the region between 165°E to 165°W. At the bottom of Fig. 2.2, arrows indicate the formation of a Southern Hemisphere cyclone within the same longitude band. Many of the westerly winds during the 1965 ENSO were associated with tropical cyclones in both the Northern and Southern Hemispheres. Southern Hemisphere cyclone formation is recorded by the New Zealand Meteorological service (Kerr, 1976) and Northern Hemisphere cyclones are recorded in the Mariners Weather Log. Northern Hemisphere cyclones are most common during the boreal warm season, from August through November. Southern Hemisphere cyclones are most common during the austral warm season, from January through March (Anthes, 1982). A tropical storm becomes a named cyclone when surface winds exceed 65 knots, so that some westerly wind events could be associated with tropical storms that are not indicated on the axes. There is only one occurrence of a cyclone pair, in December 1964.

There is also strong seasonal variability in episodes of westerly wind bursts. North of the equator (Majuro) there is very little activity from November 1964 through May 1965, whereas in the Southern Hemisphere during this time there are several strong episodes of westerly wind. By contrast, while there is significant activity at Majuro from July through November 1965 there is little activity south of the equator (Niulakita and Funafuti). Island stations near the equator show activity in both seasons.

Surface zonal winds for the same islands during the non-El Niño period from September 1966 through August 1968 are shown in Fig. 2.3. The event in December 1967 is the only episode of strong westerly wind that occurs at all near-equatorial stations and can be traced in the southern stations as well. During this period there were only three named cyclones in the Northern Hemisphere from 165°W to 165°E. These cyclones all occurred in months from August to October, the peak of the Northern Hemisphere cyclone season. Zonal winds at islands south of 5°S are not markedly different from those occurring during ENSO years.

The westerly anomalies during the ENSO years are thus composed of several episodes of strong westerly wind, with a temporary relaxation to easterlies between wind events. Consider the evolution of a such a westerly wind burst in January 1969. This feature is similar to the 1965 wind episodes, but demonstrates the evolution of the westerly winds more clearly. Figure 2.4 shows surface wind vectors from 12 island stations that span the equator near 175°E (see Fig. 2.1). Westerlies first appear on 5 January as the tradewinds start to weaken. There is no clear pattern to wind anomalies until the 7^{th} when there is a northerly cross-equatorial surge of air in the Northern Hemisphere. Strong organized westerlies south of the equator intensify from the 8^{th} through the 10^{th}. Note the strong vorticity in both hemispheres on the 9^{th} of January; pre-existing vorticity is a requirement for cyclone development (Anthes, 1982). In fact, a Southern Hemisphere cyclone spawned on 11 January and a Northern Hemisphere cyclone (Phyllis) spawned on 17 January. Zonal wind anomalies remain strong through the 15^{th}, when the westerlies start to relax. Easterlies do not return until the 25^{th}, when the winds are easterly at all stations. The stations just south of the equator show strong westerlies in excess of ten days, with peak westerlies exceeding 10 m sec^{-1}.

Information about the ensemble properties of westerly wind episodes can be obtained by using spectral analysis to characterize ENSO and non-ENSO years. The spectra can then be used to characterize the meridional dependence of wind anomalies. Three representative stations were chosen; Beru for a near-equatorial station, Butaritari for north of the equator and Nui for south of the equator. Power spectra of five El Niño years were compared with power spectra of five non-El Niño years. El Niño years include two strong events (1957 and 1972), two moderate events (1965 and 1976) and one weak event (1969) according to the classification scheme of Quinn *et al.* (1978). These spectra were computed by taking the Fourier transform of a two-year period and then averaging spectral coefficients. Each period started on the first day of November

of the year preceding warming. Thus, variability associated with the Northern Hemisphere cyclone season is included.

Spectra for Beru Island are shown in Fig. 2.5a for non-El Niño years and Fig. 2.5b for El Niño years. Confidence limits indicate the 90% confidence level. The left hand panel of each figure is an energy preserving spectrum, and total variance is printed in the upper left hand corner. Spectra were divided into six frequency bands, indicated by dashed lines at the top of the plot. Variance for each band is printed within the dashed line. The band from days 6-15 includes much of the variability associated with westerly wind bursts. Similar spectra are shown in Figs. 2.6 for Butaritari and 2.7 for Nui. Butaritari uses only four ENSO periods; data for the 1957 event is not available.

At Beru, during non-ENSO years spectra have less energy at all frequencies than during ENSO years. The band from 6-15 days has variance of 1.3 m^2 sec^{-2} during non-El Niño years and variance of 2.4 m^2 sec^{-2} during ENSO years. There are similar increases at other island stations near the equator. In contrast, spectra from off-equator stations Butaritari (to the north) and Nui (to the south) do not show variability between El Niño and non-El Niño years in the bands from 3-60 days, although these stations show an increase in variance in the lowest frequency band. Variance at Nui increases from 2.1 to 2.3 m^2 sec^{-2} and variance at Butaritari increases from 1.5 to 1.8 m^2 sec^{-2} during ENSO years.

The temporal structure of westerly wind bursts is episodic: long periods of little activity are punctuated by brief intervals of large anomalies. To capture the episodic nature of time series, an "event" style of analysis was performed on daily averaged island wind data. In this analysis monthly climatological mean winds were subtracted from daily averaged winds. A positive anomaly is then considered an event if it exceeds 9.0 m sec^{-1}.

The number of days in which wind anomalies exceeded 9.0 m sec^{-1} were averaged by months for the period from 1955 through 1979 for all years and for El Niño years alone. Averages for four island stations are presented in Table 2.1. Because ENSO years account for about one third of the total number of years, when activity during ENSO years is three times the activity for all years, then we can infer that all activity occurred during the few ENSO years. If activity during ENSO years equals activity during all years, then the distribution is fairly even, and ENSO years do not have more episodes of westerly wind than non-ENSO years.

At Nui peak activity is in January and February which corresponds to the height of the Southern Hemisphere cyclone season. In these months westerlies exceed 9.0 m sec^{-1} an average of one day per month. In September, the height of the Northern Hemisphere cyclone season, there is a minimum of activity. An episode of westerly wind which exceeds 9.0 m sec^{-1} occurs only one September day in five years. North of the equator at Butaritari the pattern is nearly reversed. Here the activity maximum is in October, just after the peak of the Northern Hemisphere cyclone season in September. The activity minimum is from February to May. At two

islands near the equator the activity season is longer, beginning in September and extending through March at Beru and Ocean.

During El Niño years the total activity of events exceeding 9.0 m sec^{-1} at equatorial stations is approximately twice the levels averaged over all years (Table 2.1). In months from August to November, El Niño activity is more than twice the activity of all years. By contrast, although activity levels at Nui (5°S) are elevated from January through April, the difference between ENSO and all years is not great. Butaritari, closer to the equator than Nui, does show an increases in the number of events during ENSO years. The number of events at Butaritari is greatest in September and October, during the peak of the Southern Hemisphere cyclone season.

C. The May 1986 Wind Event

The Mariners Weather Log begins analysis of tropical cyclone activity in May 1986 stating, "In a normal May one or two storms roam the Pacific. This year three tropical cyclones developed including a supertyphoon in the west and hurricane Agatha in the east" (p. 244, Fall 1986). Two of these cyclones formed a cyclone pair in the Western Pacific on May 16, 1986. Zonal and meridional winds from a buoy are shown in Fig. 2.8 for the month of May at 165°E on the equator (as in McPhaden *et al.*, 1988, Fig. 3). Also shown are winds from Nauru (1°S, 167°E), a nearby island. Island winds show a wind event occurring at the same time, although of weaker strength. The strength of the anomaly may appear weaker during westerly wind events at Nauru because the anemometer is in the lee of the island during westerlies (P. Freitag, personal communication). Zonal wind begins to weaken on the 6^{th}, becoming westerly on the 8^{th}. After the 10^{th} of May winds relax briefly and then intensify quickly, reaching their maximum speeds of 9 m sec^{-1} on 14 May. In the classification scheme of Sadler and Kilonsky (1983) the westerly winds rate as a strong event. The Mariners Weather Log (1986) shows the tropical depressions intensified to become cyclone Lola in the Northern Hemisphere on 17 May and Namu in the Southern Hemisphere on 15 May. There is a concomitant northerly surge of wind that begins on the 11^{th} and reaches a peak anomaly of about 7 m sec^{-1} on the 14^{th} of May. The duration and strength of the meridional surge are much less than those of the zonal surge.

Surface wind data from the Navy operational wind product enables an examination of temporal and spatial characteristics of the wind burst in detail. These data, which are a combination of both observations and model extrapolation, are available every six hours on a grid 2.5° by 2.5°. Evolution of the wind burst and subsequent generation of two cyclones is presented in Fig. 2.9. Each panel shows vector wind velocity in m sec^{-1} in the western Pacific. On the 14^{th} of May there are strong westerlies just north of the equator between 140°E and 160°E. Westerlies start to draw air equatorward to supply air divergence. This adds vorticity, one of the prerequisites for cyclogenesis (Anthes, 1982). By the 17^{th} the two cyclones have formed and start to move poleward.

A time-longitude contour of the zonal pseudo-stress in Fig. 2.10 provides an estimate of temporal and zonal scales of the wind burst. Zonal pseudo-stress is defined as the product of zonal velocity times the magnitude of the vector velocity. Westerly winds are present on the equator on 11 May, extending from 135°E to 155°E. This region of anomalous winds propagates eastward at a speed of 1.9 m sec^{-1}, until it stalls and intensifies at 145°E to 165°E. Spatially and temporally averaged westerlies reach speeds of greater than 8 m sec^{-1}. Point measurements indicate that westerlies at 155°E exceeded 10 m sec^{-1} on 18 May, a wind stress anomaly of 4 dynes cm^{-2}. The duration of the feature is about ten days and its longitudinal extent is about 20°.

The westerly anomaly that intensified west of the date line continued to propagate across the tropical Pacific. A dashed line has been superimposed onto the figure to facilitate identification of the propagating feature. Note that zonal pseudo-stress is near zero between the date line and 110°W in late May. Zonal winds at 140°W are shown in Fig. 2.11 from October 1985 through February 1987. The largest wind anomaly during this period occurs in late May 1986. The speed of the propagating anomaly can be estimated from arrival of peaks at 165°E and at 140°W. This gives a phase speed of 4.8 m sec^{-1}, consistent with the speed of a damped atmospheric 40-day wave (Weickmann *et al.*, 1989).

When the westerly anomaly propagates past 140°W, it speeds up considerably. According to the Fleet Numeric Ocean Central surface wind analysis (Fig. 2.10), east of 140°W the anomaly propagates at a phase speed of greater than 10 m sec^{-1}. The phase speed increase could be due to decoupling of the wave from convective damping. In the eastern Pacific, sea surface temperature is much cooler than in the western Pacific except in the Northern Hemisphere spring (Reynolds, 1982). When the atmospheric wave moves over cooler water, convective processes which acted to slow the wave over the western Pacific can no longer operate, thus the Kelvin wave propagates at a speed closer to the free Kelvin speed.

The development of paired cyclones shown in Fig. 2.9 indicates that there are significant westerly anomalies well before onset of cyclogenesis. In fact, westerlies existed on the equator at least five days before the named cyclones (Fig. 2.8). Westerlies intensify from 5 to 9 May and then relax briefly. A second intensification peaks on 14 May, coincident with formation of cyclone Namu.

D. Wind Burst Characteristics

It is helpful in finding the linear response to forcing to have idealized characteristics of an average westerly wind burst. Only for relatively simple forms of forcing are the equations of motion readily integrable analytically. A simple idealization of a westerly wind burst is presented here, the idealization being based on the island wind data. The meridional density of island stations is good between 165°E and 175°E (see Fig. 2.1). However, the longitudinal

distribution is sparse: there are no equatorial stations west of Nauru (167°E) or east of Arorae (177°E). It is therefore difficult to determine length scales of the wind anomaly, or if the wind patch propagates. Coherence between Nauru and Beru indicates that the longitudinal extent is at least 10°. Recent evidence indicates that wind anomalies from a strong wind episode during May 1986 span at least 30° (McPhaden *et al.*, 1988). A length of 20° between 150°E and 170°E is used for the idealized wind patch. The idealized patch has a top-hat structure longitudinally, with value unity within the forcing region and zero otherwise. The top-hat function greatly simplifies the integration of wind forcing along wave characteristics, necessary in the evaluation of linear theory.

The island data indicate that low frequency westerly wind variability is largely confined to near the equator (Harrison and Luther, 1989). Poleward of a few degrees of latitude cyclonic motion starts to become important. In the ensemble the cyclonic motion averages to zero, so that there is no clear pattern of wind anomalies. Therefore the wind patch has strong meridional structure. The idealized patch is Gaussian in y, centered on the equator, and has a width at half-maximum of 3°. The temporal structure of the wind burst is also Gaussian. Island wind data indicate that wind bursts of about ten days duration are common (see Fig. 2.2) and so the duration at half-maximum of the idealized patch is set at ten days. The peak anomaly of the wind burst is 2 dynes cm^{-2}, a strong but not exceptional wind event.

TABLE 2.1 The average number of days per month when the surface zonal wind anomaly exceeded 9 m sec^{-1} at four of the island stations through 1980. The wind anomaly is found by differencing the daily wind observation from the monthly mean climatology. The average using only El Niño years is tabulated in parentheses.

	Butaritari	Ocean	Beru	Nui
Jan	0.35 (0.89)	0.58 (1.00)	1.54 (2.58)	1.14 (1.42)
Feb	0.04 (0.11)	0.42 (0.25)	0.89 (0.83)	1.14 (1.92)
Mar	0.15 (0.22)	0.55 (0.42)	0.84 (1.42)	0.92 (1.00)
Apr	0.00 (0.00)	0.33 (0.50)	0.51 (0.75)	0.73 (0.67)
May	0.04 (0.11)	0.12 (0.33)	0.32 (0.92)	0.16 (0.27)
Jun	0.19 (0.56)	0.09 (0.17)	0.30 (0.42)	0.05 (0.00)
Jul	0.38 (1.00)	0.36 (0.92)	0.38 (1.08)	0.08 (0.00)
Aug	0.42 (1.11)	0.39 (1.08)	0.54 (1.58)	0.11 (0.25)
Sep	0.88 (2.33)	0.79 (2.00)	0.92 (2.67)	0.05 (0.17)
Oct	1.15 (2.89)	0.73 (1.67)	1.19 (3.08)	0.27 (0.50)
Nov	0.54 (1.22)	1.30 (2.83)	1.65 (4.67)	0.27 (0.50)
Dec	0.46 (0.67)	0.76 (0.67)	1.84 (3.33)	0.81 (0.33)
Total	4.62 (11.11)	6.42 (11.84)	10.92 (23.33)	5.73 (7.03)

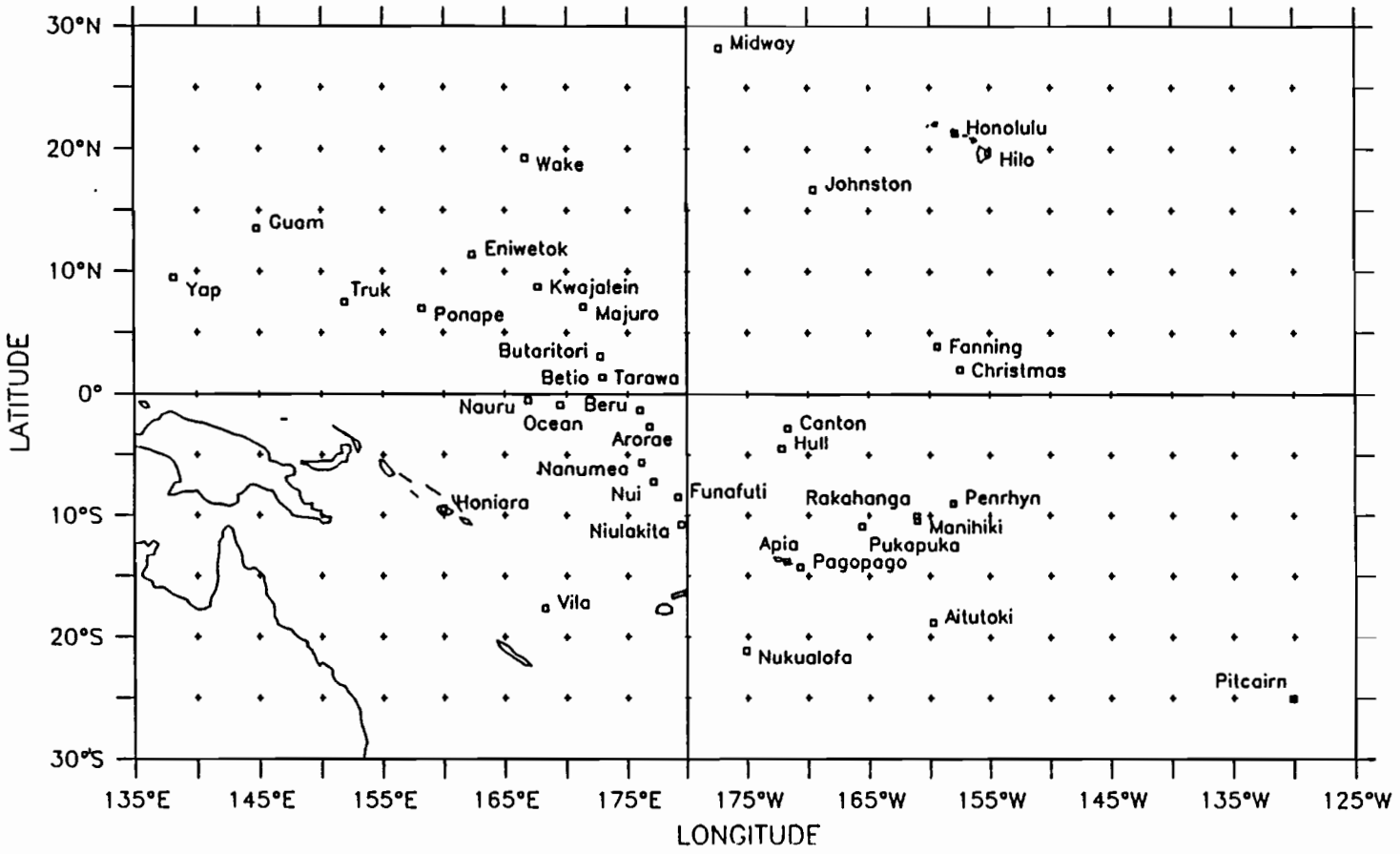

Figure 2.1. Site map of the tropical Pacific islands that are used as observation stations.

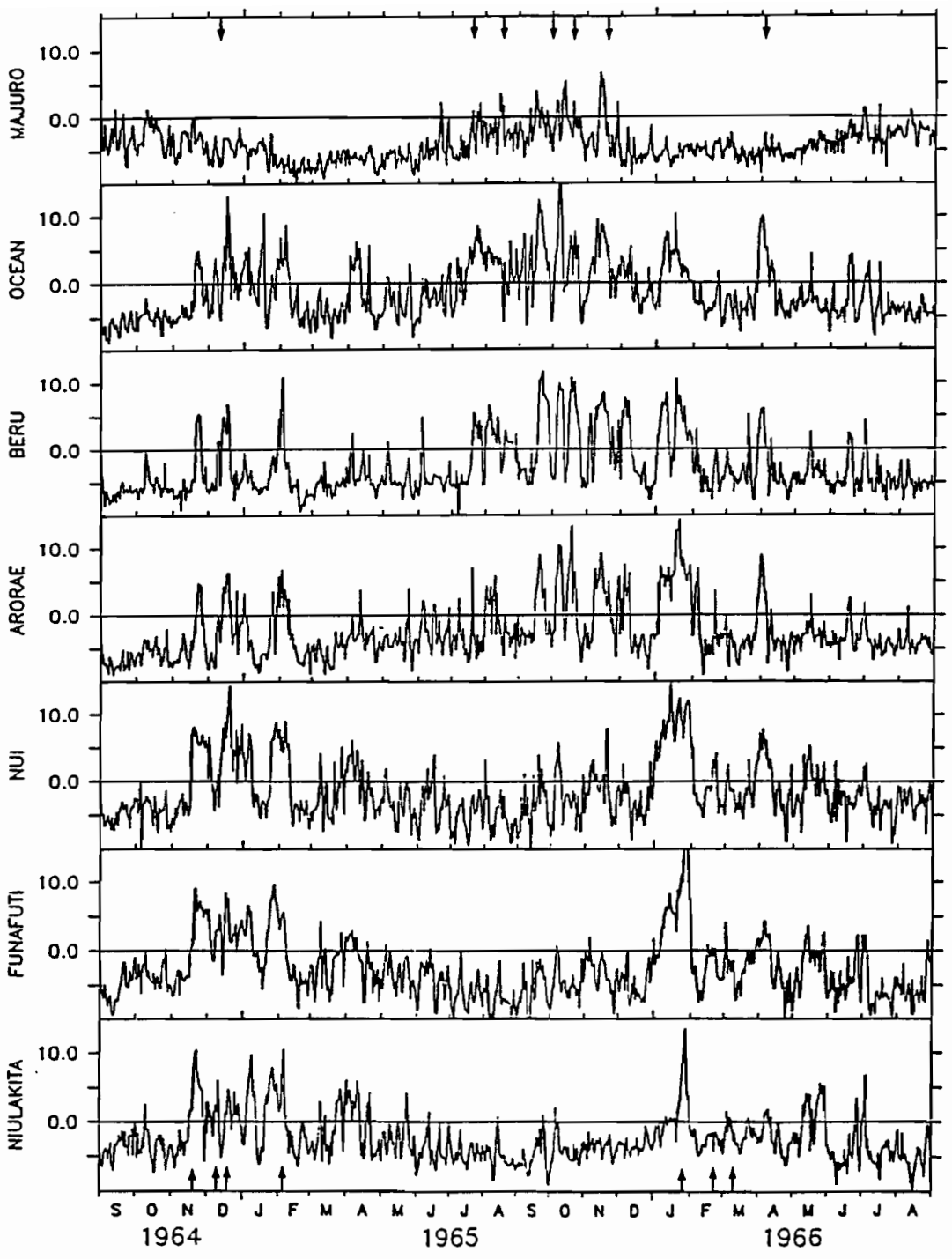

Figure 2.2 Daily averaged wind velocity from seven island stations from September 1964 to August 1966. Named cyclones that occurred from 165°E to 165°W in the Northern Hemisphere are indicated by an arrow on the top axis and Southern Hemisphere cyclones are indicated on the bottom axis.

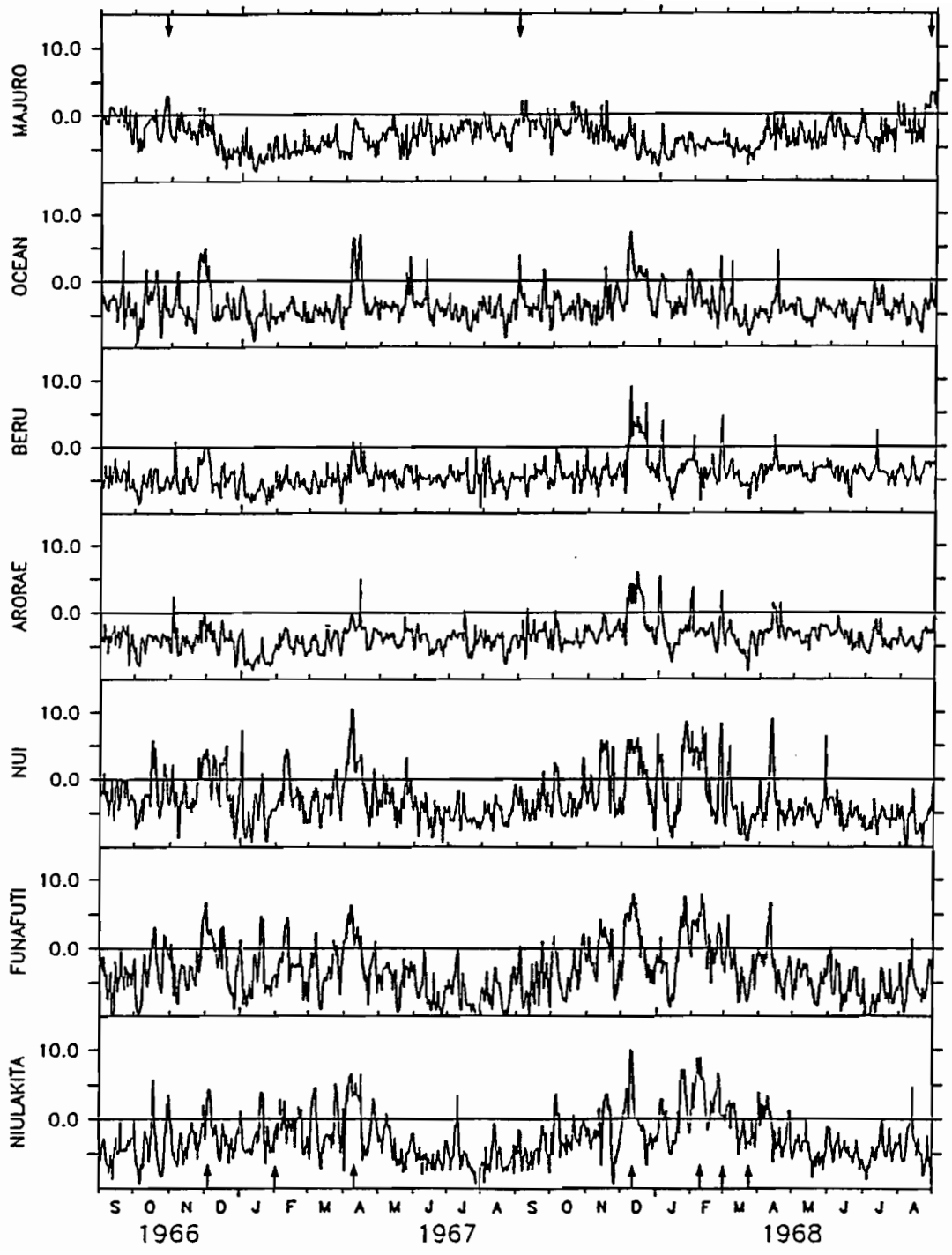

Figure 2.3 Daily averaged wind velocity from seven island stations from September 1966 to August 1968. Named cyclones that occurred from 165°E to 165°W in the Northern Hemisphere are indicated by an arrow on the top axis and Southern Hemisphere cyclones are indicated on the bottom axis.

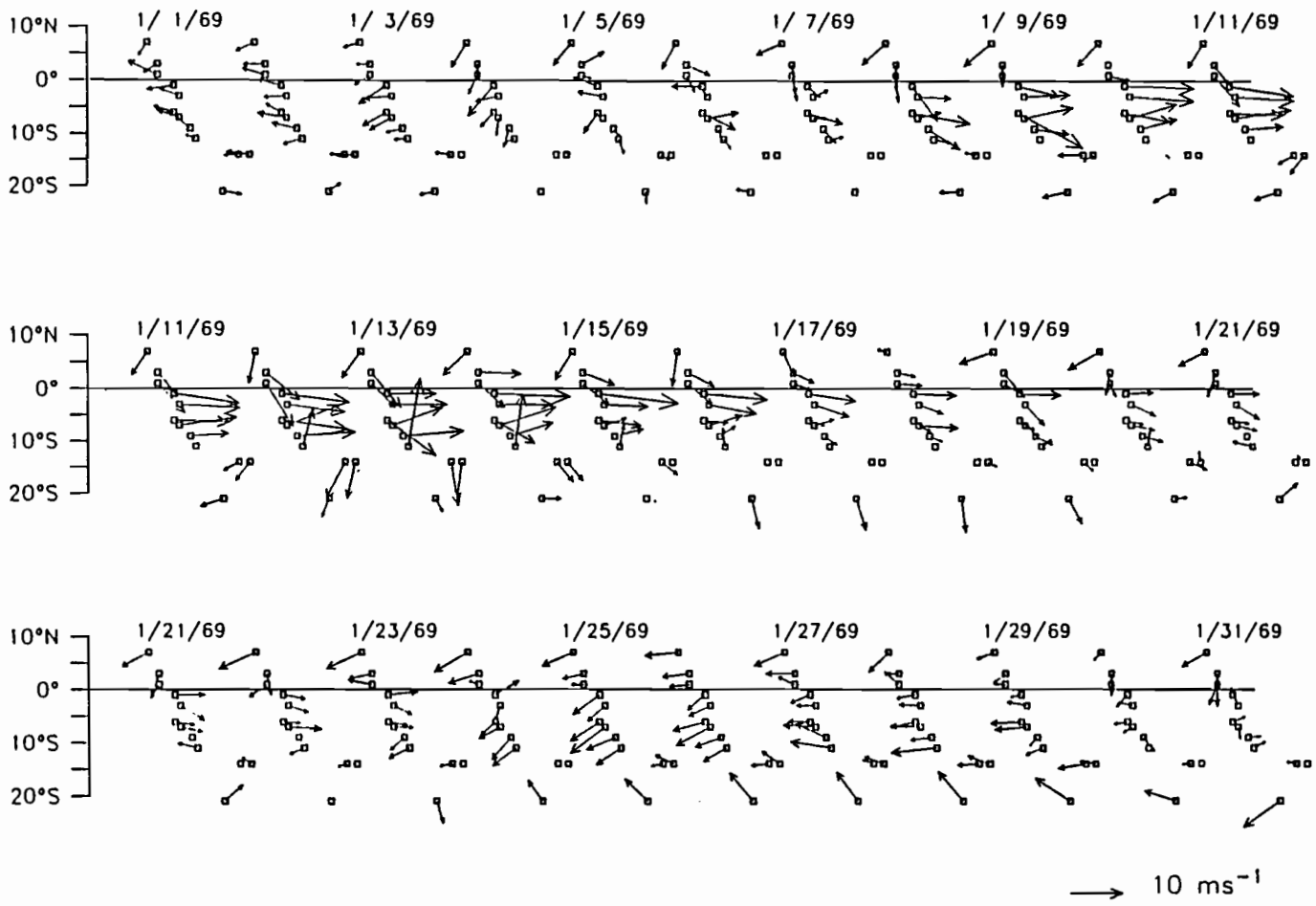

Figure 2.4. Daily averaged surface wind vectors for 12 of the island wind stations at 175°E (see Figure 2.1). A scale vector is shown in the left hand corner.

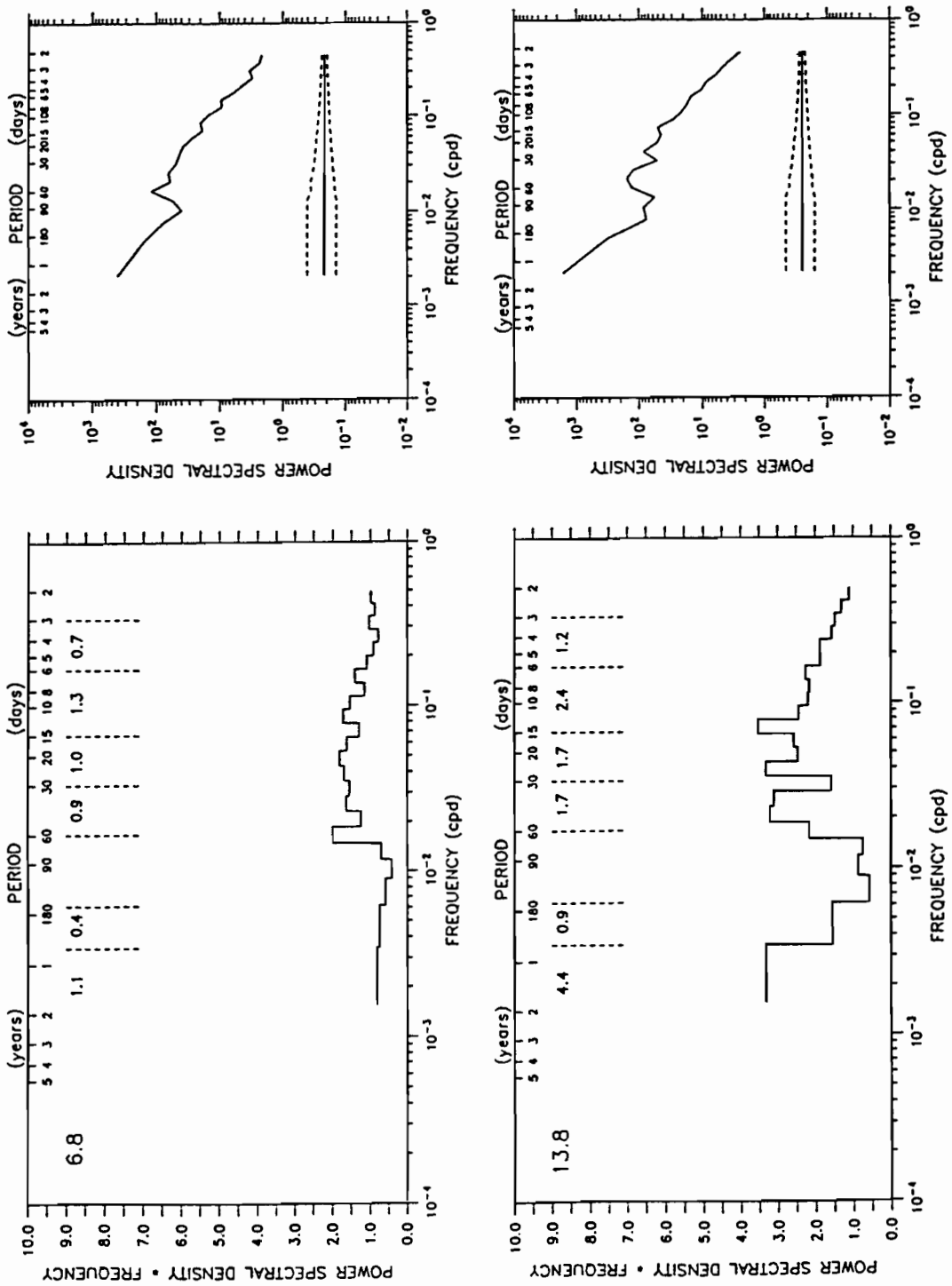

Figure 2.5. Power spectra at Beru for (top) non-El Niño years and (bottom) El Niño years. The left hand panels show energy preserving spectra.

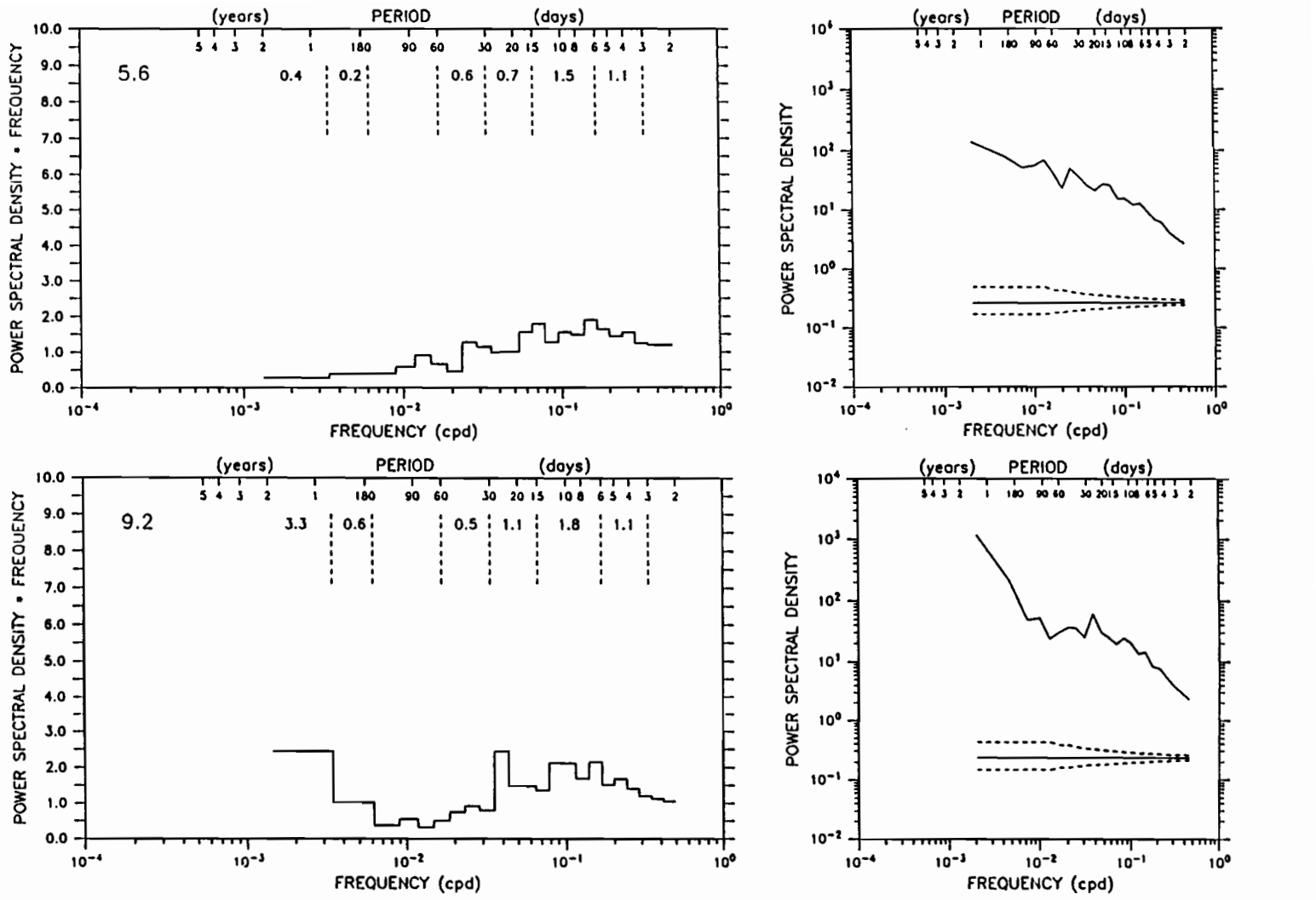

Figure 2.6. Power spectra at Butaritari for (top) non-El Niño years and (bottom) El Niño years. The left hand panels show energy preserving spectra.

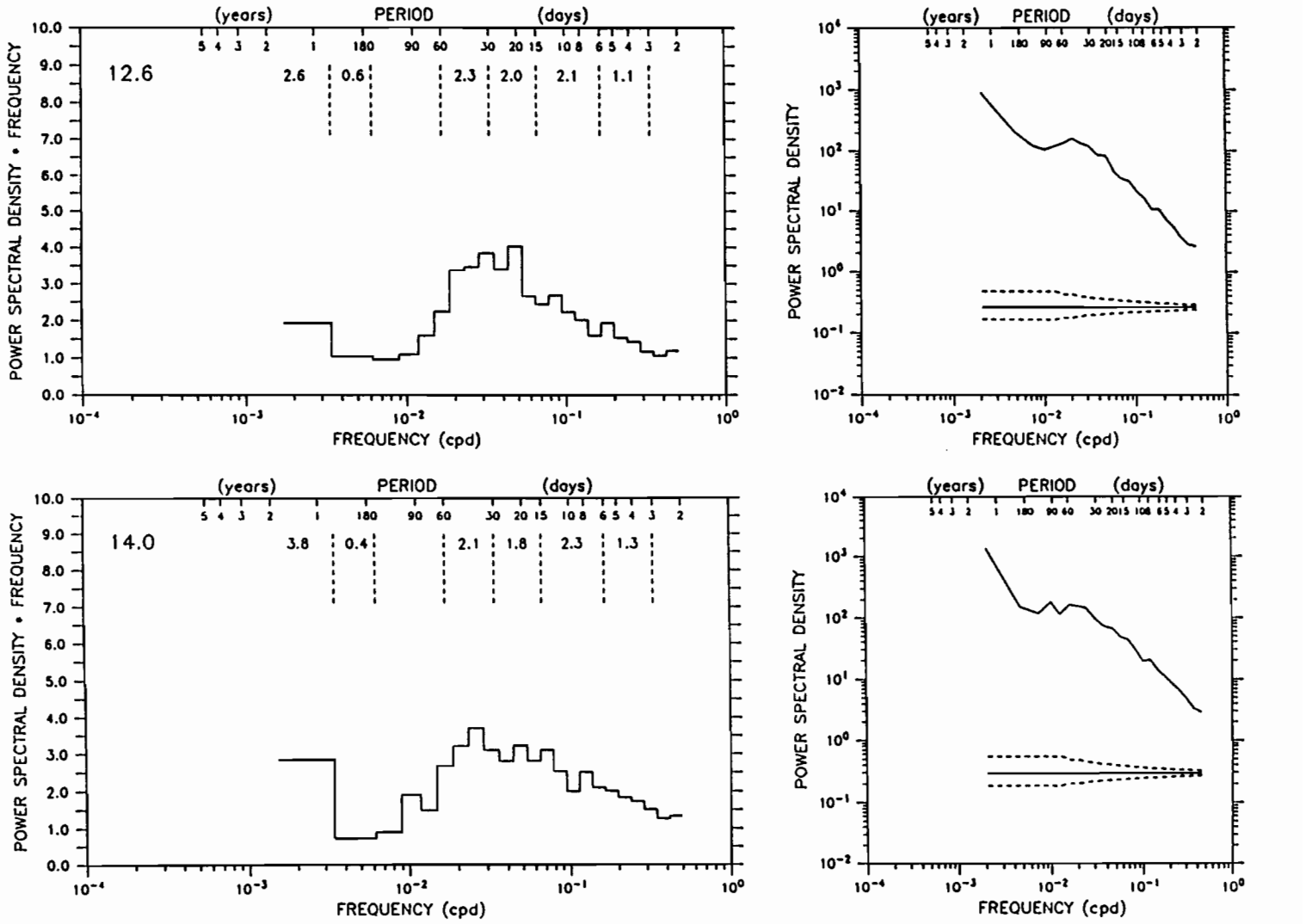

Figure 2.7. Power spectra at Nui for (top) non-El Niño years and (bottom) El Niño years. The left hand panels show energy preserving spectra.

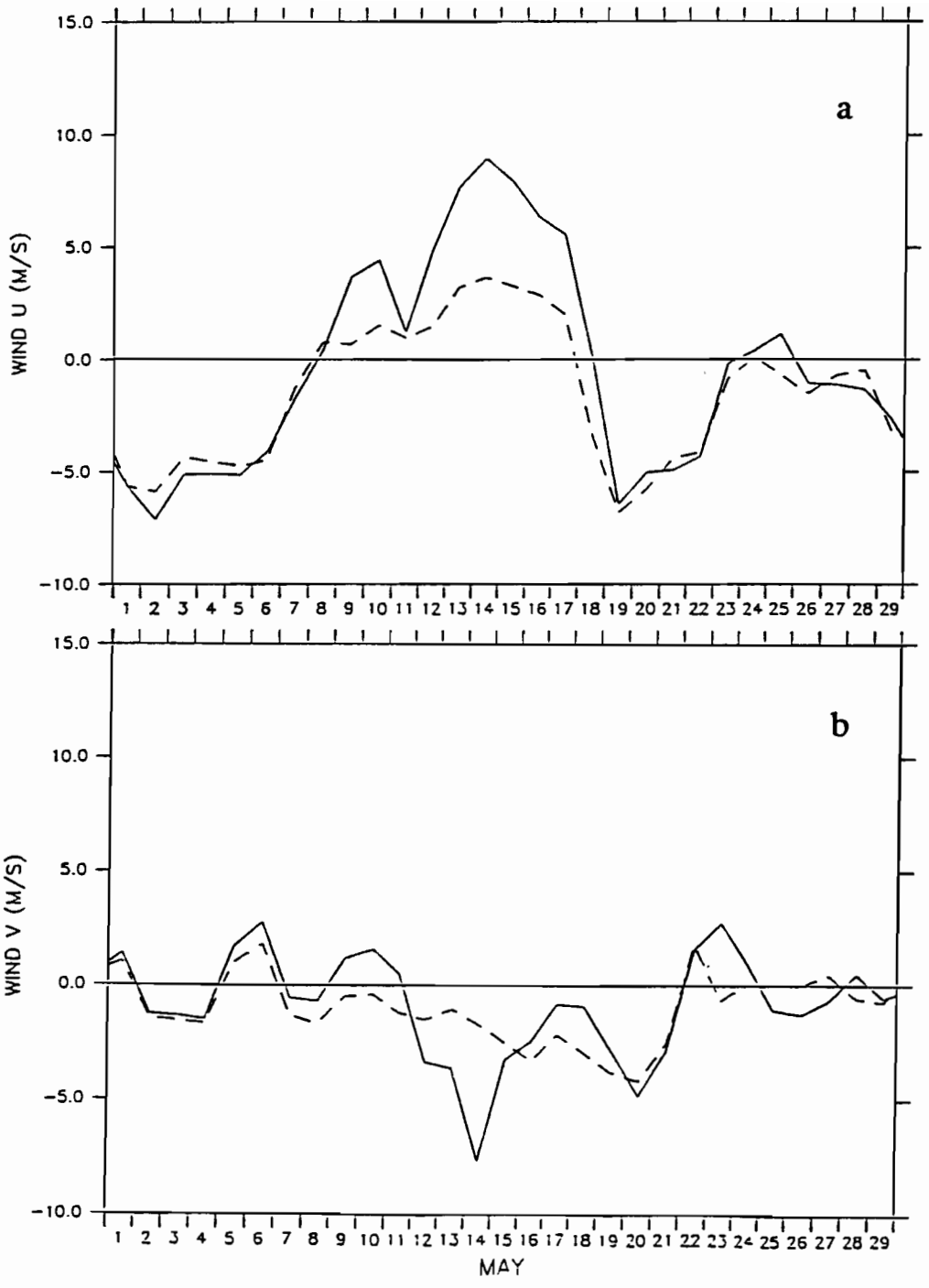

Figure 2.8 Surface (top) zonal and (bottom) meridional winds at 0°N, 165°E (solid line) and Nauru (dashed line) during May 1986.

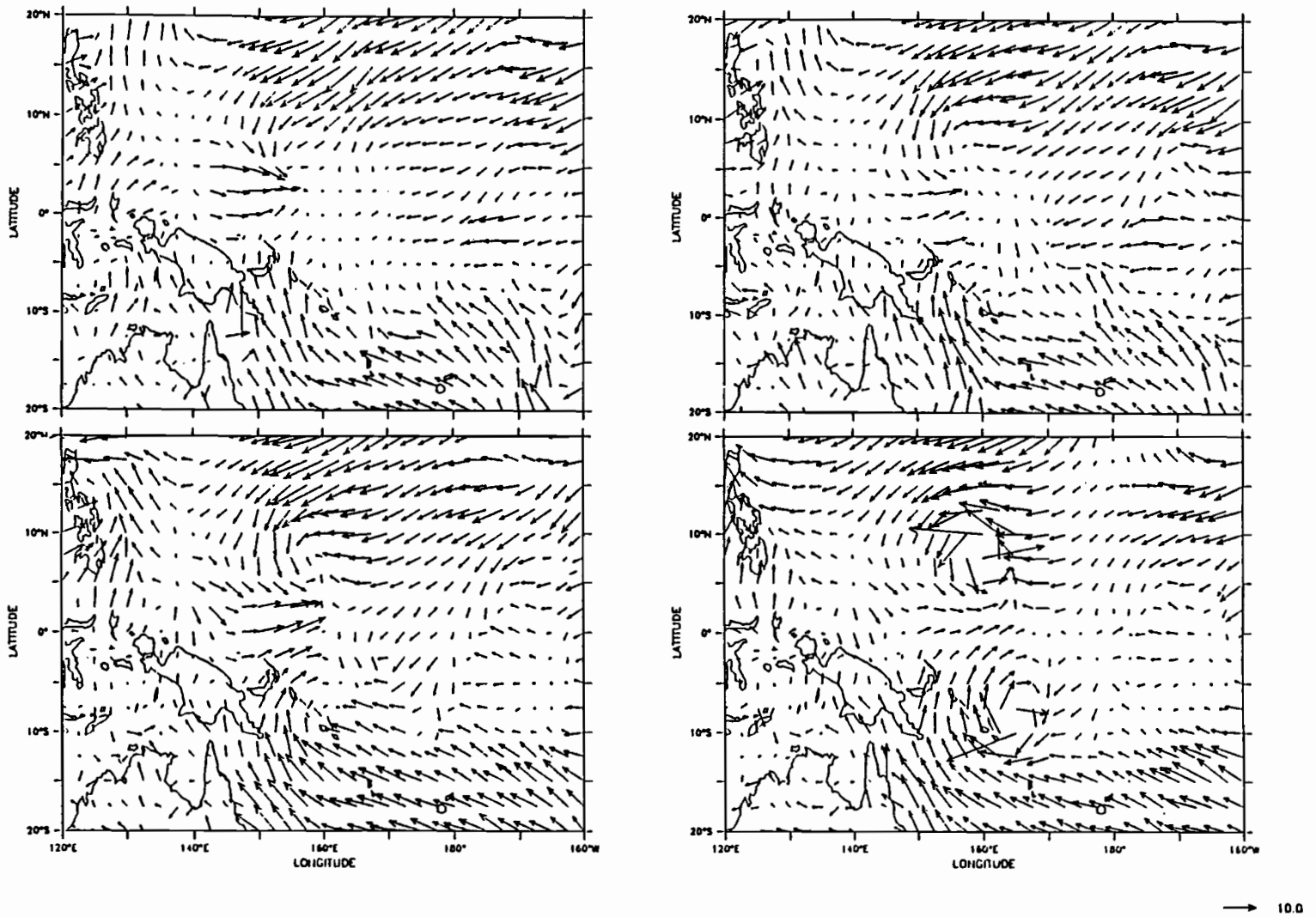

Figure 2.9. Surface wind vectors for 14 May (upper left), 15 May (upper right), 16 May (lower left) and 17 May (lower right) 1986. A vector with magnitude 10 m sec^{-1} is shown in the lower right hand corner.

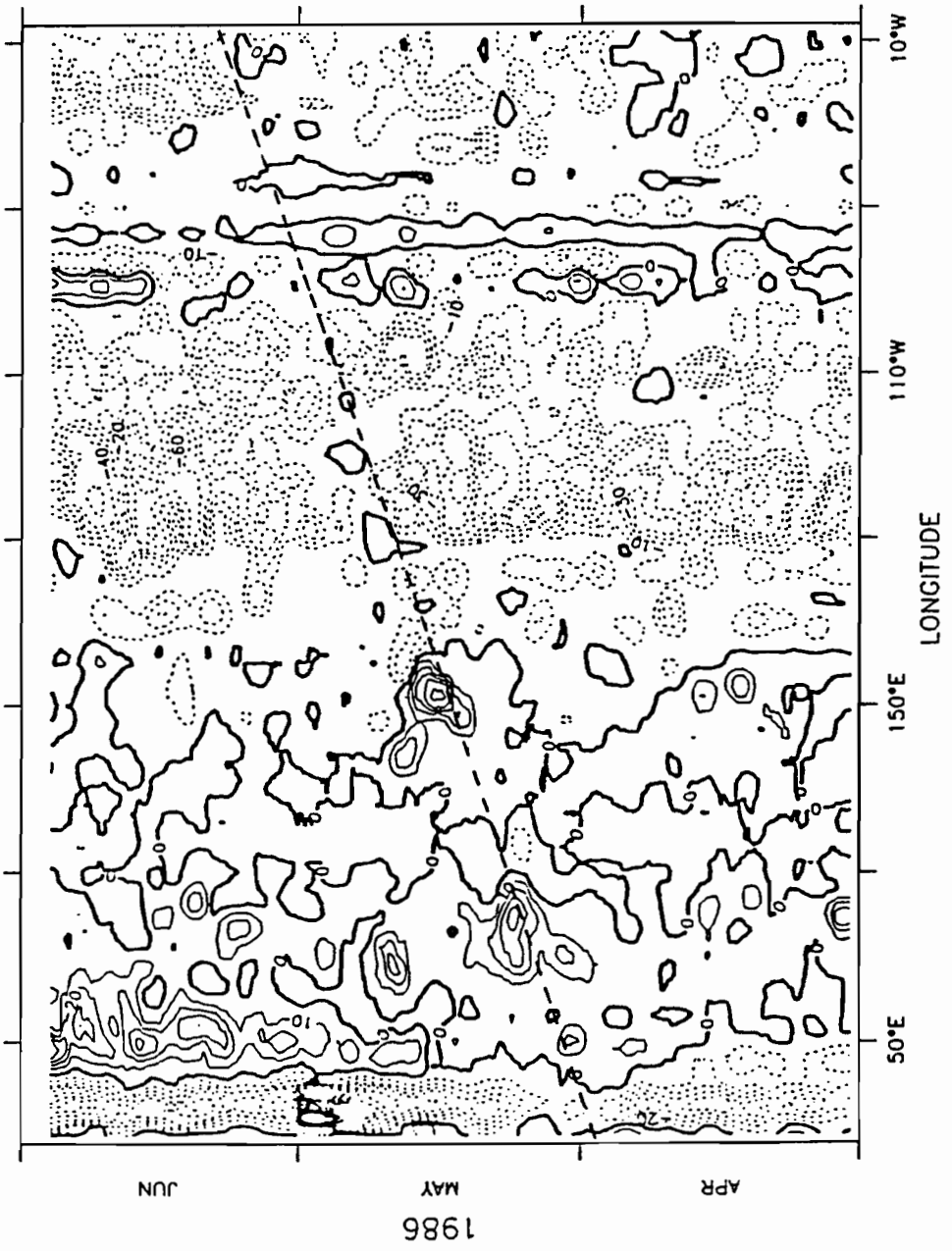

Figure 2.10. Zonal pseudo-stress at the equator for April through June 1986. Data have been averaged over 7.5° of longitude and 2.5 days.

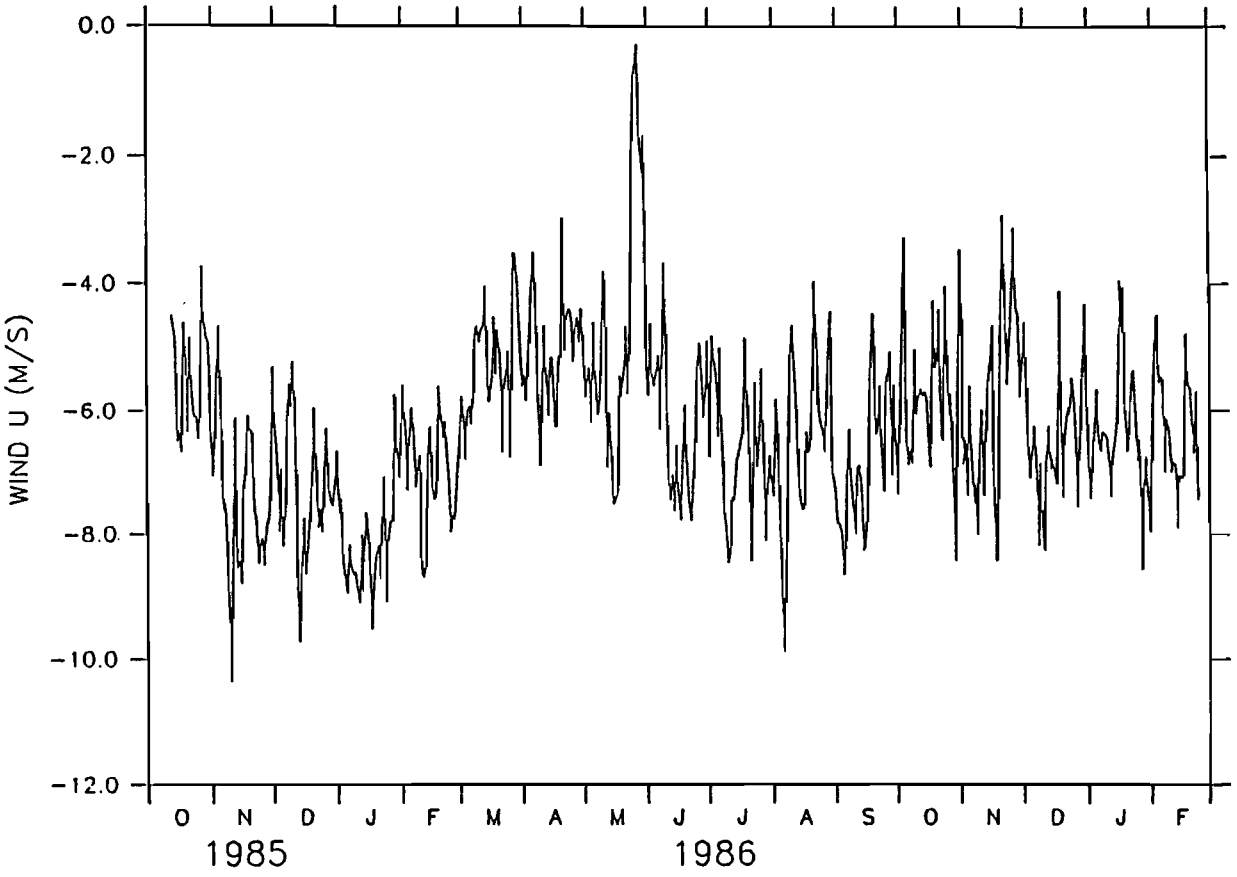

Figure 2.11. Surface zonal wind at 0°N, 140°W from October 1985 through February 1987. Courtesy of M.J. McPhaden, NOAA/PMEL.

3. FORCED EQUATORIAL WAVES

A. Introduction

The oceanic response to changes in wind forcing is one of the most successful applications of linear theory (Lighthill, 1969; Cane and Sarachik, 1976; Moore and Philander, 1977). Linear theory describes ocean response as the sum of a set of long waves, trapped to the equator. The only eastward propagating long wave excited by a zonal wind stress anomaly is the equatorial Kelvin wave, named in analogy with the coastal Kelvin wave (Matsuno, 1966). In this section the linear Kelvin pulse response to zonal wind stress is developed. A summary of linear theory of equatorial long waves can be found in appendix A. The linear response to changes in zonal wind stress is calculated in part 3.C. Two cases are examined in detail; the response to a stationary wind patch in the western Pacific and the response to a propagating wind patch that crosses the Pacific. Results from these two cases will be used in section 4 in a comparison with model results and oceanic observations. In part 3.F, one of the fundamental requirements for application of linear theory is relaxed: that background stratification does not vary as a function of longitude. Use of conservation of energy flux is the same as used by Hughes (1981). However, Hughes considered only one active layer overlaying an infinitely deep ocean. Here continuous stratification in a depth bounded ocean is considered, resulting in a different conclusion. For the remainder of the report, the term Kelvin wave refers to a waveform which can be expressed in simple sine terms. The term Kelvin pulse refers to a waveform of one sign, i.e. pure depression or elevation.

B. The Linear Approximation

The primitive equation of momentum for a parcel of water is

$$\frac{D\vec{u}}{Dt} + 2\vec{\Omega} \times \vec{u} = -\frac{1}{\rho} \nabla p - \vec{g} + \upsilon \nabla^2 \vec{u} + \vec{Q}(x,y,z,t) \tag{3.1}$$

where $\vec{u}$ is the velocity vector, $\vec{\Omega}$ is the rotation rate of the earth, ρ is the density of water, p is pressure, $\vec{g}$ is the acceleration due to gravity, υ is a coefficient of frictional dissipation and $\vec{Q}$ can be either surface wind or thermal buoyancy forcing term. The full equations of motion for oceanic flow do not in general permit analytic solutions, and only by making several assumptions about flow near the equator can solutions be readily obtained. Here the assumptions that will break down in the case of strong forcing are reviewed. Using characteristic length and time scales importance of neglected terms is estimated.

The first assumption is that flow is linear. The first term in the momentum equation is the total derivative and can be decomposed as

$$\frac{D\vec{u}}{Dt} = \vec{u}_t + \vec{u} \cdot \nabla\vec{u} \tag{3.2}$$

where the last term is advective nonlinearity. Here and for the remainder of the text, a subscript denotes partial differentiation. Using the particle velocity for u and phase speed as the characteristic length scale divided by the time scale, importance of nonlinear advection can be estimated as

$$\frac{\text{Advection}}{u_t} = \frac{U^2 T}{UL} = \frac{U}{c}. \tag{3.3}$$

This nondimensional parameter is the Froude number. For low velocity currents ($u \sim 10$ cm sec^{-1}) and relatively fast phase speeds ($c \sim 300$ cm sec^{-1}), the Froude number is small and nonlinear advection terms can be neglected. The nonlinear equatorial Kelvin wave has been discussed by Boyd (1980, 1984) and Ripa (1982). Advection can act to steepen waves, and given a long enough basin, can cause waves to break. Nonlinearity also acts to increase the phase speed of downwelling Kelvin waves and decrease the phase speed of upwelling waves.

Exclusion of nonlinear advection also eliminates the possibility that Kelvin pulses will interact with background flows via wave-mean flow or wave-wave interactions. It has been shown that presence of the equatorial undercurrent can substantially alter vertical structure of a Kelvin wave (Rothstein *et al.*, 1988). Observations made in the eastern tropical Pacific indicate that there is substantial energy on time scales of 30 days (Legeckis, 1977; Pullen *et al.*, 1987). Instability waves, produced as a result of shear in the equatorial current system, are readily produced in general circulation models (Cox, 1980; Philander *et al.*, 1986; Harrison and Giese, 1988). For purposes of developing simple linear theory, mean flow and background waves are ignored. This is clearly an unrealistic assumption, however benefits of such an assumption are great.

Importance of vertical friction can be estimated by the nondimensional inverse Reynolds number as

$$\frac{\text{Dissipation}}{u_t} = \frac{\upsilon_v t}{H^2}. \tag{3.4a}$$

Estimates of the vertical friction coefficient υ_v vary greatly, with estimates values ranging from 10 to 100 cm^2 sec^{-1} (Peters *et al.*, 1986) depending on the amount of vertical shear in the flow. Using an estimate of vertical shear as the inverse time scale and the depth of the thermocline (H) as a length scale, the inverse Reynolds number assumes a maximum value of 1×10^{-4}. Thus, ignoring vertical friction is a reasonable approximation.

Horizontal friction can be estimated as

$$\frac{\text{Dissipation}}{u_t} = \frac{\upsilon_h}{cL} \tag{3.4b}$$

where υ_h is about 2.0×10^{-7} cm^2 sec^{-1} (Pacanowski and Philander, 1981), c is about 300 cm sec^{-1} (Cane, 1984) and the length scale is about 2×10^7 cm. This gives an estimate of 3×10^{-3} for the horizontal inverse Reynolds number. It is reasonable to ignore horizontal friction terms.

With these assumptions it is possible to proceed with the linear theory of how Kelvin waves are forced by surface wind stress on the equator. The fundamentals of linear theory are presented in appendix A. Linear theory predicts that response to forcing can be expressed as the sum of baroclinic standing waves. For the specific case of Kelvin wave response, zonal velocity for any mode n can be written as

$$u_n(y,z,t) = Z_n \, \psi_n(z) \, Y_n D_0(y) \, T_n(t) \, \frac{1}{h_{mix}} \tag{3.5}$$

where h_{mix} is a mixed layer depth over which wind stress is distributed as a body force (Lighthill, 1969). Using Equation A.2b in the appendix, pressure can be expressed as

$$p = c_n \, u \, . \tag{3.6}$$

The function ψ_n in Equation 3.5 contains information about the vertical structure of baroclinic mode n, and is normalized to the value unity at the surface. The depth independent coefficient Z_n determines the amplitude of each baroclinic mode and is given by

$$Z_n = \frac{\int_0^{h_{mix}} \psi_n \, dz}{\int_0^H \psi_n^2 \, dz} \tag{3.7}$$

where the numerator is integrated from surface to the base of the mixed layer, h_{mix}. Since the structure function is approximately 1 in the mixed layer, the numerator integrates to h_{mix}, making Z_n proportional to mixed layer depth.

Meridional structure of the equatorial Kelvin wave is Gaussian (Equation A.15) and is written as

$$u(y) = e^{-y^2/2R_0^2} \tag{3.8}$$

where the quantity $R_o = (\beta/c_n)^{-1/2}$ is the Rossby radius of deformation, a scale of Kelvin wave width. Using Kelvin structure function as in Equation 3.8, the meridional projection coefficient,

Y_n, becomes

$$Y_n = \frac{\int_{-\infty}^{\infty} e^{-\beta y^2/2c_n}\, Y(y)\, dy}{\int_{-\infty}^{\infty} e^{-\beta y^2/c_n}\, dy} \tag{3.9}$$

where Y(y) is an arbitrary meridional structure of zonal wind.

Defining the spatial and temporal structure of the wind patch permits evaluation of Kelvin wave response of each vertical mode as a function of longitude and time. Amplitude of the Kelvin pulse is the result of any wind forcing that the wave encounters as it propagates from where it was formed to where it is being observed (Gill and Clarke, 1974). For forcing distributed over a mixed layer of depth h_{mix}, the integration can be written

$$T_n(t) = \int_0^t \tau\, dt \tag{3.10}$$

where the integral follows the path of the wave characteristic $x = c_n t$.

C. The Linear Response to Forcing

Equations 3.5 and 3.6 express zonal velocity and pressure for arbitrary initial and forcing conditions. There are four specific cases that are applicable to westerly wind bursts in the western Pacific. The first two involve the stationary Gaussian wind patch described in section 2. The third case treats the Gaussian wind patch averaged over one month. The fourth case is oceanic response to a translating wind patch, also described in section 2.

Meridional structure of the wind patch in all four cases is

$$Y(y) = e^{-y^2/2\lambda^2}. \tag{3.11}$$

By substituting Equation 3.11 into 3.9 and evaluating the integral yields

$$Y_n = \left[\frac{2\lambda^2}{\lambda^2 + R_0^2}\right]^{1/2} \tag{3.12}$$

When the forcing patch is narrow compared to the Rossby radius ($\lambda << R_o$), the meridional projection can be approximated by

$$Y_n = \frac{\lambda}{R_0}\sqrt{2} \tag{3.13}$$

so that meridional projection is inversely proportional to the square root of the phase speed of the

Kelvin pulse. This means that forcing projects more efficiently onto narrow high vertical modes relative to faster (and therefore broader) low vertical modes. When the forcing patch is wide compared to the Rossby radius ($\lambda >> R_o$) then the projection coefficient asymptotically approaches the constant value of the square root of two.

Since the wind patch has a finite extent in x, integration along a characteristic will make a non-zero contribution to forcing only for time $t = L\, c_n^{-1}$ where L is the longitudinal extent of the wind patch. A diagram of forcing in time and longitude is shown in Fig. 3.2. A Kelvin wave characteristic is shown as a dark solid line. For a stationary wind patch, amplitude of the Kelvin pulse at longitude $x = x_0$ will be given by

$$u(x_0,t) = \frac{\tau_0 Z_n Y_n}{h_{mix}} \int_{\frac{x_0}{c_n} - \frac{L}{2c_n}}^{\frac{x_0}{c_n} + \frac{L}{2c_n}} e^{-t^2/2\lambda^2}\, dt\,. \tag{3.14}$$

This integral gives a Gaussian probability function, which also is Gaussian. The oceanic response to a stationary wind patch can be found by numerical integration of Equation 3.14. Using a first vertical mode with a phase speed of 300 cm sec^{-1} and forced by a wind patch 20° long Equation 3.14 predicts a Kelvin pulse that is Gaussian in time with a width at half-maximum scale of 12 days. This represents a 20% increase over the time scale of the wind patch. The temporal structure for a Kelvin pulse with a phase speed of 150 cm sec^{-1} is Gaussian with a decay scale of 17 days, longer than, but not double, the decay scale of the faster Kelvin pulse.

Characteristics in Fig. 3.2 are halfway across the wind patch when the wind anomaly attains its maximum strength. A wave following this characteristic is subject to the maximum amount of forcing, therefore this ray describes the path of maximum amplitude of the Kelvin response. This maximum is found by

$$T_n(\max) = \int_{-L/2c_n}^{L/2c_n} e^{-t^2/2\lambda^2}\, dt \tag{3.15}$$

and so depends on both phase speed c_n and length of the wind patch L. Figure 3.3 presents T_n as a function of c_n for a wind patch 20° wide. At a value for the first mode Kelvin wave of 300 cm sec^{-1} the characteristic receives about 2/3 of total available forcing. At phase speeds less than about 150 cm sec^{-1} there is little effect on T_n.

A vertical stratification typical of the eastern tropical Pacific is shown in Fig. 3.1. The thermocline is near the surface with a maximum value of N at 10 cycles per hour at a depth of 20 m. Eigenvectors for this stratification can be found numerically. Structure functions of zonal velocity for the lowest four vertical modes are also presented in Fig. 3.1, normalized such that the value at the surface is unity. Each mode, n, has n zero crossings; each zero crossing corresponds

to a maximum in vertical displacement. The profile of vertical velocity is the depth integral of these structure functions (see Equation 3.7d), with value zero at surface and bottom.

The N profile shown in Fig. 3.1 was used in an eigensolver to determine the structure and phase speed of vertical normal modes. Using Equations 3.7, 3.9 and 3.10, projection coefficients Z_n, Y_n, and T_n were determined. They are presented in Table 3.1. Maximum amplitude of surface velocity for any Kelvin mode, n, can be found east of the forcing region as $u_n(max) = Z_n Y_n T_n (h_{mix})^{-1}$. Since surface velocity of the Kelvin pulse is proportional to the inverse of h_{mix}, and Z_n is proportional to h_{mix}, the zonal velocity anomaly is not sensitive to depth of the mixed layer for low vertical modes. With a maximum wind stress of 0.2 dynes cm^{-2}, the first vertical mode has a maximum velocity anomaly of 2.1 cm sec^{-1}. In the absence of mean flow sea level perturbation is calculated as

$$\eta = \frac{p_n}{g} = \frac{c_n \, u_n}{g} \tag{3.16}$$

where u_n is surface velocity.

Zonal velocity and sea level perturbations expected from linear theory are presented in Table 3.1 for the first four vertical modes. The third baroclinic mode is most strongly forced for this density stratification. When the thermocline is thin and near the surface, as in the representation of the eastern Pacific, forcing projects most efficiently onto the third and fourth vertical modes (Eriksen, 1988). After the fourth vertical mode, the projection coefficient Z_n starts to decrease rapidly. Although velocity perturbation increases by a factor of three from mode 1 to mode 3, there is little difference in sea level expression of various modes. Linear theory predicts that all vertical modes will have about the same surface expression of about 0.50 cm. This is because of the effect of decreasing phase speed with mode number. Since sea level is proportional to phase speed (Equation 3.16), an increase in velocity anomaly is compensated for by a decrease in phase speed. Thus, it is possible to have very energetic high mode waves which have very little sea surface expression.

The western Pacific is characterized by a deep and broad thermocline, so that the N profile has substantially different characteristics from the one just presented. Such a density structure is shown in Fig. 3.4, with the first four vertical structure functions. Velocity and sea level anomalies derived from linear theory are presented in Table 3.2. The phase speed of the first vertical mode is 303 cm sec^{-1}, a reasonable value for the western Pacific (Cane, 1984). Vertical projection coefficients suggest that the first vertical mode would be most energetic, with second vertical mode projection less than half of the first vertical mode. However, when integration along characteristics and meridional projection are computed, dominance of the first mode is not as evident. Here a mixed layer of 80 m is used, and the peak wind stress is 2.0 dynes cm^{-2}. Linear theory predicts that the first vertical mode will a have peak velocity of 32.8 cm sec^{-1}. The

second vertical mode will be smaller, but still significant at 23.9 cm sec^{-1}. Linear theory predicts a sea level increase of 10.1 cm for the first mode. Sea level expression for the second vertical mode is 4.2 cm.

Many of the numerical experiments of the tropical Pacific have used monthly averaged winds (Busalacchi and O'Brien, 1981; Cane and Zebiak, 1985; Harrison *et al.*, 1988). Response to a westerly wind burst that has been included in a monthly mean can easily be evaluated. Consider a month in which the above ten-day wind burst occurs at mid-month. The wind anomaly increases linearly for the first fifteen days, until it reaches its maximum anomaly of approximately one third of the maximum of the ten-day burst. Over the next fifteen days, the wind anomaly decreases to zero again. Because oceanic stratification is identical to that in the above example, projection coefficients are the same except for T_n, which is now given by

$$T_n(\max) = 2 \int_0^{L/2c_n} t\,dt = \frac{L^2}{4c_n^2} . \tag{3.17}$$

Because T_n grows proportional to the inverse of c_n squared, higher vertical modes are favored in the monthly averaged wind burst. Maximum zonal velocity and sea level perturbations for the month-long burst are presented in Table 3.2b. The surface velocity of the first vertical mode is 24 cm sec^{-1}, a 27% reduction over the shorter, but more intense ten-day wind burst. In contrast, the third and fourth vertical modes grow relative to the shorter wind burst.

The structure of the month-long burst is also significantly different. Instead of being Gaussian in longitude and time, the wind burst averaged over one month will result in Kelvin pulses which ramp up and down linearly in longitude and time. Because the month patch is longer in duration, the forced response of each vertical mode will be wider. Different baroclinic modes will overlap, and remote response will be a gradual increase in zonal currents over a period of several months.

The final case of wind stress anomaly is that associated with a translating wind patch, as discussed in section 2. Here the linear response to an idealized representation of the translating patch is considered. The idealized translating patch has a top-hat structure in longitude with a length of 20° and is Gaussian in y, and is centered on the equator with a width of 3° of latitude. The wind anomaly within the patch does not vary in time, although the patch propagates eastward with a speed c_f.

Since the observed phase speed of atmospheric forcing is about 10 m sec^{-1} (section 2), it is faster than the fastest equatorial internal wave. A schematic diagram of the translating wind patch is presented in Fig. 3.5a. In this case the wind patch is propagating at 10 m sec^{-1}, indicated by characteristics c_f. Characteristics of the first baroclinic mode Kelvin pulse are labeled c_w. At longitude $x = x_0$, the response can be determined as a function of time, as presented schematically in Fig. 3.5b. Perturbation begins when the leading edge of the wind patch propagates to x_0.

The velocity perturbation grows linearly with time until the trailing edge of the wind patch passes x_0, at time $(x_0 - L)c_f^{-1}$. At this time the velocity anomaly attains its maximum value of

$$u_{max} = \frac{Z_n Y_n \tau_0 L}{h_{mix}(c_f - c_w)} . \tag{3.18}$$

Velocity is unchanged until the leading edge of the free oceanic Kelvin wave arrives at x_0. The time that the velocity anomaly has its maximum value depends on observation longitude, and is given by

$$T(max) = \frac{x_0}{c_w} - \frac{x_0}{c_f} - \frac{L}{c_f} . \tag{3.19}$$

Zonal velocity then decreases linearly with time until the trailing edge of the oceanic free Kelvin wave passes x_0.

Consider a translating wind patch that formed at 160°E and moves eastward at a constant 10 m sec^{-1}. The wind patch will arrive at 140°W seven days after the start of the wind burst. The velocity anomaly will achieve its maximum value three days after the patch arrives at 140°W, when the trailing edge of the wind anomaly passes. Perturbation zonal velocity will be constant until 21 days after the beginning of the atmospheric Kelvin wave. It takes another eight days for the ocean to return to its unperturbed state.

D. Kelvin Waves and Anomalous Advection

There are two mechanisms by which a Kelvin pulse can alter sea surface temperature. Surface temperature is determined in large part by a balance between heating by the sun and cooling by upwelling of cold water. A change in depth of the thermocline alters the cooling by entrainment of cool water into the surface. This results in sea surface heating in the case of a downwelling wave and cooling in the case of an upwelling wave (McCreary, 1983).

When a Kelvin pulse is created by a uni-directional wind anomaly, as in the examples above, upwelling or downwelling associated with the pulse has one sign. The thermocline is displaced only when the Kelvin pulse is present; after passage of the Kelvin pulse the thermocline returns to its original depth. Although the Kelvin pulse alters sea surface temperature, depth of the thermocline remains unaltered. Then the balance between entrainment and solar heating resumes, at a new surface temperature.

Another mechanism that has been suggested for alteration of sea surface temperature by Kelvin pulses is advection against the horizontal temperature gradient (Philander, 1981; Gill, 1983; Harrison and Schopf, 1984). This requires a zonal temperature gradient, a typical feature of both tropical Pacific and Atlantic during much of the year. Harrison and Schopf introduced an anomalous advection equation

$$\frac{dT'}{dt} = -u'\frac{dT}{dx} - v'\frac{dT}{dy} \tag{3.20}$$

in which temperature change T′ could be estimated by knowing background temperature gradients and perturbation velocities, u′ and v′. Although the meridional temperature gradient is strong (up to 4°C in a few degrees of latitude), recall that the Kelvin wave has no meridional velocity. Linear theory predicts that the Kelvin wave will not result in a heating or a cooling by advecting the meridional temperature gradient. When there are strong temperature gradients there will be strong anomalous temperature changes; regions of weak or no gradient will have no changes. For Gaussian pulses that are discussed in section 1, the zonal velocity anomaly is always greater than zero and there is a net warming. There is also a possibility that advecting subsurface thermal structure results in a change of thermocline depth. Then anomalous heating or cooling can occur as in the first mechanism.

During Austral summer the zonal temperature gradient is weak in the central Pacific. However, there are strong coastal temperature gradients. A Kelvin pulse propagating toward the eastern Pacific during this time will generate little temperature anomaly in the central Pacific, yet may lead to significant warming at the coast of South America (Harrison and Schopf, 1984). In Austral winter, there is a cold tongue of water that extends from the coast of South America into the central Pacific. Due to this strong temperature gradient, as Kelvin pulses propagate through the central Pacific there will be temperature anomalies.

To find the temperature anomaly expected from Kelvin pulses discussed in the above examples, Equation 3.20 is integrated with respect to time. Since the Kelvin pulse has no meridional velocity perturbations, only the zonal temperature gradient is needed for the anomaly equation. Assuming the zonal temperature gradient is constant, the temperature anomaly equation becomes

$$T_{anomaly} = \frac{dT}{dx}\int_0^t u\,dt\,. \tag{3.21}$$

In May, the horizontal temperature gradient in the central Pacific is about 1.5°C per 10° of longitude (Reynolds, 1982). Using the first mode pulse which has maximum surface currents of 32.8 cm sec^{-1} and a Gaussian time scale of 12 days, the expected temperature anomaly is 0.4°C.

E. Reflection and Transmission at the Eastern Boundary

Eventually equatorially trapped Kelvin waves will propagate to the boundary of the ocean basin. Energy is partitioned into westward propagating Rossby waves and coastally trapped Kelvin waves (Moore, 1968). Kelvin waves of very low frequency reflect efficiently into westward propagating Rossby waves. Kelvin waves of very high frequency also reflect effi-

ciently into westward propagating inertia-gravity waves. Between these two extremes there is a band from about one month to two days, for which a first baroclinic mode inbound Kelvin wave must transmit 100% of its energy into coastally trapped Kelvin waves.

The frequency content and vertical structure of the inbound Kelvin wave thus determines the reflection coefficient. For a sinusoidal wave with a six-month period, 84% of incident wave energy will be reflected as westward propagating Rossby waves. The remaining 16% of energy will be transmitted as coastally trapped Kelvin waves (Clarke, 1983).

Because the Kelvin response to episodic forcing is Gaussian, there is no single frequency for the inbound Kelvin pulse. Then, to determine the nature of reflected and transmitted signals, the frequency content of the Kelvin pulse must be known. The Fourier transform of the Kelvin pulse is

$$\mathrm{FT}\left(e^{-t^2/2\gamma^2}\right) = \sqrt{2\pi}\,\frac{\gamma}{2}\,e^{-s^2\gamma^2/2}\ . \tag{3.22}$$

Since the transform of the Kelvin pulse is also Gaussian, most of the power is at zero frequency. At zero frequency there is perfect reflection into outbound Rossby waves. However, there is also significant power at a period of five days in the Kelvin wave forced by the stationary patch. Since this is within the gap for which there can be no reflected Rossby wave, there will also be energy transmitted into coastally trapped Kelvin pulses.

In the wind burst example above in which a downwelling Kelvin pulse is excited, there is no upwelling following the wave pulse. When the wave hits the coast of South America and reflects an outgoing Rossby wave the sign of velocity at the surface changes. This in turn excites an upwelling Kelvin wave which travels up the coast of the Americas. Thus a purely downwelling equatorial wave excites both downwelling and upwelling coastal waves. When coastal waves advect the temperature field they will act not only to warm but also to subsequently cool the coast of South America. Furthermore, the amplitude of upwelling versus downwelling waves will depend on the relative amplitude of the reflected Rossby wave. Waves that have a period within the gap from a month to two days have perfect transmission into coastally trapped Kelvin waves. The resulting coastal Kelvin pulse is therefore only downwelling. However, if 50% of the incoming Kelvin wave is reflected as equatorially trapped Rossby waves, upwelling and downwelling waves will have comparable amplitude.

F. Interaction with a Sloping Thermocline

In a study of thermal changes during the 1972-73 ENSO, Gill (1982) found that movement of the thermocline in the western Pacific could be adequately described by the first vertical mode. However, changes in thermal structure in the eastern Pacific were dominated by the second vertical mode. Gill speculated that the first mode scattered energy into the second mode as it

encountered the shoaling thermocline. However, it has been shown that scattering becomes important only for periods greater than six months (Gill and King, 1985) and that even scattering at these long periods is not sufficient to explain Gill's observation (Busalacchi and Cane, 1988).

There is no direct way for linear theory to accommodate horizontal changes in thermal structure. However, if changes in thermal structure occur over distances which are large compared to the length scale of the Kelvin pulse, a WKB approximation can be made. Here the length scale is taken as the full width at half maximum of the Kelvin pulse. The thermocline shoals from near the date line to about 100°W, a distance of 80°. Since the pulse length scale is about 20° the pulse is short compared to changes in thermal structure. In the WKB limit it is assumed that the vertical structure of any mode can change to reflect changes in background thermal structure. Hence there can be no scattering of energy from one mode to another and there is no reflection of the Kelvin wave into westward propagating Rossby waves. Changes of vertical structure of each mode are estimated by finding the structure of the waves in their local environment.

It is instructive to consider first the limit of waves which are long compared to the distance over which significant changes occur in thermal structure. In this limit, waves impinge on a jump discontinuity. Using a model with two regions, a western and an eastern Pacific, Busalacchi and Cane (1988) found that energy flux of a single mode is nearly conserved across the jump discontinuity. Thus, even in this limit of rapidly varying background stratification, scattering of energy into westward propagating Rossby waves is not important. Busalacchi and Cane also found that surface currents of the first and second modes undergo an amplitude increase as they propagate from the western to the eastern Pacific. In their model the amplitude increase is due to a change in the Rossby radius of deformation. As waves propagate into the eastern Pacific, their phase speed decreases. Equation 3.8 shows that an increase in phase speed narrows the wave. Hence, to conserve the flux of energy the amplitude must increase.

The density stratification used by Busalacchi and Cane (1988) is shown in Fig. 3.6. The N profile averaged from 150° to 170°W from XBT measurements is also shown. Although the overall shape of the two curves are similar, the N profile used by Busalacchi and Cane has a thermocline which is too shallow to be characteristic of the western Pacific. Repeating their calculations, but using observed stratification yields a significantly different interpretation of evolution of first and second vertical mode Kelvin waves that propagate into the eastern Pacific.

Conserving energy flux (J) through a meridian (Ripa, 1982) as

$$J = \int_0^H \int_{-\infty}^{\infty} p(x,y,z)\ u(x,y,z)\ dy\ dz \tag{3.23}$$

an expression for changes in velocity (u) or pressure (p) as a function of longitude can be found. Substituting the meridional and vertical structure functions gives

$$J(x) = u_{0n}^2 \int_0^H \int_{-\infty}^{\infty} c_n \, \psi_n^2(z) \, e^{-\beta y^2/c_n} \, dy \, dz \tag{3.24}$$

where the above integrals extend over the entire depth of the ocean and from pole to pole. The meridional integral in Equation 3.24 can be evaluated to give

$$J(x) = \sqrt{\frac{\pi}{\beta}} \; u_{0n}^2 \, c_n^{3/2} \int_0^H \psi_n^2(z) \, dz \tag{3.25}$$

where c_n and ψ_n are found using the local stratification. Using different stratifications for the western and eastern Pacific allows us to estimate change of zonal velocity and sea level anomalies. Equating the expression for energy flux in the eastern Pacific with energy flux in the western Pacific yields

$$u_E^2 c_E^{3/2} \int_0^H \psi_E^2(z) \, dz = u_W^2 c_W^{3/2} \int_0^H \psi_W^2(z) \, dz \tag{3.26}$$

where the subscript for baroclinic mode has been dropped. The quantities u_E and u_W represent surface velocity in the eastern and the western Pacific, respectively. Solving for the surface zonal velocity in the eastern Pacific as a function of surface zonal velocity in the western Pacific gives

$$u_E = u_W \left[\frac{c_W}{c_E}\right]^{3/4} \left[\frac{\int_0^H \psi_W^2(z) \, dz}{\int_0^H \psi_E^2(z) \, dz}\right]^{1/2} \tag{3.27a}$$

and for surface pressure (or sea level)

$$p_E = p_W \left[\frac{c_E}{c_W}\right]^{1/4} \left[\frac{\int_0^H \psi_W^2(z) \, dz}{\int_0^H \psi_E^2(z) \, dz}\right]^{1/2} \tag{3.27b}$$

Since the phase speed in the western Pacific is always larger than the phase speed in the eastern Pacific for the sloping thermocline case, the first term implies a surface zonal velocity increase for any vertical mode. Sea level, on the other hand, always experiences a decrease in amplitude, although not as great a difference as in zonal velocity. Changes in zonal velocity and sea level due to a change in phase speed is discussed in Busalacchi and Cane (1988).

Changes in zonal velocity and sea level in a two layer model can now readily be found. In this model the depth of the upper layer changes, but the relative difference in density between the

two layers remains the same. The equation for energy flux (3.25) then becomes

$$J(x) = \sqrt{\frac{\pi}{\beta}}\ u_1^2\ c^{3/2}\ \frac{H_1}{H_2}\ D \tag{3.28}$$

where H_1 is the depth of the upper layer, H_2 is the depth of the lower layer and D is the constant total depth. Since the phase speed c is a function of H_1 and H_2, the function J(x) can be found as a function of H_1 and H_2 alone. Then the amplitude increase of a Kelvin wave propagating into a region with a different upper layer is

$$u_E = u_W \left[\frac{H_{2E}}{H_{2W}}\right]^{1/8} \left[\frac{H_{1W}}{H_{1E}}\right]^{7/8} . \tag{3.29}$$

If a wave propagates from a region where the upper layer has a depth of 100 m (western Pacific) into a region where the upper layer is 50 m (eastern Pacific) then Equation 3.29 predicts that the wave will undergo an amplitude increase of 1.8. The same power law (7/8) is found when considering a single active layer overlaying an infinitely deep lower layer (Hughes, 1981).

When realistic N profiles are used for eastern and western Pacific, conservation of energy flux (Equation 3.27) predicts that the surface velocity of the first vertical mode will decrease by about 15%. In contrast, the surface velocity of the second mode will increase by 70%. The increase in phase speed explains some of the increase in the second mode, but it cannot explain a decrease of the first mode.

The explanation for the amplitude decrease of the first mode rests in the ratio of the vertical structure functions in Equation 3.27. In the eastern Pacific, where the thermocline is sharp and close to the surface, structure of the first vertical mode is broad. Structure functions therefore tend toward the solution when the stratification is constant. The integral of the square of these functions is greater than in the western Pacific. Energy in the first vertical mode has been redistributed vertically, such that surface velocity decreases. For the second vertical mode, which is more sensitive to changes in thermal structure near the surface, the opposite is true, and surface velocity increases.

TABLE 3.1 The predicted linear Kelvin pulse response to the 0.2 dyne cm^{-2} westerly wind burst for the density stratification as in Figure 3.1. Z_n and Y_n are dimensionless projection coefficients as discussed in the text.

Mode	c_n cm sec^{-1}	Z_n	T_n sec	Y_n	u_n cm sec^{-1}	Sea Level cm
1	218	0.277	7.68×10^5	0.59	2.1	0.46
2	122	0.342	9.07×10^5	0.74	4.6	0.57
3	83	0.377	9.19×10^5	0.85	5.9	0.50
4	64	0.328	9.19×10^5	0.92	5.5	0.34
5	52	0.281	9.19×10^5	0.97	4.9	0.26
6	44	0.180	9.19×10^5	1.02	3.4	0.15

TABLE 3.2. (A) The predicted linear Kelvin pulse response to the 2.0 dynes cm^{-2} westerly wind burst for the density stratification in the western Pacific shown in Figure III.4. Z_n and Y_n are dimensionless projection coefficients as discussed in the text. (B) The response for the month averaged burst.

Mode	c_n cm sec^{-1}	Z_n	T_n sec	Y_n	u_n cm sec^{-1}	Sea Level cm
1	303	0.402	6.28×10^5	0.52	32.8	10.1
2	174	0.175	8.42×10^5	0.65	23.9	4.2
3	105	0.085	9.15×10^5	0.78	15.2	1.6
4	79	0.106	9.19×10^5	0.86	20.9	1.7
(B)						
1	303	0.402	4.58×10^5	0.52	23.9	7.4
2	174	0.175	7.51×10^5	0.65	21.3	3.8
3	105	0.085	11.31×10^5	0.78	18.8	2.0
4	79	0.106	13.70×10^5	0.86	31.2	2.5

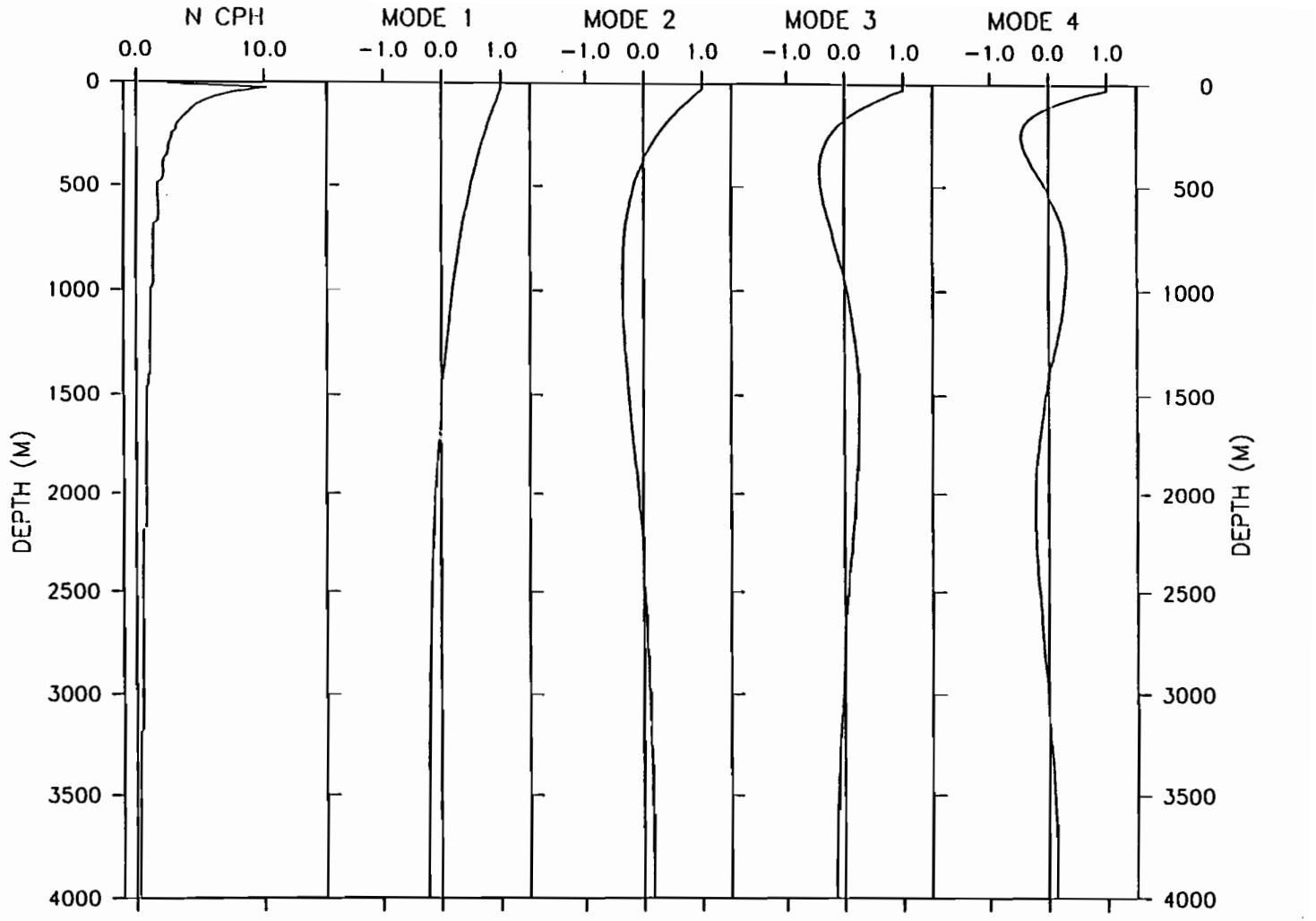

Figure 3.1. The vertical density structure and first four zonal velocity structure functions for the quiescent ocean initial condition.

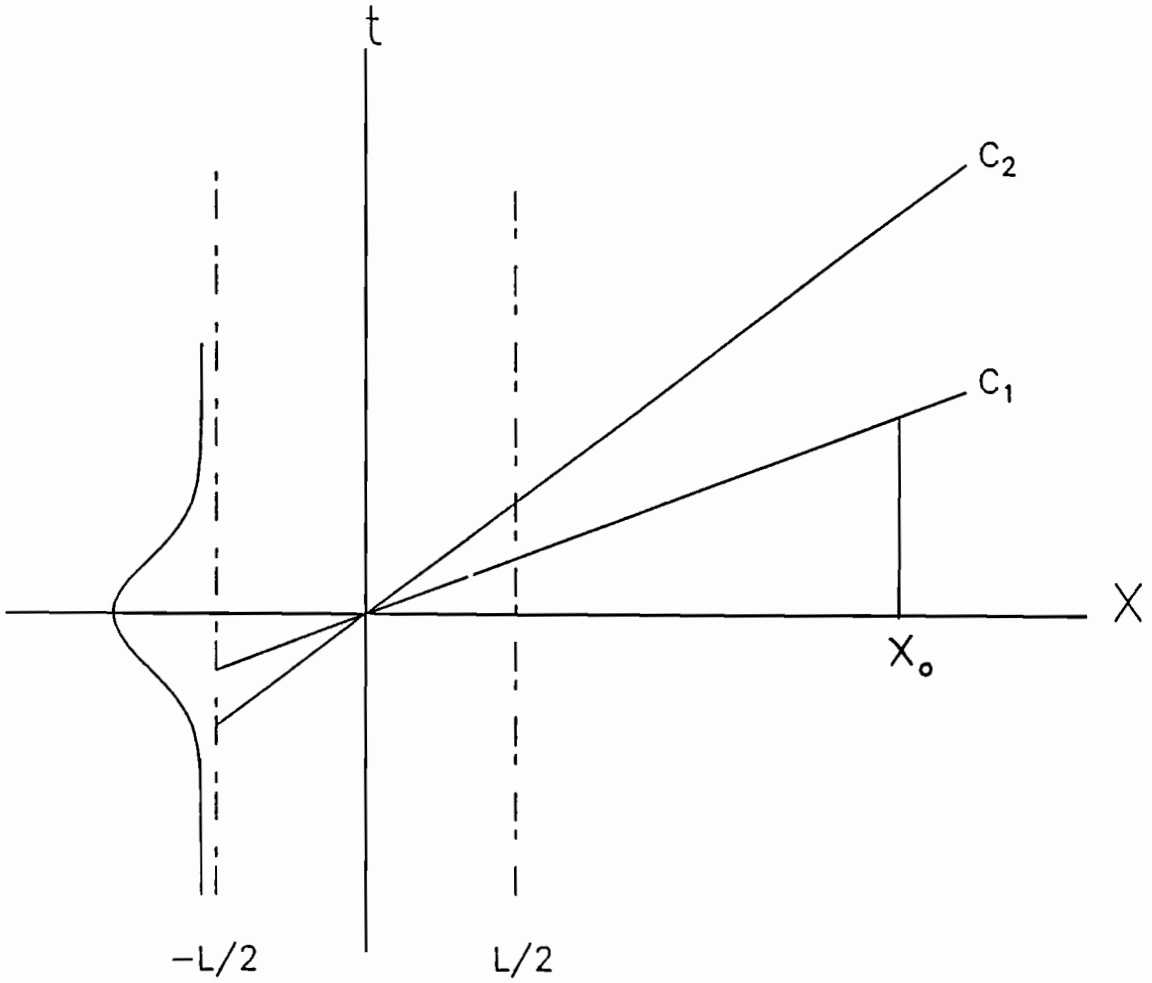

Figure 3.2. Kelvin pulse characteristics for the first (C_1) and second (C_2) baroclinic modes. The forcing region extends from -L/2 to L/2 with time dependence as indicated by the curve to the left of -L/2.

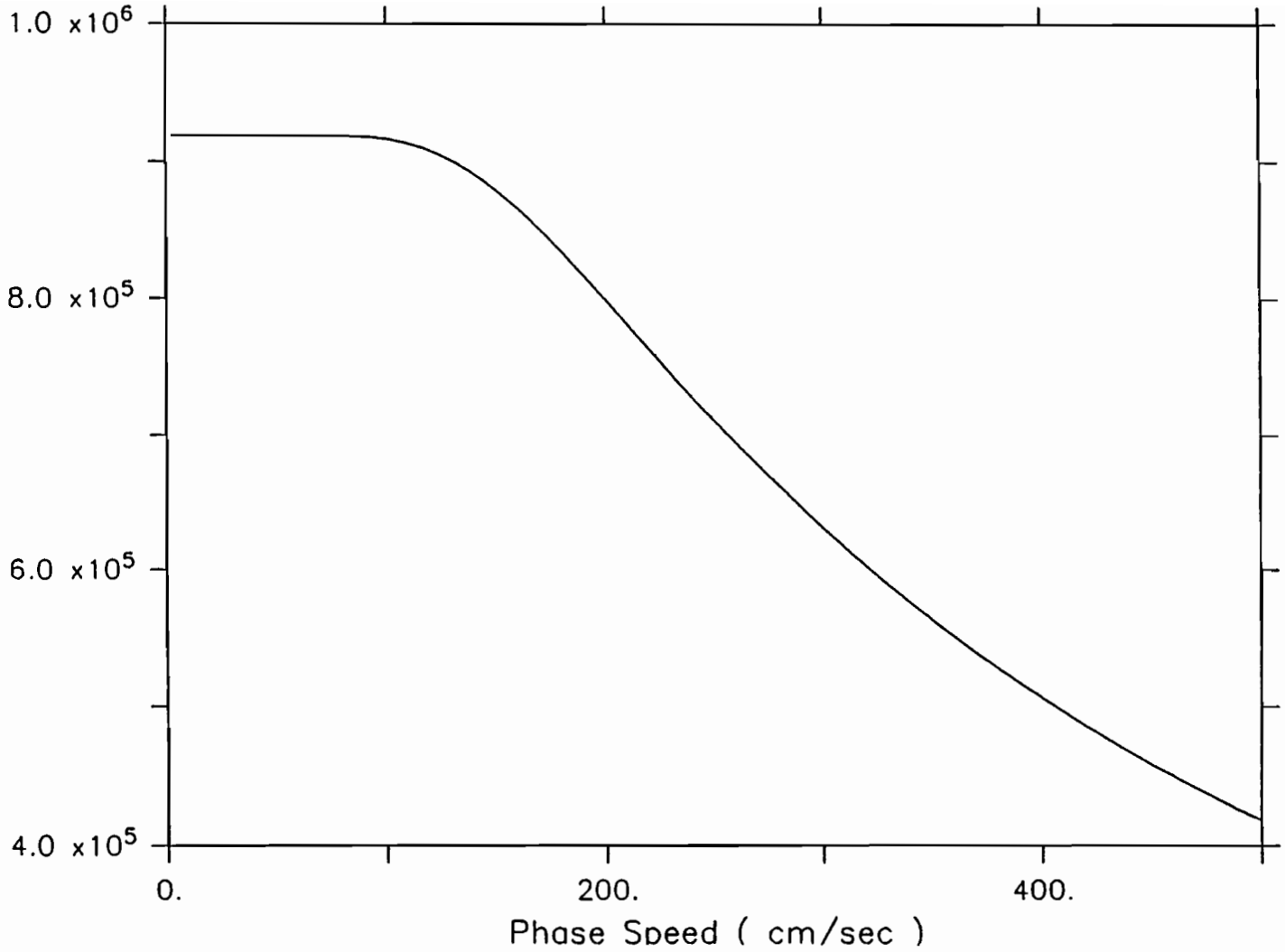

Figure 3.3. The time integrated forcing coefficient (T_n) in units of seconds plotted as a function of phase speed. The wind patch is 20° of longitude wide and Gaussian in time with a half-width of ten days.

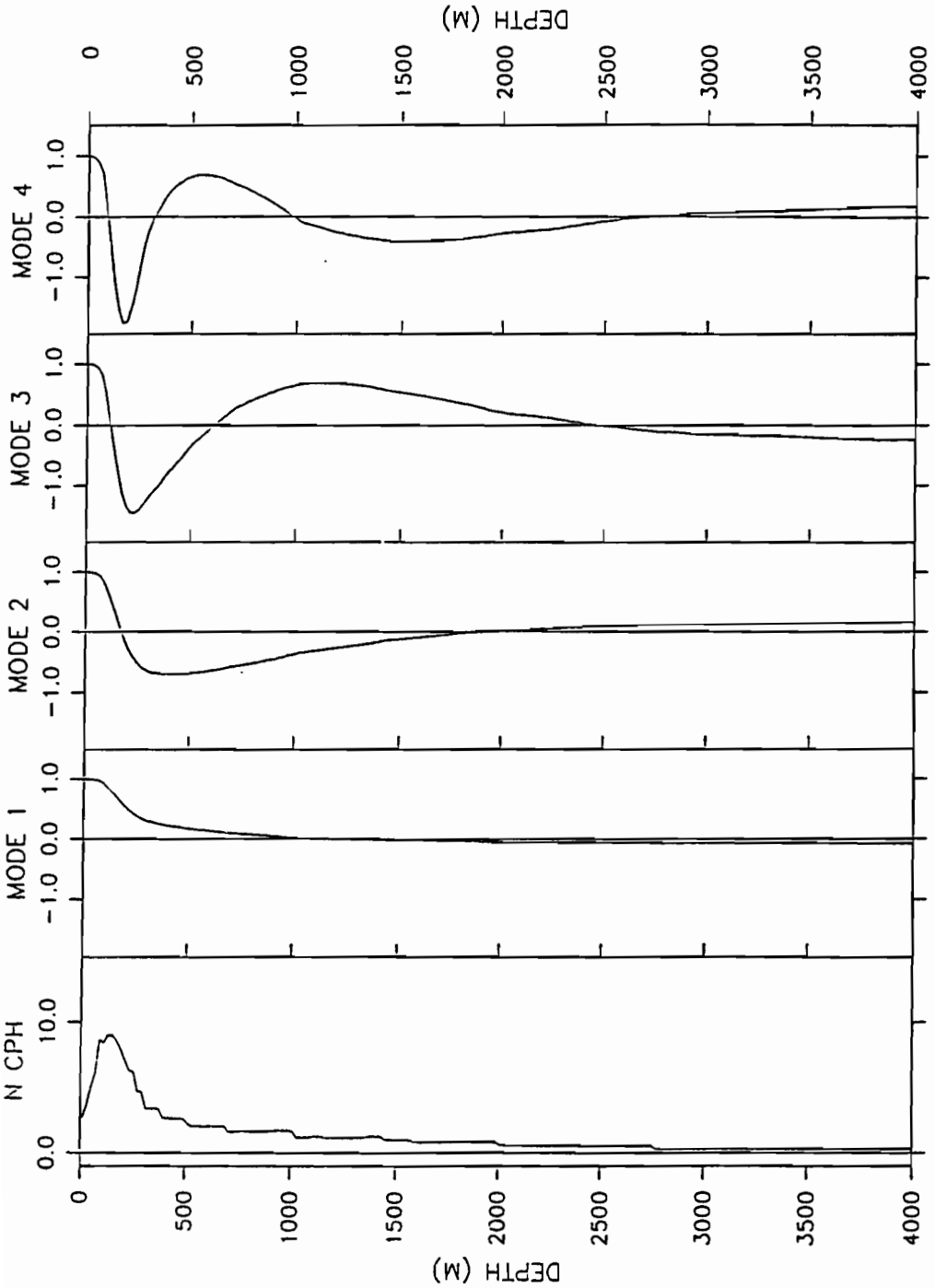

Figure 3.4. The vertical density structure and first four zonal velocity structure functions for the climatological model conditions at 0°N, 160°E.

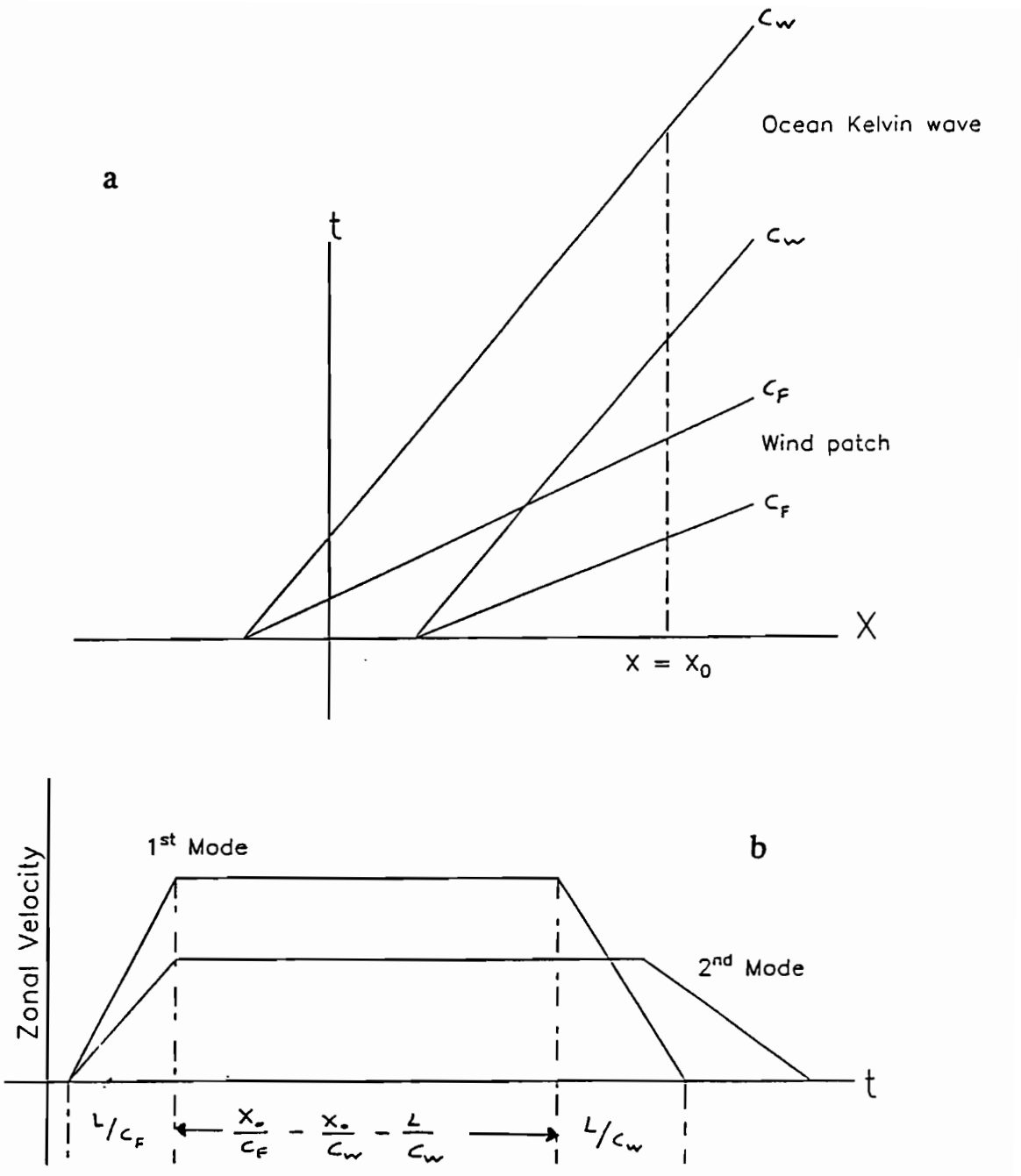

Figure 3.5 (Top) A schematic of the time-longitude structure of the linear oceanic response to a propagating wind patch. In this case the wind patch travels faster than the first mode oceanic Kelvin pulse. (Bottom) The zonal velocity response at $x = x_0$.

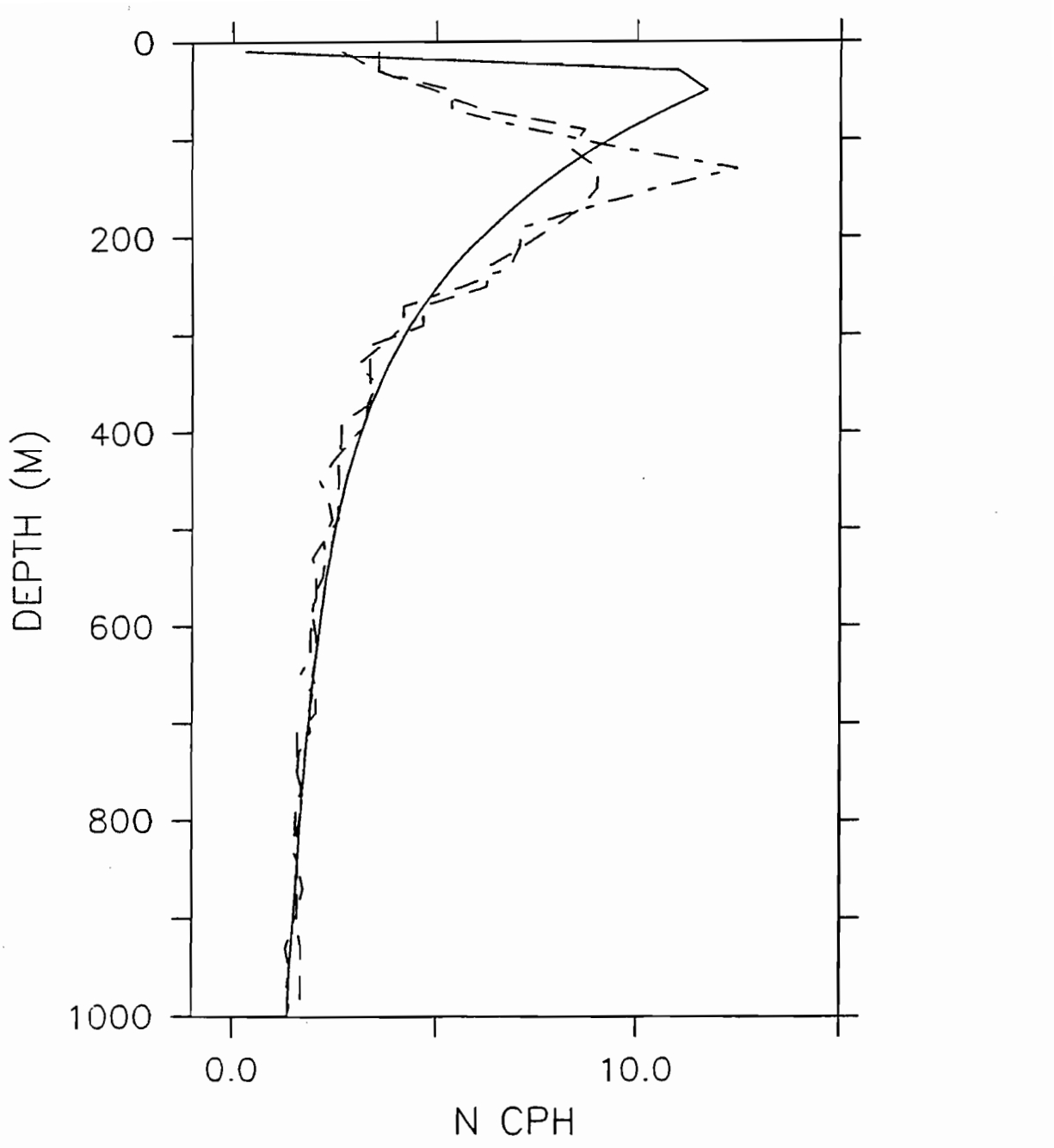

Figure 3.6 The vertical density structure as used in Busalacchi and Cane (1988) (solid line). The model vertical structure from 160°E is shown as a dashed line and the observed structure averaged from 150°E to 170°E is shown as a dotted-dashed line.

4. MODELING EFFORT

A. Introduction

Linear theory provides a useful framework for predicting the oceanic response to episodic forcing in the western Pacific when the wind anomaly is weak. However, when the wind anomaly becomes strong, assumptions that were made to linearize the equations of motion break down. By multiplying zonal velocity in Table 3.1 by a factor of ten, the linear response to a 2.0 dyne cm^{-2} wind anomaly is obtained. For the third and fourth modes, these linear zonal velocities are nearly equal to the phase speed. This violates the necessary condition for linear flow, that the Froude number remain much less than one. Furthermore, there are sources of nonlinearity in background oceanic flow which affect propagation of equatorial Kelvin pulses. These sources include shoaling of thermocline from west to east and interactions with both equatorial undercurrent and instability waves.

Because shoaling of the thermocline alters the vertical structure functions, the equations of motion are not separable. Although linear theory is useful in the WKB limit of short wavelength compared to changes in thermal structure, it is not always true that changes in thermal structure are smooth.

Since the sloping thermocline is in balance with a zonal baroclinic pressure gradient with a deeper vertical scale than that associated with wind stress mixing, a compensating flow from west to east is created. Thus, the shoaling thermocline is inextricably linked to the eastward flowing equatorial undercurrent. The undercurrent interacts with Kelvin pulses nonlinearly, and can alter their vertical structure.

The equatorial Pacific is full of variability on time scales from days to years. In particular, 30-day instability waves are a dominant feature of the eastern Pacific during Boreal summer. There are also seasonal changes in the strength of the undercurrent and thermal structure and interannual changes associated with ENSO.

These sources of nonlinearity prohibit analytic solutions to the equations of motion so solutions must be found numerically. One possibility is to isolate these dynamics in an ocean general circulation model. Such a model contains enough resolution in the vertical to allow a realistic representation of the equatorial undercurrent and shoaling thermocline. Since the seasonal cycle of the ocean is sensitive to seasonal changes in wind stress, using monthly mean winds drives a realistic ocean seasonal cycle. Because there are realistic horizontal shears in the general circulation model, instability waves are formed (Cox, 1980).

Philander and Pacanowski (1980) used a numerical model to examine response of the equatorial Pacific to relaxation of the tradewinds. They point out that the ocean will respond differently to forcing at time scales less than 150 days than to forcing at time scales greater than 150 days. Their results indicate that in the slowly varying case the ocean can adjust to forcing in equilibrium with the wind whereas fast forcing will generate propagating wave fronts which can

very effectively advect warm water to the east. Philander and Pacanowski go on to show that the system can have a highly nonlinear response if the wind not only relaxes, but actually reverses and become westerly. This is due to meridional circulation which is set up by an Ekman flux of water toward the equator at the surface and a subsequent downwelling of water at the equator. Convergence at the surface must be balanced by a divergence away from the equator near the thermocline. Westerlies accelerate water at the surface towards the east while convergent flow contains eastward momentum at the equator. Easterlies, on the other hand, tend to advect westward zonal momentum from the South Equatorial Current away from the equator and bring up eastward momentum from the undercurrent which opposes surface forcing. The net result is a weaker South Equatorial Current than is predicted from purely linear considerations.

B. Model Description

The most complete model for examining oceanic response to episodic forcing is the GFDL ocean model as modified by Philander and Seigel (1985). The model was first built by Bryan and Cox (1967) and was modified extensively by Semtner (1974). A thorough discussion of model formulation and solution technique is found in a GFDL technical paper (Cox, 1984).

The tropical Pacific version of the model extends from 130°E to 70°W and from 30°S to 50°N, as shown in Fig. 4.1. In longitude the grid spacing is a constant 1°. Meridionally the grid is 1/3° of latitude equatorward of 10°; poleward of 10° latitude the grid expands as a cosine function. At the northern boundary at 50°N meridional grid spacing is 3°. The mesh was constructed to gain high resolution in the equatorial waveguide at expense of resolution in northern and southern latitudes. There are 27 levels in the vertical with 10 levels in the upper 100 meters. Below 100 m the vertical grid expands to fit the remaining 17 grid points in 3900 m. The model uses an "Arakawa B grid" (Arakawa, 1988), an example of which is shown in Fig. 4.2. The grid describes boxes, with horizontal components (u,v) calculated at corners and with temperature calculated at the center of each box. In the vertical, horizontal components of velocity and temperature are found at midpoints of boxes with vertical velocity found on the face of each box.

Boundary conditions are much the same as in linear theory. There is a flat bottom at 4000 m and a rigid-lid surface, so that the vertical component of velocity is zero at the bottom and at the surface. At the surface vertical shear is proportional to wind stress and at the bottom vertical shear is proportional to a bottom boundary friction term. Boundaries are solid walls, with horizontal components of velocity and the normal derivative of temperature set to zero. The Boussinesq approximation is made and the fluid is assumed hydrostatic. A polynomial expresses the density of seawater as a function of temperature, salinity and depth (Bryan and Cox, 1972).

Several parameterizations have been added to the GFDL ocean model (Philander and Seigel, 1985). Motions which occur at length scales smaller than the grid spacing are parameterized by assuming an eddy viscosity formulation. In the vertical, a Richardson number

mixing parameter has been incorporated (Pacanowski and Philander, 1981) as

$$\upsilon = \frac{50.}{(1 + 5\mathrm{Ri})^2} + 1. \tag{4.1}$$

for momentum, and

$$\kappa = \frac{\upsilon}{(1 + 5\mathrm{Ri})} + 0.1 \tag{4.2}$$

for mixing of heat. When density is statically unstable, mixing is assumed to be strong enough to completely mix the fluid within the two boxes in which instability existed. Otherwise, the mixing parameter can assume a value from 1 to 50 $cm^2\ sec^{-1}$. The mixing coefficient of momentum assumes a minimum value of 10 $cm^2\ sec^{-1}$ in the upper grid box. Horizontal friction is determined by a latitudinally dependent friction coefficient, which is a constant $2 \times 10^7\ cm^2\ sec^{-1}$ equatorward of 10° latitude and increases to $50 \times 10^7\ cm^2\ sec^{-1}$ at the northern boundary. These latitudinally dependent friction coefficients damp out basin modes that would otherwise dominate the numerical solution.

North of 30°N and south of 20°S model temperature and salinity fields include a Newtonian damping term $[\lambda(T-T_c)]$ to force them toward Levitus (1982) climatology (T_c). The time scale of this damping (λ) is half a day at zonal boundaries and decreases linearly to zero at 30°N and 20°S. The model driven with climatological monthly mean winds does not generate a realistic zonal temperature gradient (Harrison, personal communication) as compared with observations (Reynolds, 1982). Because the model lacks an active atmosphere, the possibility that warm sea surface temperatures reduce solar insolation by formation of cumulus clouds is not included. Therefore a parameterization of cloud formation by adjusting incoming heat flux is included. Incoming solar radiation is decreased linearly with temperature when the sea surface exceeds a temperature of 27°C. When SST is 30°C, incoming solar radiation is decreased by 22%.

Air temperature, used in the heat flux calculation, is prescribed by climatological conditions. There is no flux of water through the surface due to evaporation or precipitation. A minimum wind speed of 4.88 m sec^{-1} is introduced in the heat flux equation to simulate effects of short time scale winds which would be lost in monthly averages.

The model code has been designed to use monthly averaged wind stress as the atmospheric boundary condition (Philander and Seigel, 1985). For the purpose of modeling episodes of westerly wind stress, a separate subroutine was included in the model code. The subroutine is executed once per time step to calculate the wind anomaly from the wind burst. The wind anomaly is then added to background monthly wind values. The model is then run twice, once with anomaly and once without, to determine the effect of bursts on the model ocean.

The region of anomalous winds is indicated by a rectangle superimposed onto the model grid in Fig. 4.1. The wind patch has a Gaussian dependence in latitude with a width at half-maximum of 3°. In longitude the wind patch is a top-hat function, so that it assumes a value of one within the patch and is zero outside. In experiments described herein, the patch is 20° long, from 150°E to 170°E. The stationary patch has Gaussian structure in time, with a width at half-maximum of 10 days.

The wind burst experiments and some of their important characteristics are presented in Table 4.1. The first set of experiments are those in which the wind burst was imposed onto a horizontally uniform and quiescent ocean. Ocean temperature and salinity fields are initialized to a stable configuration and there are no background currents. Because there are also no background winds, there are no currents except those due to the wind anomaly. With these experiments, sensitivity to strength of the wind anomaly is examined. When the wind anomaly is weak, the model response should agree well with predictions of linear theory. Comparing the response for different wind strengths gives an indication of importance of nonlinear mechanisms in the model. It is also possible to alter initial temperature and salinity stratification, thereby determining sensitivity of the model to initial density structure.

The second set of experiments are those which were imposed onto more realistic background conditions. The model was initialized with observed temperature and salinity vertical structure from the Pacific ocean (Levitus, 1982). The model was integrated for three and a half years with climatological monthly mean winds before the wind burst was imposed onto background winds. These experiments are used to investigate interaction of the response from the wind burst with the equatorial undercurrent, shoaling thermocline and realistic horizontal temperature gradients.

C. Experiments on a Quiescent Background

Five experiments were conducted using quiescent background initial conditions; four have a density stratification as shown in Fig. 3.1. This stratification is an idealization of the eastern Pacific, with a shallow and sharp thermocline. The wind anomaly in these experiments range from very weak (0.2 dynes cm^{-2}) to very strong (5.0 dynes cm^{-2}). The fifth experiment is initialized with density stratification of the western Pacific, as in Fig. 3.4.

The model zonal velocity response 57 days after the peak of the 0.2 dynes cm^{-2} burst is shown in Fig. 4.3 as a function of longitude and depth. Evolution of standing vertical modes is quite evident. The first vertical mode, with greatest phase speed, has one zero crossing and is found at 90°W. Using the center of the patch as starting point for the pulse maximum, the model gives an average phase speed of 219 cm sec^{-1}. Comparison with the predicted phase speed of 218 cm sec^{-1} (Table 3.1) shows close agreement with linear theory. The first vertical mode has a maximum zonal velocity of 1.6 cm sec^{-1} at the surface, somewhat less than the 2.1 cm sec^{-1}

predicted by linear theory. Exact agreement is not assured, because the model is sampled once every 24 time steps, and there is no guarantee that the maximum is captured at any given snapshot. The meridional shape of the pulse is Gaussian, with a width scale of 329 kilometers. This can be compared with 307 kilometers expected from linear theory (Equation 3.18). Because the meridional grid resolution is 33 km, the two estimates agree to within resolution.

Following the first mode are second and higher vertical modes. The second vertical mode has a surface particle speed of about 4 cm sec^{-1}, in good agreement with linear theory. The third mode at 8.2 cm sec^{-1}, and the fourth mode at 9.7 cm sec^{-1}, are larger than linear predictions of 5.9 and 5.5 cm sec^{-1} respectively. Because slower pulses have longer length scales (see section 3), these modes tend to overlap more than the low vertical modes. The model amplitude of the fifth and sixth drop off more rapidly than predicted by linear theory.

When Kelvin waves encounter the coast of South America wave energy is partitioned into reflected wave energy and transmitted coastally trapped energy. The reflected part propagates westward as equatorially trapped Rossby waves. The transmitted part propagates poleward as coastally trapped Kelvin waves and is lost from the equatorial waveguide. Because horizontal friction increases rapidly as a function of latitude poleward of 10°, coastal Kelvin waves are quickly attenuated beyond 10° latitude. Vectors of zonal and meridional velocity due to the first vertical mode Kelvin wave are shown just prior to impact in Fig. 4.4a and just after impact in Fig. 4.4b. The inbound Kelvin wave gives rise to a narrow coastal pulse which propagates along the coast of South America. Because the coastal trapping scale decreases as the wave moves poleward, surface currents become both stronger and more narrowly constrained to the coast. The reflected wave shows structure consistent with a first meridional mode Rossby wave propagating westward. The reflected wave generates an upwelling coastal pulse which also propagates poleward. However the coastal wave is now an upwelling wave that, in contrast to the downwelling wave, will lead to cooling.

Two tenths of a dyne cm^{-2} is not a reasonably strong wind burst; actual wind bursts in the western Pacific tend to be about 2.0 dynes cm^{-2} (section 2). Burst experiment B24 was started with the same quiescent initial condition as above, however now the wind stress maximum is increased to 2.0 dynes cm^{-2}. Corresponding depth-longitude contours of zonal velocity are shown in Fig. 4.5. Although the general structure is the same, there are important differences between the two runs. There is still clear evidence of vertical modes, with lower modes traveling faster than higher modes. There is evidence, however, of nonlinear processes, especially in the evolution of the second baroclinic mode. In the strongly forced case, after 57 days the second mode is east of 120°W. In the weakly forced case the second mode is west of 120°W after 57 days (Fig. 4.3).

A time-series of surface velocity at 140°W is shown in Fig. 4.6 for the four different wind anomalies. The abscissa has been scaled according to maximum wind burst strength, so that if

linear theory governed wave evolution the four time series would be identical. Arrival of the second baroclinic mode wave is indicated on the ordinate by an arrow. The top panel shows response to the 0.2 dynes cm^{-2} case. Amplitude and phase speed of the first four baroclinic modes agrees well with linear theory. Note that the fourth baroclinic mode is the largest amplitude Kelvin pulse.

When the wind burst is 1.0 dyne cm^{-2} the first three vertical modes have greater amplitude relative to the weakly forced case. There are two reasons for larger relative amplitudes in the strongly forced case. There is a nonlinear interaction between wind forcing and fluid velocity underneath the wind patch. Since work done on the ocean is proportional to the dot product of wind stress and fluid velocity, the amount of work done increases as fluid speed underneath the wind patch increases. Work done on the ocean by the atmosphere increases by a factor of 30 when wind stress increases by a factor of 10. Additional work done goes into deepening the mixed layer, and this affects wave amplitude in two ways. First, the phase speed of each mode decreases and so T_n is larger. Second, the deeper thermocline changes vertical projections, increasing P_n for lower vertical modes at expense of higher vertical modes.

The fourth vertical mode is markedly less energetic than in the weakly forced case. Linear theory predicts that the phase speed of the second mode is 64 cm sec^{-1} and that surface zonal velocity is 40.5 cm sec^{-1}. This represents a Froude number of 0.63, indicating that nonlinear processes cannot be neglected.

Zonal velocity for the 2.0 dynes cm^{-2} case is shown in Fig. 4.6c. Again, the first two vertical modes have larger surface velocities relative to the weakly forced case. Now, however, it is the third vertical mode which has become supercritical. Linear theory predicts a surface velocity of 77 cm sec^{-1} and a phase speed of 83 cm sec^{-1} for the third mode. The second vertical mode indicates two other effects of nonlinear behavior. The first is an increase in phase speed of the wave; the second mode arrives at 140° almost two weeks earlier than in the weakly forced case. This implies a phase speed of 1.56 m sec^{-1}, a 25% increase over the weakly forced case. A phase speed increase of 15-20% above calculated linear phase speed has been observed in the tropical Pacific for first baroclinic mode Kelvin waves (Knox and Halpern, 1982; McPhaden *et al.*, 1986). This increase has been attributed either to Doppler shifting of waves by the mean flow, most notably by the equatorial undercurrent (McPhaden *et al.*, 1986), or from non-linear self advection of the pulse (Ripa, 1984). Since there is no mean flow in these experiments, the phase speed increase in the model must be attributed to a self-advection of the pulse.

Examination of vertical structure of the four peaks following the first vertical mode peak in the 2 dynes cm^{-2} case reveals that all have vertical structure consistent with a second vertical mode wave. The pattern is suggestive of a solitary wave train, similar to those described by Osborne and Burch (1980). The governing equation for a solitary wave train is the KdV equation given by

$$u_{ttt} + c_0 u_x + \alpha u u_x + \gamma u_{xxx} . \tag{4.3}$$

The crucial balance in the KdV equation that leads to evolution of solitons is between self-advection (third term) which tends to steepen the wave and dispersion (fourth term) which tends to broaden the wave. When these two terms are of comparable magnitude and opposite sign, their effects cancel, and waves can propagate without change over large distances (Osborne and Burch, 1980). The Kelvin wave is non-dispersive however, and presumably cannot form solitons (Boyd, 1980). However, presence of shear can provide dispersion which thus allows Kelvin solitons to form (Boyd, 1984). Again, in this particular experiment there are no background currents, so dispersion could not come from a mean flow. However the second mode propagates in the presence of the first mode over a distance of at least 40° of longitude. It is possible that shear from the first mode provides the dispersive term to allow the second mode to form Kelvin solitons which then propagate to the coast of South America as individual solitary waves.

By knowing the number of solitary waves in the packet, the decrease of amplitude and increase of phase speed relative to linear theory of each soliton can be determined (Osborne and Burch, 1980). Examination of Fig. 4.6c indicates that there are six solitons in the wave packet. The amplitude decrease as a function of soliton number is

$$A_n = \frac{\lceil N\text{-}n \rceil^2}{\lfloor N\text{-}1 \rfloor} \tag{4.4}$$

where N is the total number of solitons in the wave packet. A corresponding increase in phase speed is given by

$$c = c_0 + \frac{u_0 A_n}{2} \tag{4.5}$$

where c_0 is the linear wave speed, A is the non-dimensional amplitude coefficient and u_0 is the particle speed of the Kelvin pulse. Because the phase speed of a soliton is proportional to amplitude, solitons are ordered according to their amplitudes. Fig. 4.6c shows that the amplitude of the fastest Kelvin pulse is largest, with solitons of lesser amplitude following. Equation 4.5 predicts that maximum sub-critical phase speed increase is 50%.

Using Equations 4.4 and 4.5, the predicted time series of Kelvin solitons at 110°W is calculated for a packet of six solitons. This time series is shown in Fig. 4.7a as a solid line. Also shown is a time series of model surface zonal velocity at 110°W as a dashed line. The amplitude of the waves have been normalized to the amplitude of the first Kelvin pulse. Note in this figure that Kelvin pulses are rank-ordered, in the sense that the first Kelvin pulse has greatest amplitude

and largest phase speed. Subsequent pulses have smaller amplitudes and slower phase speeds. There is remarkable agreement in amplitude and timing of predicted and modeled time series.

Spatial structure of the first Kelvin pulse can also be compared with the expected hyperbolic secant squared form (Osborne and Burch, 1980). Using a length scale of 220 kilometers, predicted zonal velocity amplitude is shown in Fig. 4.7b. Again, velocity of the model response is shown as a dashed line, normalized to a value of unity at its maximum.

Higher vertical modes (three and above) are quite effectively damped in the strongly forced case. Because of Richardson-number dependent mixing in the model, vertical mixing is large when vertical shear is large. Higher vertical modes have vertical structure near the surface, and therefore are more strongly mixed. Also, because higher vertical modes have slower phase speeds they will tend to be close to each other near the forcing region. Since vertical mixing is proportional to total velocity of the fluid, summation of these high vertical modes will create a shear which will tend to dissipate them.

Because episodes of westerly wind are most often found in the western Pacific, where the thermocline is both deep and broad, a model experiment was run using density initial conditions of the western Pacific. Temperature and salinity structure from 160°E were taken from the model in climatological May. The model was then initialized, again with no currents, with the density structure presented in Fig. 3.7. For comparison with model results, predictions of linear theory are listed in Table 3.2.

Zonal velocity from the 2.0 dynes cm^{-2} wind burst is shown in Fig. 4.8, from the date line to the coast of South America. In agreement with linear theory, the first baroclinic mode has largest amplitude at 20-30 cm sec^{-1}. The second baroclinic mode also has a significant amplitude of 15-20 cm sec^{-1}. The third and higher baroclinic modes are attenuated as they propagate eastward. By the time any of these modes propagate to 140°W their amplitude has been reduced to insignificant levels.

D. Experiments on a Climatological Background

The second set of experiments was to impose the burst onto the model ocean which includes full climatological background velocity and temperature fields. Added complexities involve a sloping thermocline and a strong thermocline. Because of asymmetries in the wind field there are differences between the two hemispheres. There are also seasonally strong 30-day waves and strong upwelling along the equator. The burst was centered on 15 May on top of the EDIT2 climatological wind field. Sea surface temperatures (SST) of the climatological run are shown in Fig. 4.9. For comparison observed temperature fields (Reynolds, 1982) are shown in Fig. 4.10. The model background is too warm in the far Western Pacific, 30°C, as compared with 29°C in Reynolds' climatology. In the Eastern Pacific the model background is too cool, 23°C, as compared with 25°C in climatology. As a result, the cross-equatorial temperature

gradient is too large by 3° over 100° of longitude. The cold tongue which extends up the coast of South America is 20°C adjacent to the coast, whereas in climatology the minimum temperature is 18-19°C at 10°S. The longitudinal temperature gradient in the model cold tongue is quite realistic; this is important if longitudinal advection of warm water is the primary source of heating along the South American coast.

The vertical structure of temperature and zonal currents of the model climatology is shown in Fig. 4.11. The temperature shows characteristic shoaling of the thermocline to the east. The thermocline in the western Pacific is characteristically deep, although much more diffuse than that observed. The equatorial undercurrent is similarly more diffuse in the model simulation than that observed. Zonal currents shown in Fig. 4.11b indicate an undercurrent maxima between 160° and 120°W of greater than 110 cm sec^{-1} at a depth of 75 to 125 meters.

Figure 4.12 presents anomalous equatorial surface zonal and meridional velocity components resulting from the westerly episode; results are shown east of the date line and between 15 April and 15 October 1986. To facilitate identification of the forced response, first and second baroclinic mode Kelvin wave speeds (derived from linear theory for model central Pacific conditions) are used to construct first and second mode characteristics, which are superimposed on Fig. 4.12. Note that the zonal velocity signal in the first and second modes are roughly comparable (about 20 cm sec^{-1}), but that the first mode signal decreases east of about 110°W. The second mode signal remains strong right up to the model South American coast. The SST (sea surface temperature) anomaly, shown in Fig. 4.13, begins as a result of anomalous zonal advection of warm water, as expected.

Zonal and meridional components of surface velocity at the equator at 110°W are shown in Fig. 4.14, to illustrate the magnitude of the phenomenon at a particular location. Subsequent to passage of the second mode Kelvin pulse, zonal velocity decreases to about 20 cm sec^{-1} below climatological values, and then returns to a state similar to climatology. In meridional velocity there are both phase shifts and amplitude changes of instability waves. Kelvin pulses result in induced meridional velocity changes of as much as 10 cm sec^{-1} in late July and early August, but return toward climatology is clear in September. Reflected Rossby waves do not contribute substantially to the cooling process; the first vertical mode Rossby pulse arrives in the region of cooling well after cooling has begun.

Surface heat budget analyses show warming begins due to zonal advection. During the period when the sea surface temperature anomaly rises from about 0.4°C to 1.0°C, meridional advection becomes as important as zonal advection. Sea surface temperature changes resulting from meridional advection deserve comment, because only zonal velocity changes are associated with linear Kelvin waves. Most of the year there are energetic instability waves present along the equator in the eastern Pacific, that result from complex vertical and horizontal shear field of local current systems (North Equatorial Counter Current, South Equatorial Current and Equatorial

Undercurrent). Any perturbation of the shear field presumably alters the strength of the instability and characteristics of resulting instability waves. Also unexpected is cooling that immediately follows warming. Cooling is affected both by meridional and zonal advection of heat, as shown in Fig. 4.15. It is important to note that while there was non-trivial transient warming and cooling, no significant net temperature changes occurred as a result of the warming/cooling event. Note also that the forced SST response depends very much on location along the equator; near the center of the cold tongue (110°W to 120°W in the model) there can be no anomalous zonal advection.

After passage of the first two vertical modes, anomalous zonal flow becomes strongly negative. Because the background zonal temperature gradient is negative throughout most of the central Pacific this leads to cooling along the equatorial waveguide. Unexpected negative anomalies arise from upwelling caused by the usually strong tradewinds found near the equator. Because the first and second vertical modes have their first zero crossings fairly deep (1500 and 500 m respectively), upwelling has only a small effect on vertical structure. However, higher order vertical modes have zero crossings near the surface, often above the thermocline. It is then possible that upwelling could entrain enough water to bring the zero crossing to the surface. In this case the sign of the velocity anomaly would change, and instead of having anomalous warming there is anomalous cooling. Because the strength of high vertical modes is weak by the time they have propagated to the central Pacific this tends to be a small effect.

The temperature anomaly at the coast of South America at 5°S is presented in Fig. 4.16. Arrival of the first and second mode Kelvin pulses at the coast is shown by arrows. Also shown is the time of the wind burst in mid-May. There is no heating until arrival of the first vertical mode when temperature rises to nearly 0.5°C above climatology in late June. The temperature then rebounds to 0.5°C below climatology when the upwelling Kelvin wave, which has been forced by the reflected equatorial Rossby wave, passes. In early August the second vertical mode Kelvin pulse encounters the coast of South America. It also sends downwelling, as well as upwelling, coastally trapped Kelvin waves. Because the second vertical mode had more energy when it encountered the coast of South America, resulting coastally trapped Kelvin waves have correspondingly more energy. In mid to late August there is a sharp temperature increase, followed by an equally rapid return to climatological values. In late September there is another rapid heating, the anomaly reaching 2°C, again followed by a very rapid drop to below climatology. The experiment stopped on 15 October, when temperatures were slightly below climatological values.

Heating at 5°S associated with the Kelvin pulses is predominantly that due to the alongshore advection of heat. Vertical advection of heat, those changes associated with deepening of the thermocline, are small. Depressing the thermocline does not by itself heat the surface;

it is only through suppression of upwelling that the surface can warm. This is a small effect in the model warming.

Analysis of the May wind burst indicates that peak westerly wind speeds were 12 m sec^{-1} (see section 2). This corresponds to a wind stress anomaly of nearly 4 dynes cm^{-2}. In the interest of modeling this May wind event, an experiment was performed using a wind anomaly of 4 dynes cm^{-2}. Zonal and meridional velocities at 110°W in this experiment are presented in Fig. 4.17. Also shown in this figure are results from the 2 dynes cm^{-2} case and results from the climatological run. The zonal velocity anomaly is generally what is expected from a linear increase in forcing by a factor of two. The first vertical mode anomaly is about 40 cm sec^{-1}, nearly twice the anomaly of the more weakly forced case. The second baroclinic mode is larger than twice the weaker anomaly, but this could be in part due to a more pronounced overlapping of modes in the more strongly forced case. There are differences in the phase speeds of the strongly and weakly forced cases. The peak of the second baroclinic mode arrives at 110°W, about six days before the peak of the weakly forced second mode. This represents a 10% increase in phase speed. The phase speed increase for the first baroclinic mode is not as pronounced. This is expected because self advection scales inversely proportional with phase speed. Higher modes experience larger phase speed modification because of larger nonlinear self-advection.

Modification of instability wave energy is again considerable in the strongly forced case. Timing of the amplification depends, however, on pre-existing instability wave patterns. Note that for both strong and weak cases, timing of the amplification due to the first mode is nearly simultaneous. The second baroclinic mode arrives too early to be synchronized with the second instability wave pulse. The first instability wave has a secondary maxima, and the resulting instability wave field is forced 180° out of phase with climatology.

Wind anomalies during May 1986 consisted of two parts; a stationary wind anomaly in the western Pacific and a propagating anomaly which crossed the entire Pacific in about 15 days (section 2). Linear theory predicts that a propagating feature can alter the Kelvin pulse response in two ways. When the forcing region propagates, integration along characteristics must take into account the speed of translation of forcing. In the special case where the forcing region propagates at the same speed as a Kelvin mode a resonance occurs between forcing and the Kelvin pulse, such that the pulse experiences constant forcing. The second way that propagating forcing alters the ocean response is that the wind anomaly continuously generates waves as it propagates, leaving a train of Kelvin pulses in its wake.

To examine changes brought about by including a propagating anomaly, the model was run with both the 4 dynes cm^{-2} stationary anomaly as above and the propagating anomaly described in section 2. The patch propagates at a speed of 10 m sec^{-1} from the region of the stationary patch to the coast of South America. The surface zonal velocity anomaly is shown in Fig. 4.18

as a function of time and longitude. Evolution of the second baroclinic mode is similar to that of the stationary wind patch experiment (B31). The first baroclinic mode has a 10-20% increase in magnitude of surface zonal currents. Also evident in the propagating wind patch experiment is a rapid local acceleration of surface currents as the patch moves across the basin. The temperature anomaly at 5°S, 81.5°W for the propagating wind patch experiment is presented in Fig. 4.19. Note that warming from late July onwards is virtually the same for experiments with and without the propagating wind patch. However, warming that starts in mid-June is much greater in the propagating patch experiment.

Models currently being used to study inter-annual variability in the tropical Pacific are driven with monthly averaged wind stress (Busalacchi and O'Brien, 1981; Philander and Seigel, 1985; Harrison *et al.*, 1988). In section 2 we found, however, that much wind variability in the western Pacific is contained in a band from 3 to 15 days. Linear theory predicts that the month-averaged burst excites a train of Kelvin pulses of less amplitude than the ten-day burst, but of much longer duration. Vertical modes do not have sufficient time to separate from one another before they encounter the coast of South America. Thus, identification of individual modes may be difficult.

Experiment B29 includes the ten-day burst as though it had been incorporated into the monthly mean wind field. The meridional and zonal structure of the patch remains the same. The magnitude of the wind stress anomaly is approximately 1/3 of the ten-day burst, so that the time integral of wind stress remained constant.

The temperature anomaly at the coast of South America is shown in Fig. 4.20 for the month-long burst experiment. For the purposes of comparison, the temperature anomaly from the ten-day experiment (B16) is plotted as a dashed line. Response to the ten-day has greater amplitude and is characterized by higher frequency variability than for the month-averaged wind burst. The peak temperature anomaly from the ten-day burst is 1°C warmer than the peak temperature anomaly resulting from the month-averaged burst. Although details of the two responses are different, response to the slow burst is approximately the same as the month-averaged response of the fast burst. This indicates that, away from the forcing region, the model tropical Pacific behaves linearly.

For the purposes of modeling long term sea surface temperature changes, using a month-averaged wind burst is certainly adequate. A month-averaged burst does not capture details of westerly wind bursts, which have much shorter time scales. Because the month-averaged burst does not reproduce the magnitude of the temperature anomaly, processes sensitive to SST, such as atmospheric convection, may not be captured by the month-averaged burst.

E. Comparison with Data

Current meters and thermistor chains at 140°W and 110°W provide the first detailed observations of oceanic changes subsequent to a strong wind burst. The data have been discussed by McPhaden *et al.* (1988) who concluded that the wind event had little effect on the equatorial waveguide and therefore was not causative of the 1986-87 ENSO. The observed Kelvin pulse at 110°W had surface zonal currents of about 10 cm sec^{-1} over a period of about 3 days. This is smaller than both the Kelvin response predicted by linear theory and the Kelvin pulses in the ocean general circulation model. Because the wind burst was strong according to the index of Sadler and Kilonsky (1983), the May wind burst is a crucial test of linear theory as well as model results. An independent, and somewhat different, evaluation of the current data is provided here.

Zonal winds at 165°E and zonal currents at 140°W and 110°W are presented in Fig. 4.21. The time series are separated by an amount proportional to their longitudinal separation. The zonal wind anomaly lasts for at least ten days, with peak westerlies of almost 10 m sec^{-1}. Because normal tradewinds are easterly, westerlies represent anomalies of 12 to 15 m sec^{-1}.

Linear theory, as discussed in section 3, indicates that a westerly episode of wind lasting at least ten days and with maximum wind stress of 3 dynes cm^{-2} will force a first baroclinic Kelvin pulse with a zonal current anomaly of 50 cm sec^{-1}. Duration of the pulse will depend on the width and the phase speed of the Kelvin pulse; however, the Kelvin pulse cannot be of shorter duration than the wind pulse itself. Using stratification characteristic of the western Pacific, the second baroclinic mode should also have comparable significant zonal currents (Table 3.2).

As Kelvin pulses propagate eastward away from the forcing region the phase speed of each pulse should decrease because of changing background stratification. The first mode Kelvin wave speed is 2.91 m sec^{-1} in the western Pacific (Cane, 1984), 2.46 m sec^{-1} in the central Pacific (Rothstein, 1984) and 2.10 m sec^{-1} in the eastern Pacific (Hayes and Halpern, 1984). Using these estimates, an average speed of 2.75 m sec^{-1} is used from the forcing region to 140°W and a speed of 2.25 m sec^{-1} is used from 140°W to 110°W. For the second baroclinic mode the phase speed is taken to be 60% of the first mode wave, which is consistent for density stratifications in Tables 3.1 and 3.2. Wave characteristics with these speeds have been drawn in Fig. 4.21, at the beginning and the end of the wind anomaly. Again, wave characteristics denote the minimum time period during which oceanic perturbations are expected.

At 140°W zonal currents rise rapidly in late May and remain as strong eastward currents until mid June. A rise in speed from 50 to 100 cm sec^{-1} is consistent with the 50 cm sec^{-1} anomaly expected from linear theory. It is also in agreement with the 40 cm sec^{-1} anomaly found in the strong May wind burst experiment (Fig. 4.17). Careful examination of Fig. 4.21 indicates that the zonal velocity anomaly begins before the expected arrival of the first baroclinic Kelvin pulse. Recall that there was a relaxation of the trades in late May at 140°W (Fig. 2.10),

possibly as part of an equatorially trapped, eastward propagating atmospheric anomaly. Such a wind anomaly causes a local acceleration of water, and thus confuses timing of the onset of the remotely forced signal. The current anomaly at 140°W lasts for over 30 days: too long in duration for the first mode alone. Note however, that at 140°W wave characteristics of the first and second baroclinic modes have barely separated. The data are consistent with the interpretation of having both first and second baroclinic modes which overlap at 140°W.

Zonal currents at 110°W also experience rapid changes following the May wind burst. The first increase in zonal velocity occurs in mid-June, consistent with arrival of the first baroclinic wave propagating at 2.25 m sec^{-1} from 140°W. Duration of the pulse is over ten days, expected from a single first vertical mode. A second increase in zonal current occurs in mid-July, consistent with arrival of the second baroclinic mode wave. The velocity perturbation of the second pulse is much larger than the expected 50 cm sec^{-1}. As noted above, an increase in importance of the second mode has been noted in observations of changes in thermal structure in the eastern Pacific (Gill, 1982) as well as in numerical experiments described above and in Harrison and Giese (1988).

Meridional velocity at 110°W experiences a sudden relaxation from 50 cm sec^{-1} southward flow to near zero flow coincident with an increase in zonal flow (McPhaden *et al.*, 1988). Because the magnitude of meridional changes are of the same order as zonal changes, and meridional temperature gradients are stronger than zonal temperature gradients, changes in meridional flow will likely be important in the thermodynamic balance of the equatorial waveguide. In both experiments using realistic background fields, amplification of existing instability wave field was found to induce meridional anomalies of up to 20 cm sec^{-1} (Fig. 4.14b). In the 2 dynes cm^{-2} May wind experiment, these meridional anomalies occurred simultaneously with zonal anomalies.

A potentially important surface warming mechanism expected east of a westerly forcing event is anomalous zonal advection of heat (Schopf and Harrison, 1983; Harrison and Schopf, 1984). Equation 3.24 gives an expression for estimating the temperature anomaly expected from a single pulse of zonal velocity. Using observed zonal velocity anomalies and a zonal temperature gradient of -6.7×10^{-9} °C cm^{-1} (1.5 °C in 20° of longitude), the pulse at 140°W gives a temperature anomaly of about 0.6 °C.

At 140°W the sea surface temperature increased from about 26.2°C in mid-May to about 26.8°C in mid-June. An anomalous zonal current of 50 cm sec^{-1} acting on a zonal surface temperature gradient of about -6.7×10^{-9} °C cm^{-1} for 20 days would warm about 0.6°C, so that warming is consistent with anomalous zonal advection.

At 110°W surface temperature increased from about 24.3°C on 10 June to about 25.3°C on 18 June. Estimating the zonal SST gradient at 110°W is not so easy as at 140°W, because 110°W can be near the center of the equatorial cold tongue and there are large month-to-month gradient

changes in this region. But a zonal current anomaly of 70 cm sec^{-1} working against a zonal surface temperature gradient of 1×10^{-8} °C cm^{-1} for ten days would cause warming of 0.7°C, which is similar to that observed. We cannot say from available data what the zonal SST gradient was at 110°W, so this is a very imprecise estimate, but it does establish that the SST change was of the correct sign, at the correct time and of roughly correct amplitude for remotely forced zonal anomalous advection to be acting.

There was also a period of warming in the third week of July, from about 23°C on 15 July to about 25°C on 20 July. Anomalous zonal advection cannot account for this warming; McPhaden *et al.* (1988) indicate that meridional advection was acting to warm at this time. Although timing of the zonal current pulse is correct for remote forcing, the substantial pulse of meridional flow suggests that eastern Pacific instability waves may have been reappearing. Interestingly, in the numerical study reported by Harrison and Giese (1988) passage of the first mode pulse appears to modulate reappearance of the model instability waves in a way similar to that observed here.

The May 1986 wind burst was a strong event, from which linear theory and model experiments predict a substantial remote oceanic response. In the model experiments, changes induced by Kelvin pulses are as large as the Kelvin pulses themselves. This tends to confuse and obscure the Kelvin signal. Similarly, the data are difficult to interpret because of large changes in zonal and meridional velocity which are not directly associated with Kelvin pulses. Furthermore, because of changes in local winds, the remote signal can become confused with locally forced oceanic changes. At two mooring sites at 140°W and 110°W, observed upper ocean current and sea surface temperature response is consistent with passage of first and second baroclinic mode Kelvin pulses. The amplitude and duration of Kelvin pulses are consistent with values expected from linear theory as well as from numerical experiments described above.

Observations of sea surface temperature are made five days a week at Paita (81.5°W, 5°S). These observations are presented in Fig. 4.22 from May through September 1988. Where values are missing the line has been connected by linear interpolation indicated by a dashed line. Monthly mean temperature is shown by a broken line. There is a sharp rise from 16 to 19°C in the first week of July, consistent with arrival of the first baroclinic Kelvin wave.

This first pulse of warming lasts about 20 days, consistent with the duration of the Kelvin pulse at 110°W. The first pulse is followed by a second pulse of warming which starts in late July and lasts through mid-August. The second pulse is comparable in magnitude (2-3°C) and duration to the first pulse. When the two pulses are considered together, there is a period of over a month and a half of anomalous warming.

This alternative interpretation of available data presented above is consistent with both predictions of simple linear theory and results from an ocean general circulation model. The warm anomaly at the coast of South America is particularly encouraging. Along the equatorial

waveguide, where the zonal temperature gradient is much weaker, agreement is not as clear. Unfortunately, there is not enough data available to confirm, or rule out either the interpretation presented here, or the one presented by McPhaden *et al.* (1988).

TABLE 4.1 The experiments discussed in the report. The wind burst anomaly is given in dynes cm^{-2}.

		Anomaly	Description
Quiescent Background			
B24	linear	0.2	No motion, exponentially decreasing N profile
B20	non-linear	2.0	Same
B27	intermediate	1.0	Same
B30	strong	5.0	Same
B32	non-linear	2.0	N profile from 160°E of climatology (G22)
Climatological Background (EDIT2 Winds)			
B16	May 15	2.0	One burst centered on 15 May
B29	Month burst	0.66	The 2.0 dyne burst is averaged over one month
B31	May 15	4.0	As in B16 with a 4 dyne burst
B33	Prop. Patch	0.25	As in B31, plus a patch of westerly wind stress propagating at 10 m sec^{-1}

TABLE 4.2 A comparison between the predicted amplitude and phase speed of a solitary wave train and the amplitude and phase speed of the second baroclinic waves in the model. The model wave amplitudes have been normalized to the amplitude of the first wave in the packet.

Soliton	THEORY		MODEL	
	Amplitude	Speed cm sec^{-1}	Amplitude	Speed cm sec^{-1}
1	1.00	203	1.00	183
2	0.64	174	0.66	167
3	0.36	151	0.24	156
4	0.11	135	0.18	144

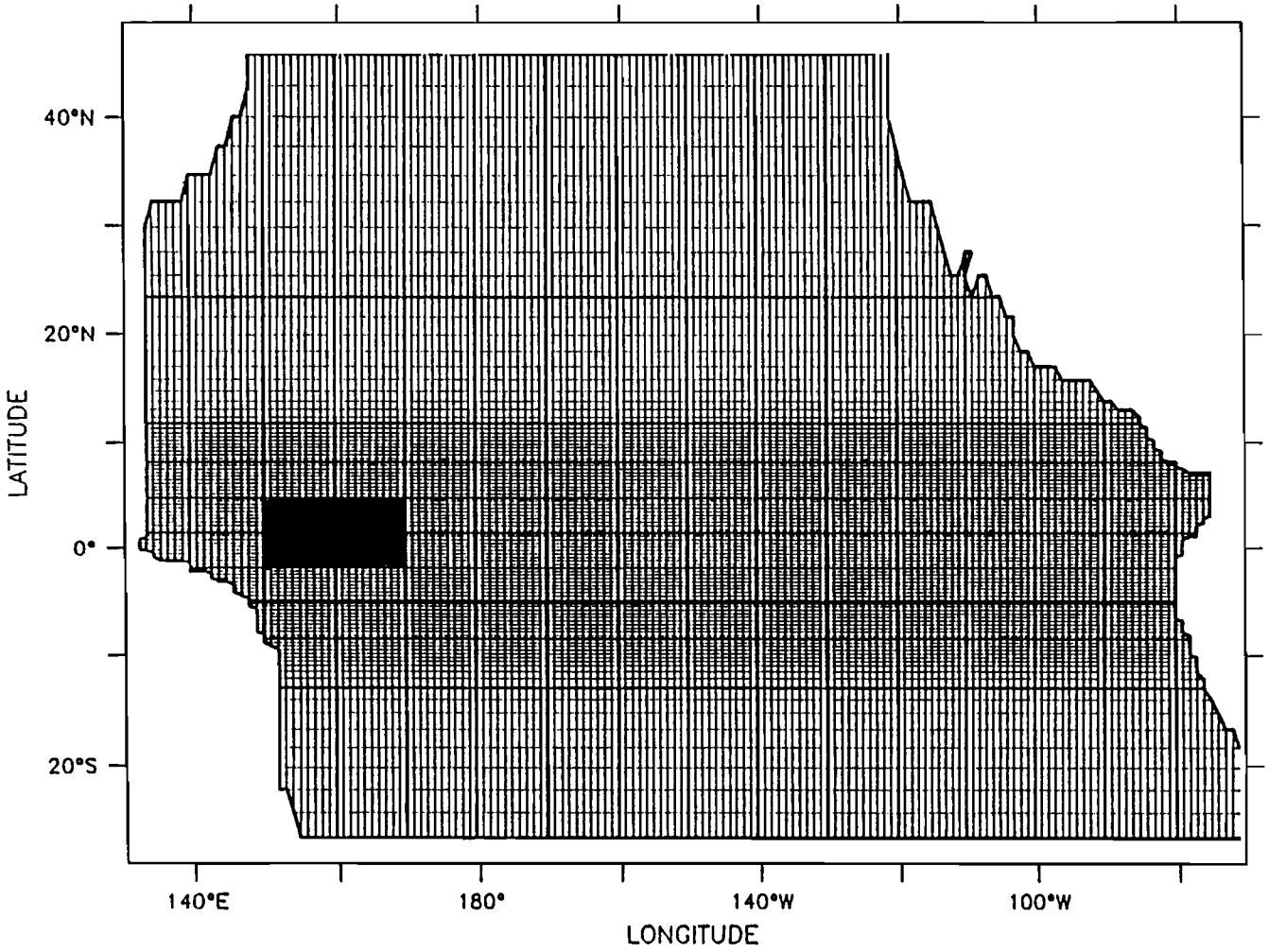

Figure 4.1. The model grid for the tropical Pacific general circulation model. In longitude the spacing is a constant 1°, in latitude the spacing is more fine within the equatorial waveguide. Bold lines indicate every 10^{th} grid point. There are 27 levels in the model. The darkened rectangle shows the region of anomalous forcing.

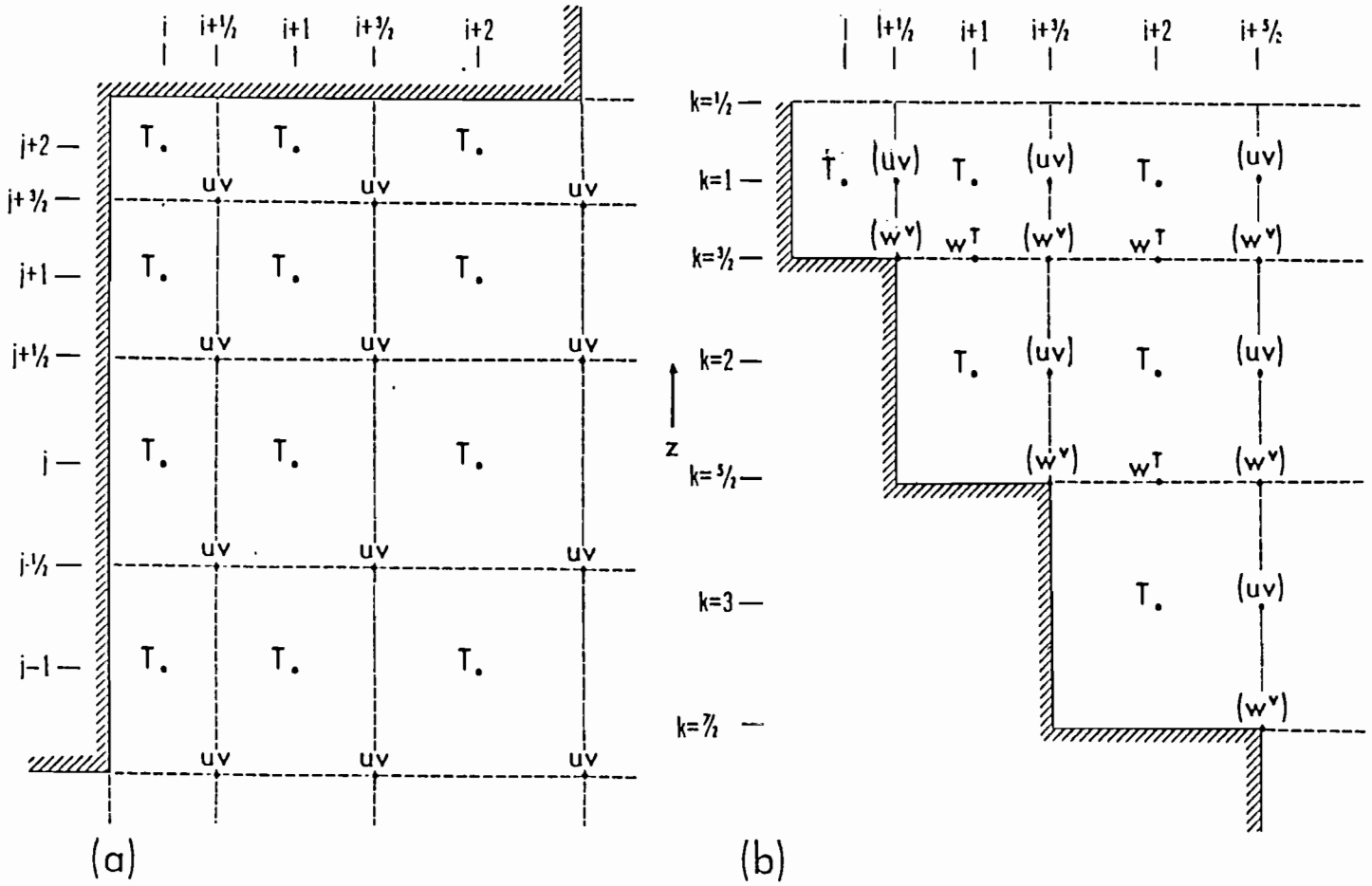

Figure 4.2. The placement of variables in the Arakawa B grid as used by the GFDL ocean model. In the horizontal (a), velocity components are at the corner of boxes and temperature is calculated at the center of the box. In the vertical (b), velocity is at the center of each face and temperature is again at the center of each box.

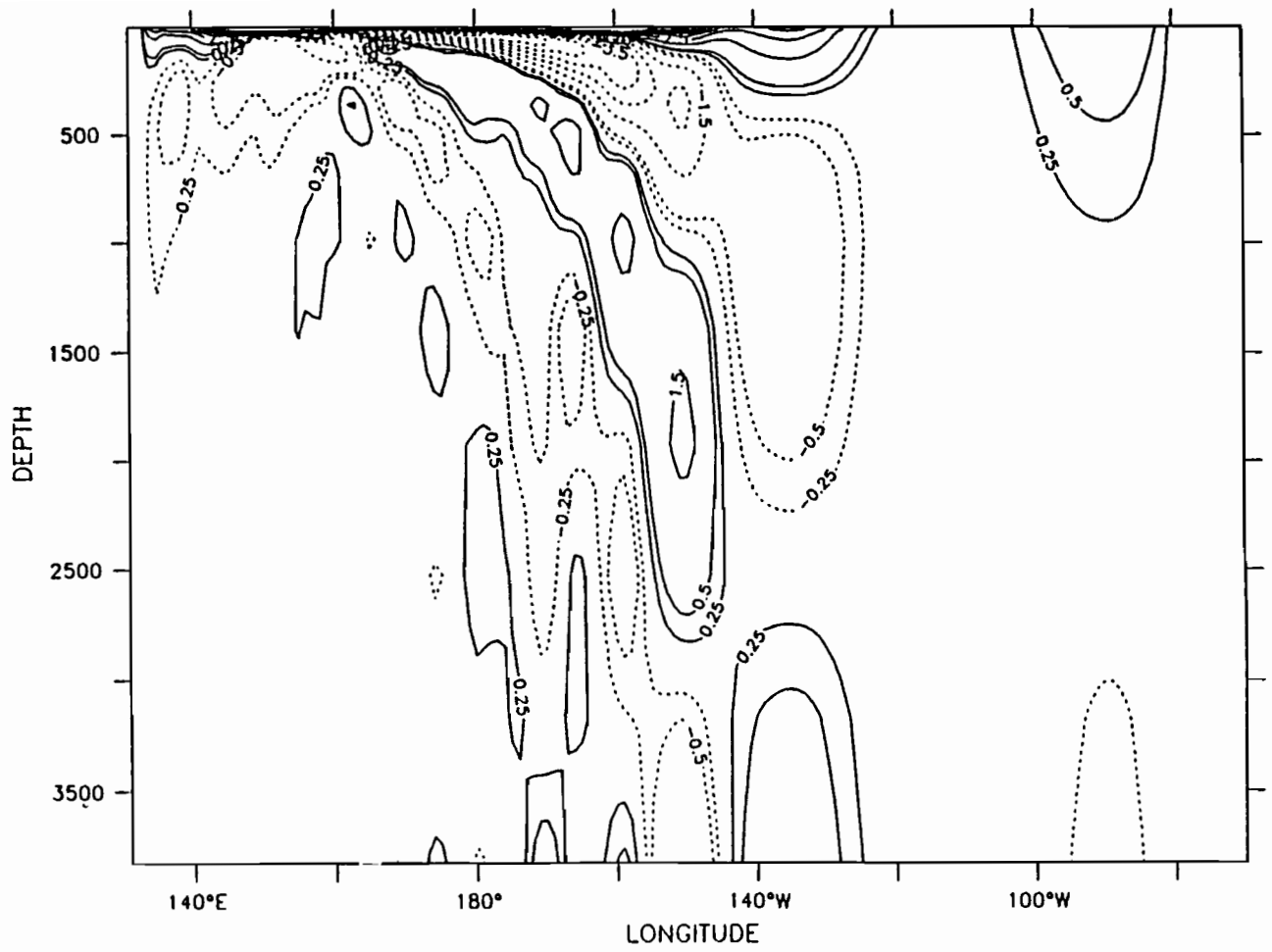

Figure 4.3. Zonal velocity 57 days after the peak of the weak (0.2 dynes cm^{-2}) wind burst. The contour interval is 0.5 cm sec^{-1} from -0.25 to 0.25 cm sec^{-1} and the contour interval is 1.0 cm sec^{-1} between -9.5 and 9.5 cm sec^{-1}. The forcing region is between 150°E and 170°E.

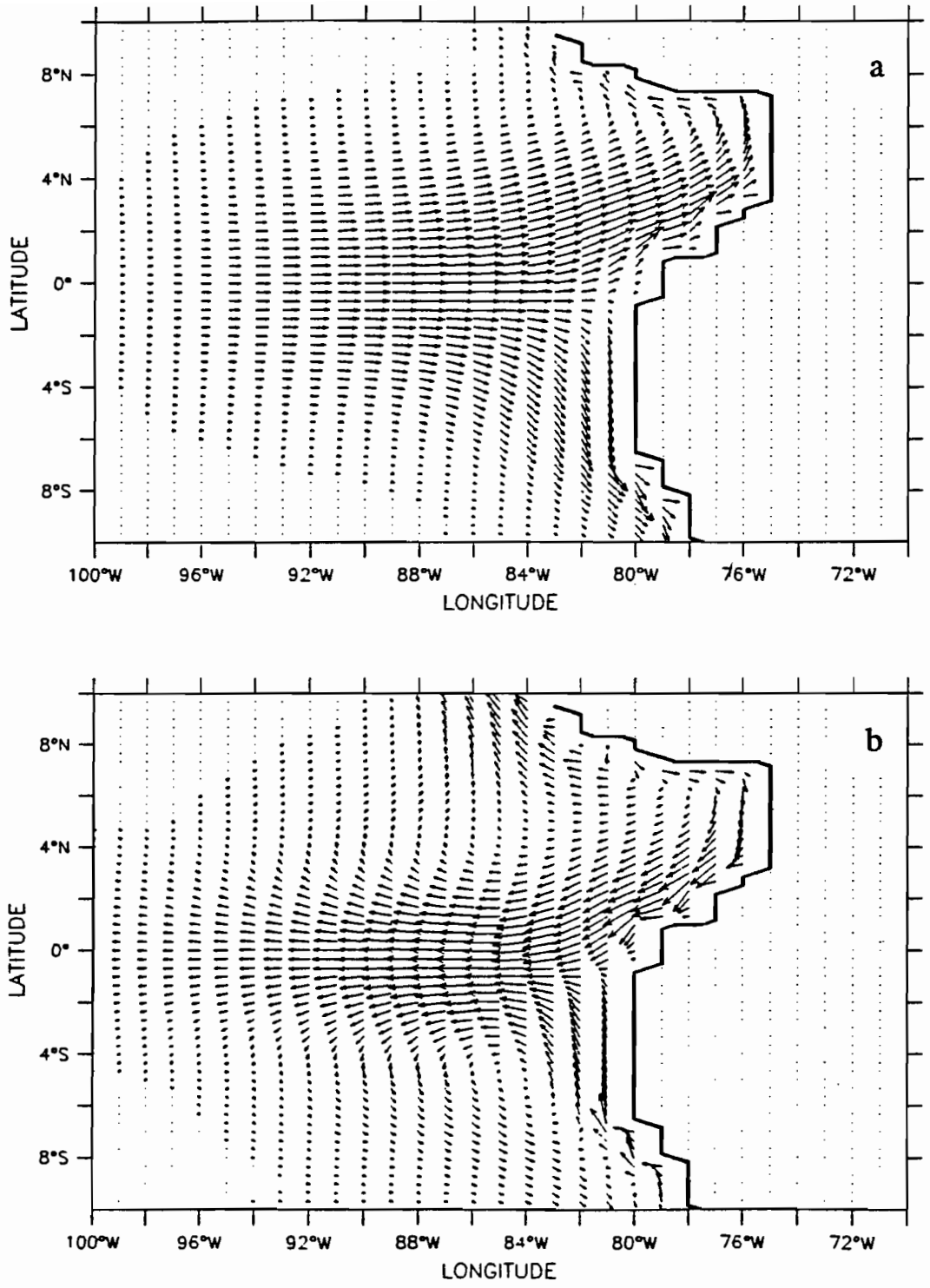

Figure 4.4 Surface current vectors associated with the first baroclinic mode Kelvin pulse (top) just prior to impact and (bottom) just after reflection from the coast of South America. A scale vector is shown in the lower left hand corner.

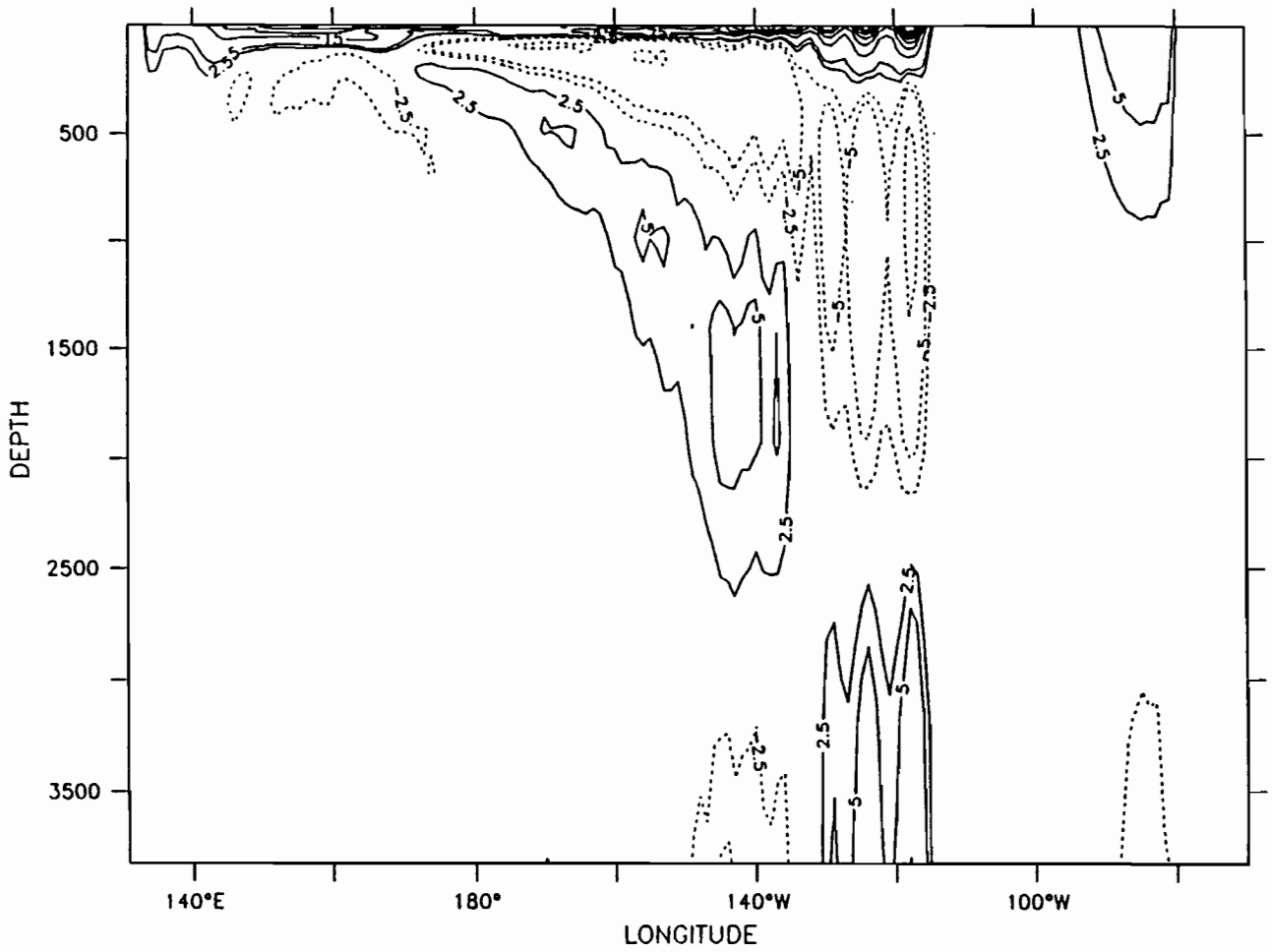

Figure 4.5. Zonal velocity 57 days after the peak of the strong (2.0 dynes cm^{-2}) wind burst. The contour interval is 5 cm sec^{-1} from -2.5 to 2.5 cm sec^{-1} and the contour interval is 10 cm sec^{-1} between -95 and 95 cm sec^{-1}.

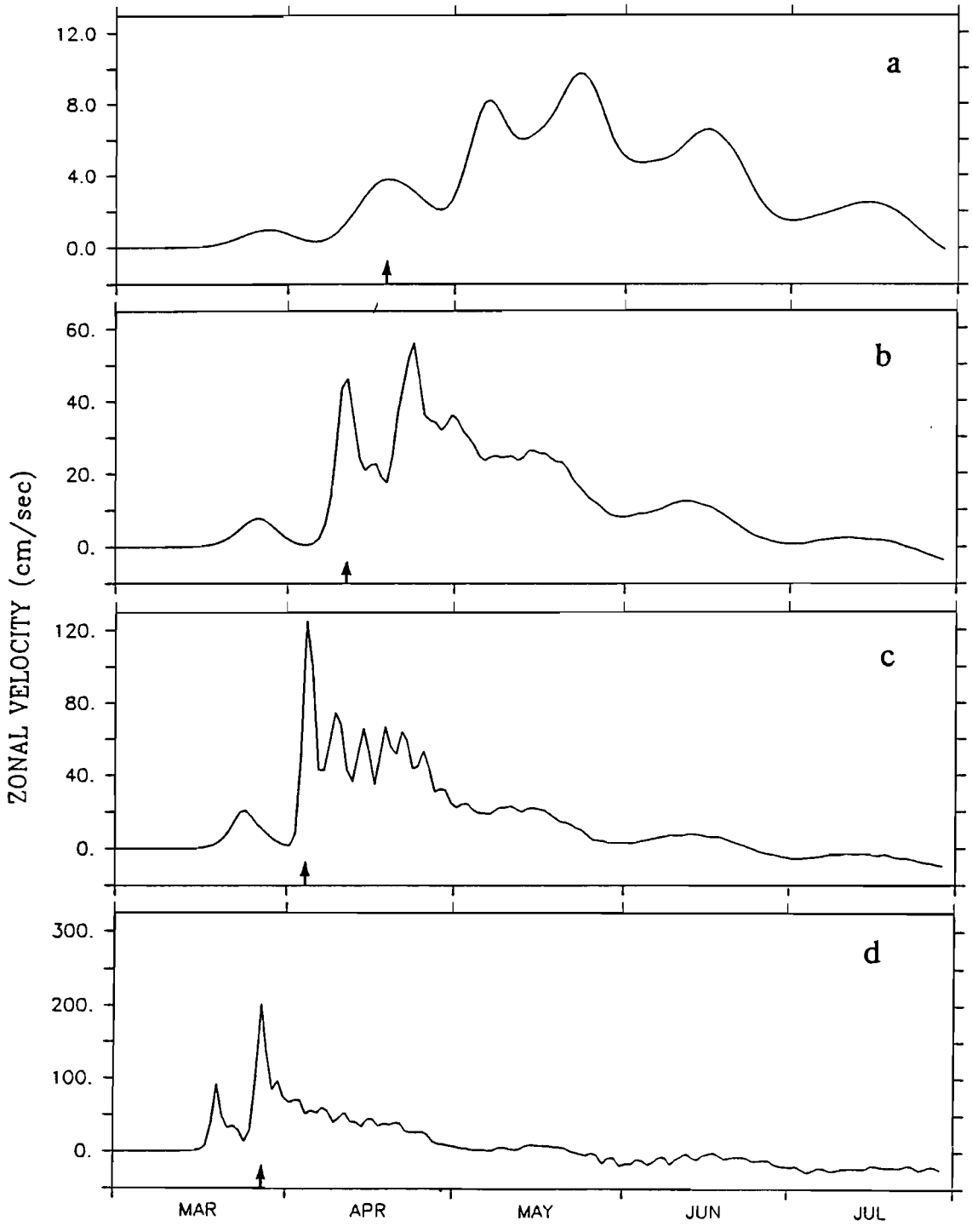

Figure 4.6 Surface zonal current at 110°W for experiments (a) B24, (b) B27, (c) B20 and (d) B30. The second baroclinic mode is indicated by an arrow on the axes. The vertical axes are scaled proportional to the magnitude of the wind burst.

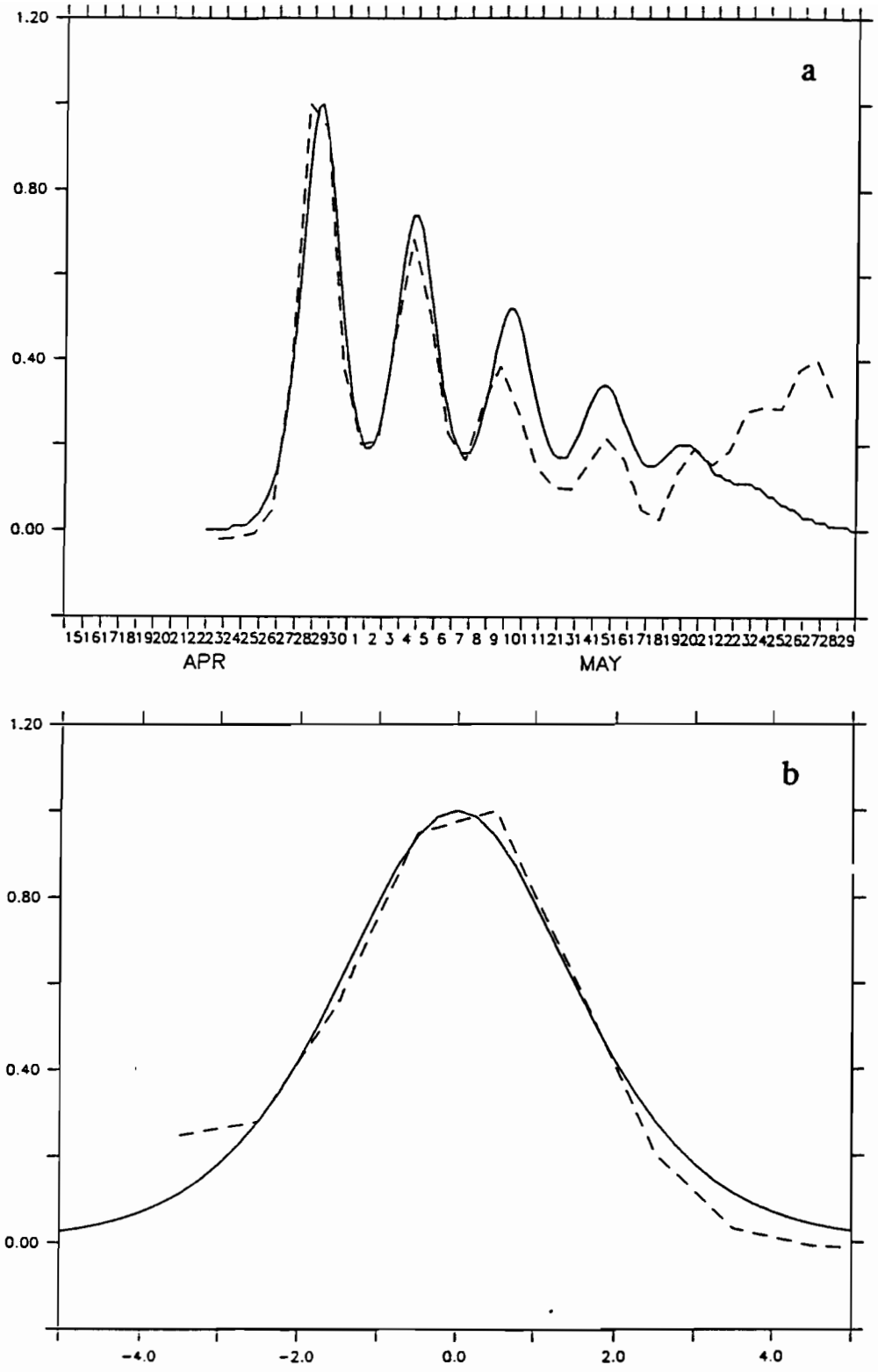

Figure 4.7 (Top) The predicted (solid line) and modelled (dashed line) evolution of solitons at 110°W. (Bottom) The predicted (solid line) and modelled (dashed line) longitudinal structure of the first soliton in Figure 4.7a.

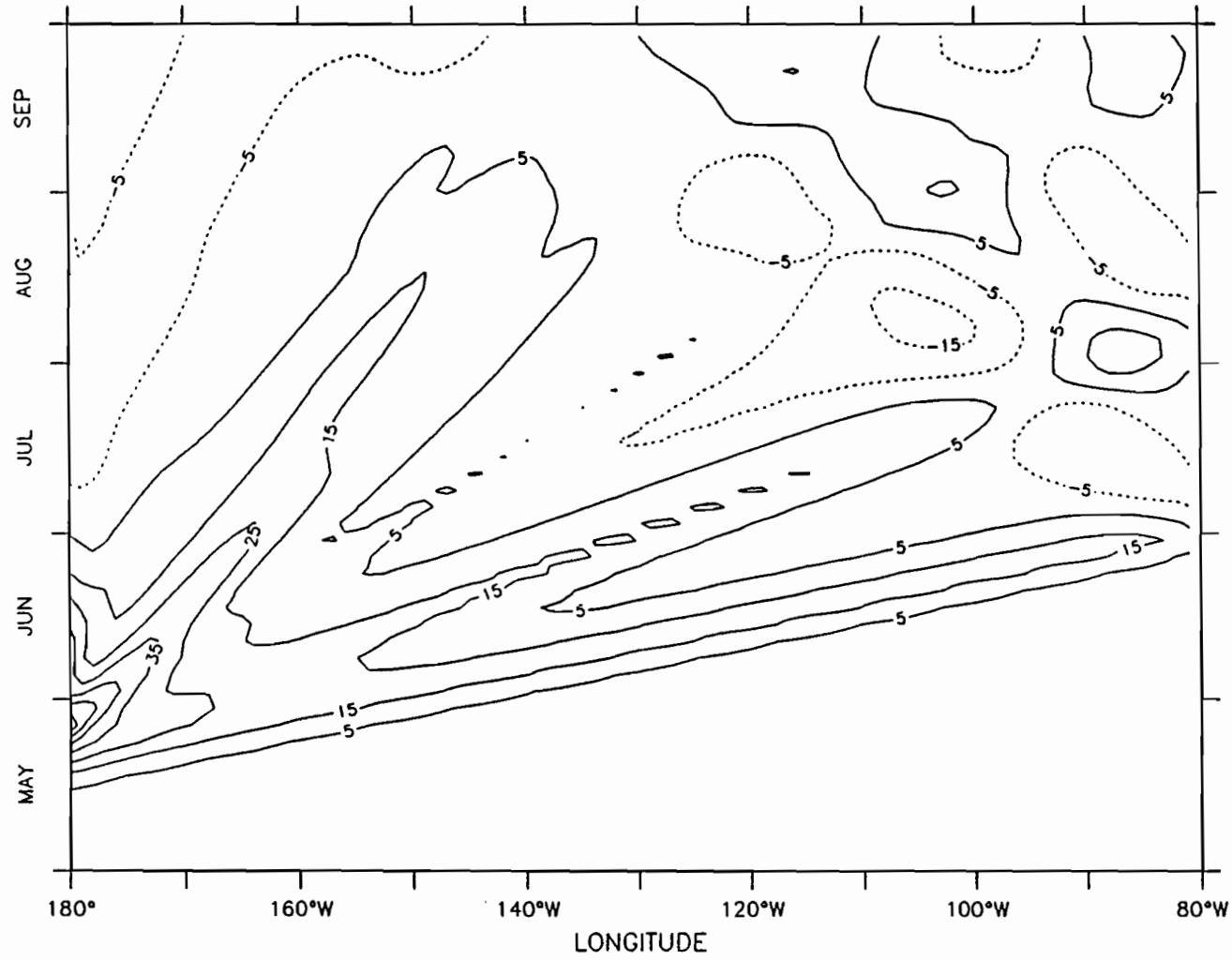

Figure 4.8. A time-longitude contour of zonal velocity in experiment B32. The contour interval is 10 cm sec^{-1} from -95 to 95 cm sec^{-1}.

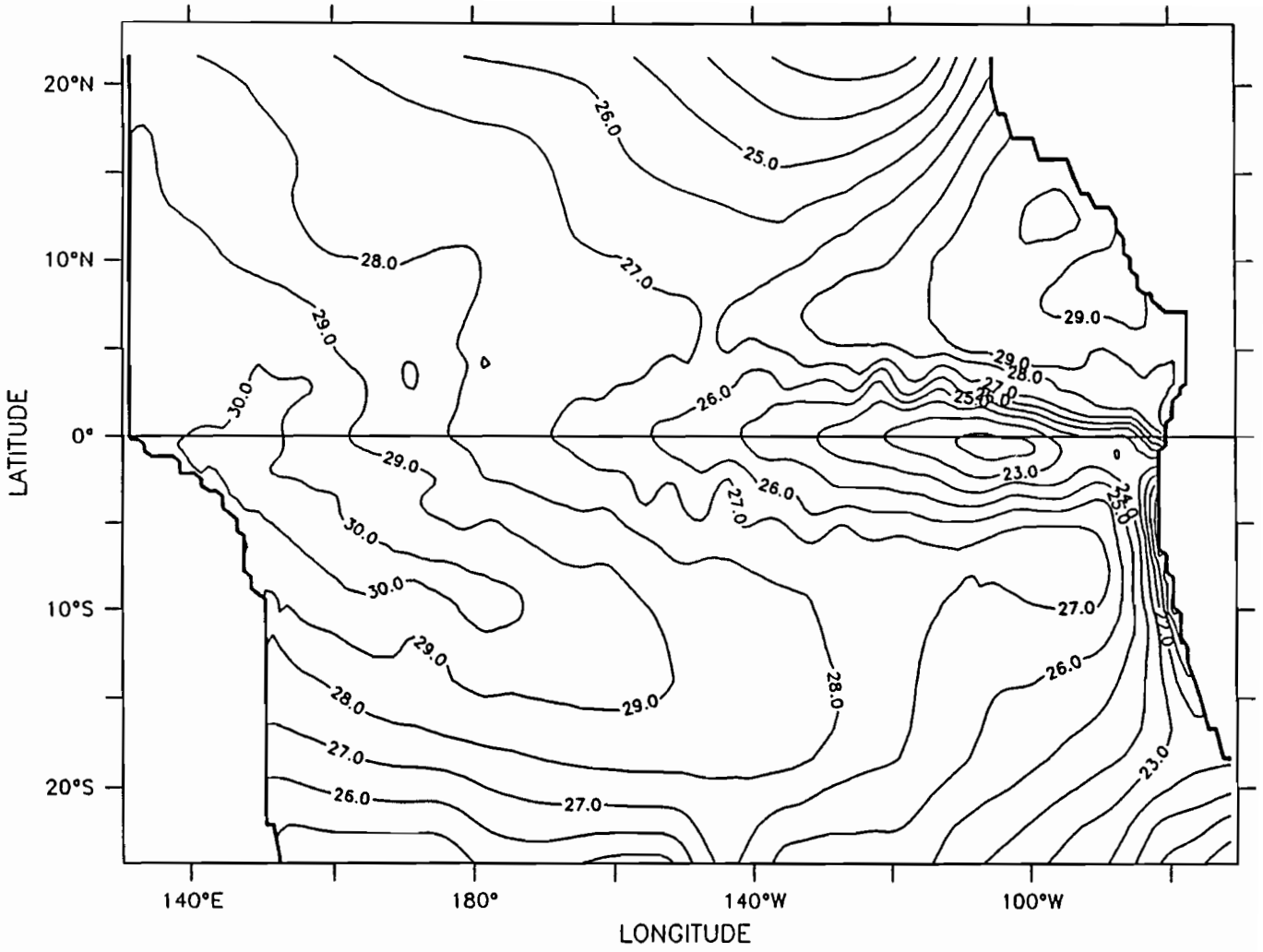

Figure 4.9. The climatological sea surface temperature for May from the model. The contour interval is 1°C.

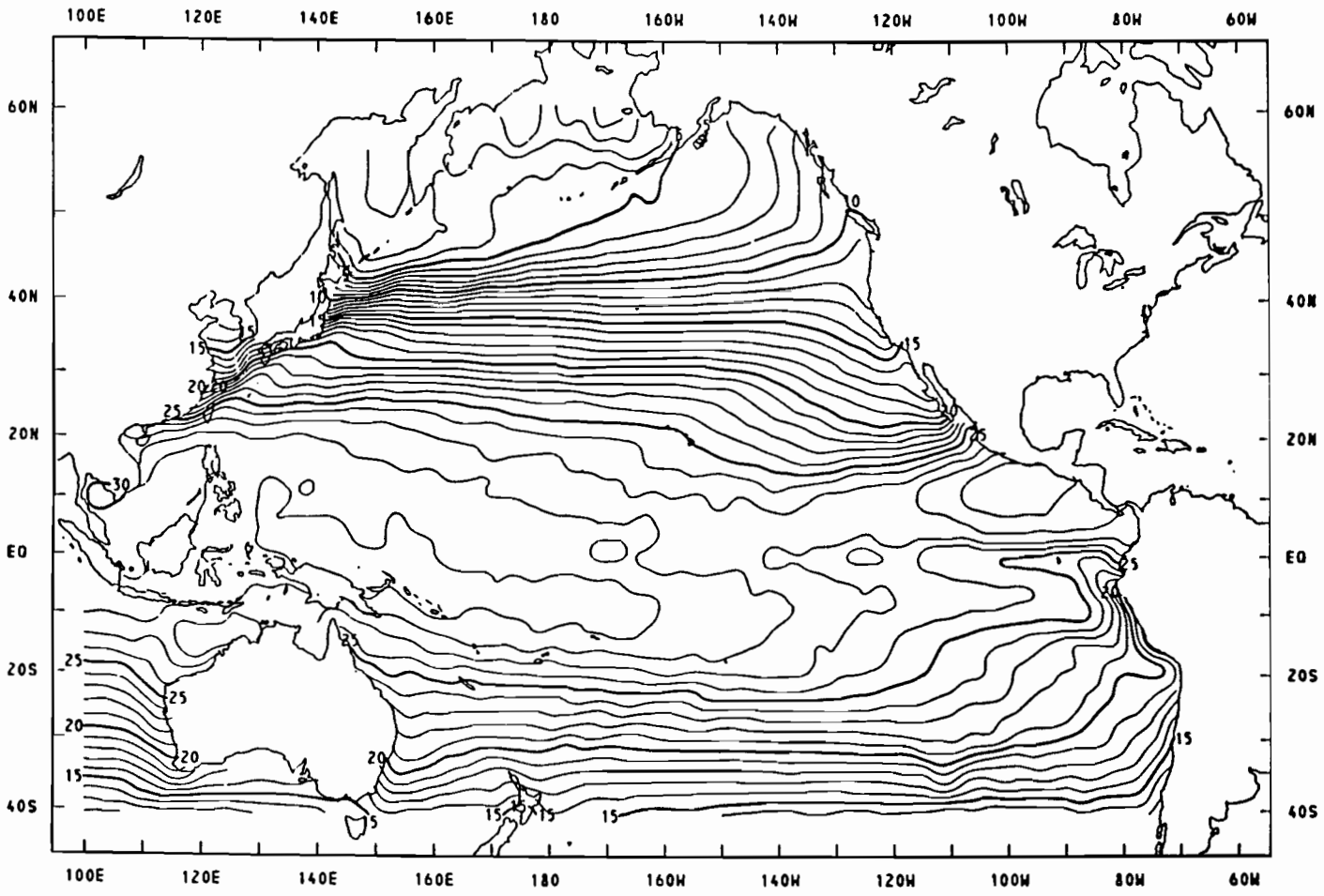

Figure 4.10. The observed climatological sea surface temperature for May, after Reynolds (1982). The contour interval is 1°C.

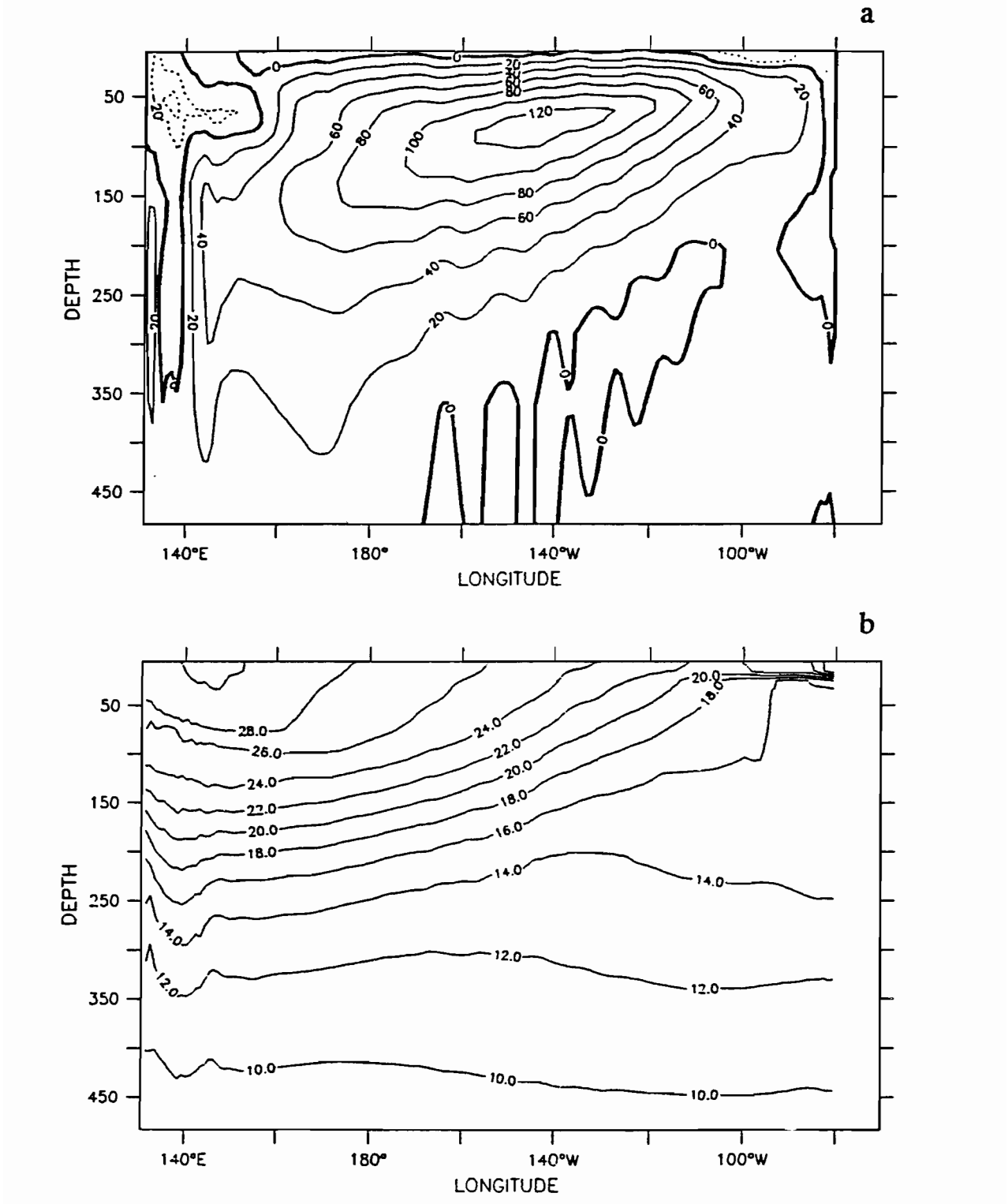

Figure 4.11 Depth-longitude contours of model (top) zonal velocity and (bottom) temperature from climatological May.

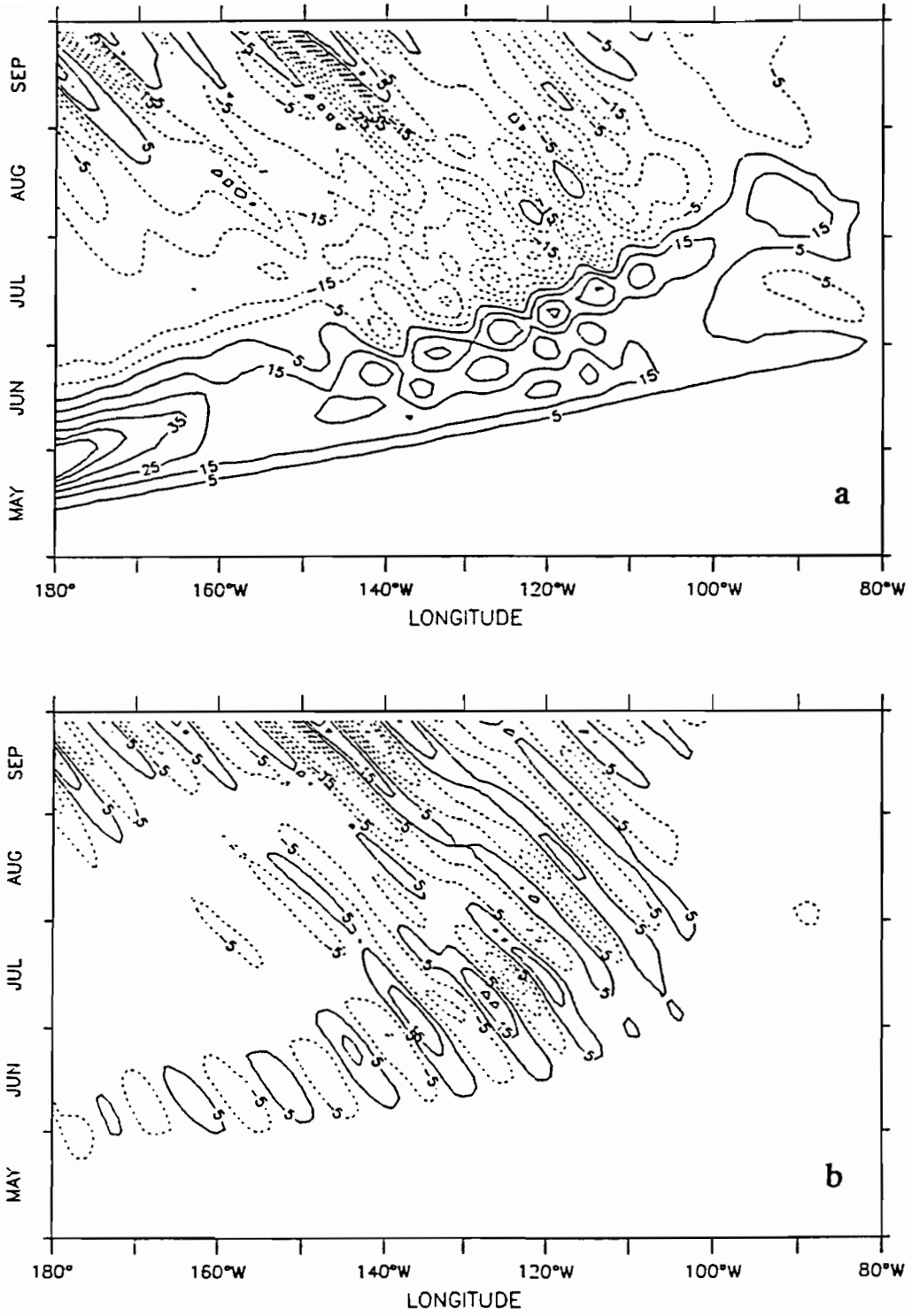

Figure 4.12 Time-longitude contours of surface (top) zonal and (bottom) meridional velocity anomalies for experiment B16. The contour interval is 10 cm sec^{-1} from -125 to 125 cm sec^{-1}.

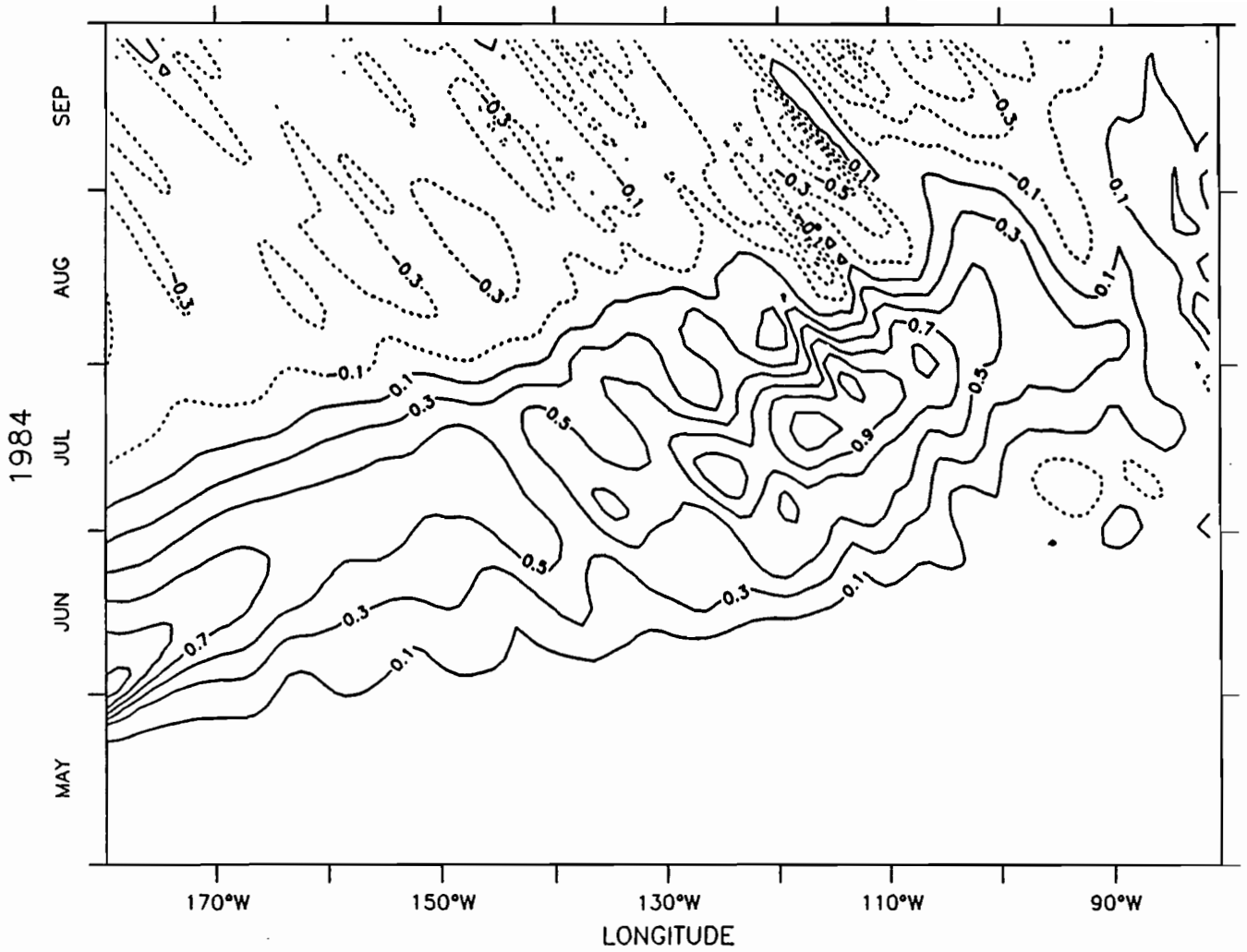

Figure 4.13. Time-longitude contour of the temperature anomaly from experiment B16.

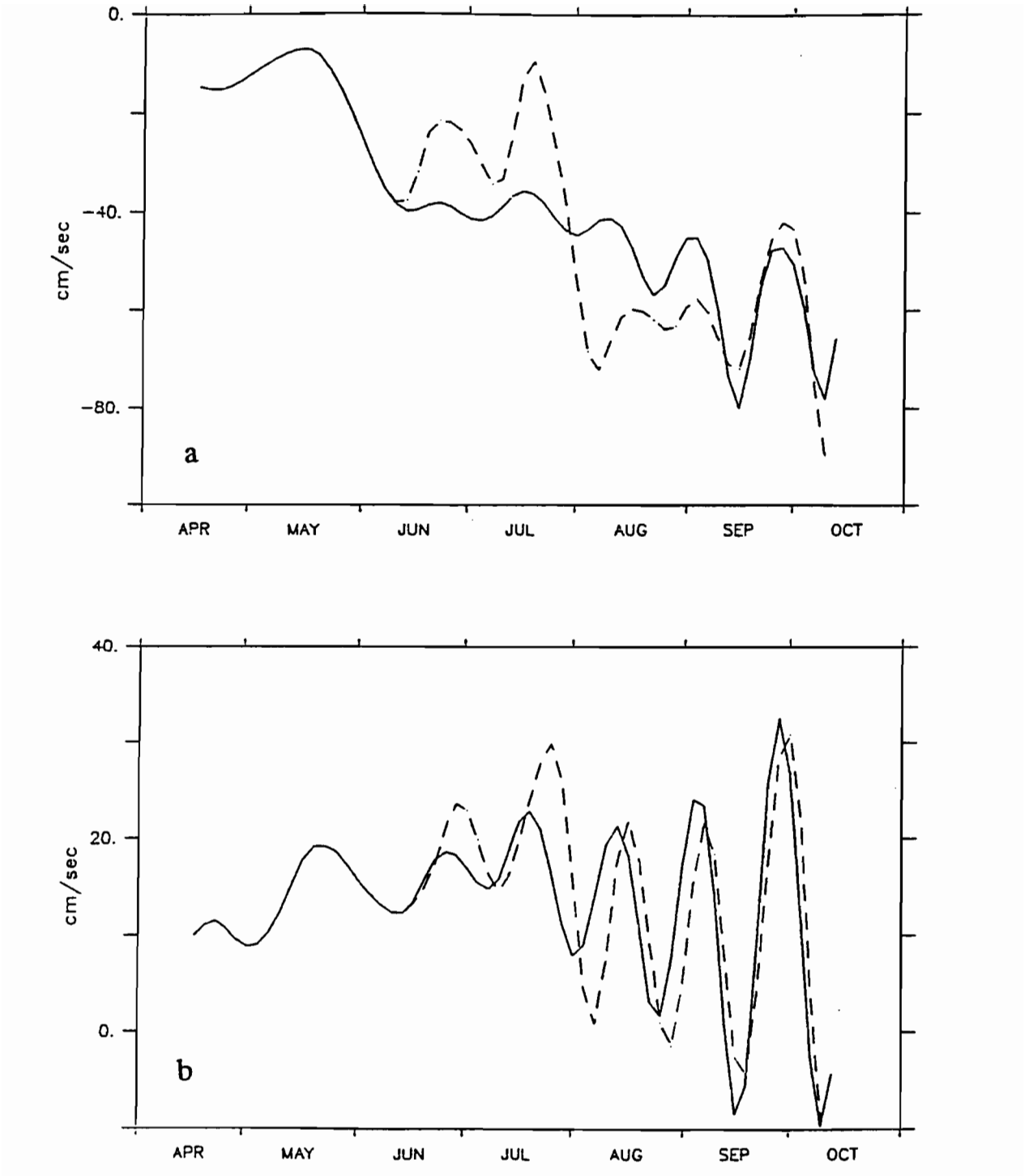

Figure 4.14 Plots of (top) zonal and (bottom) meridional velocity at 0°N, 110°W for climatology (solid line) and the wind burst experiment B16 (dashed line).

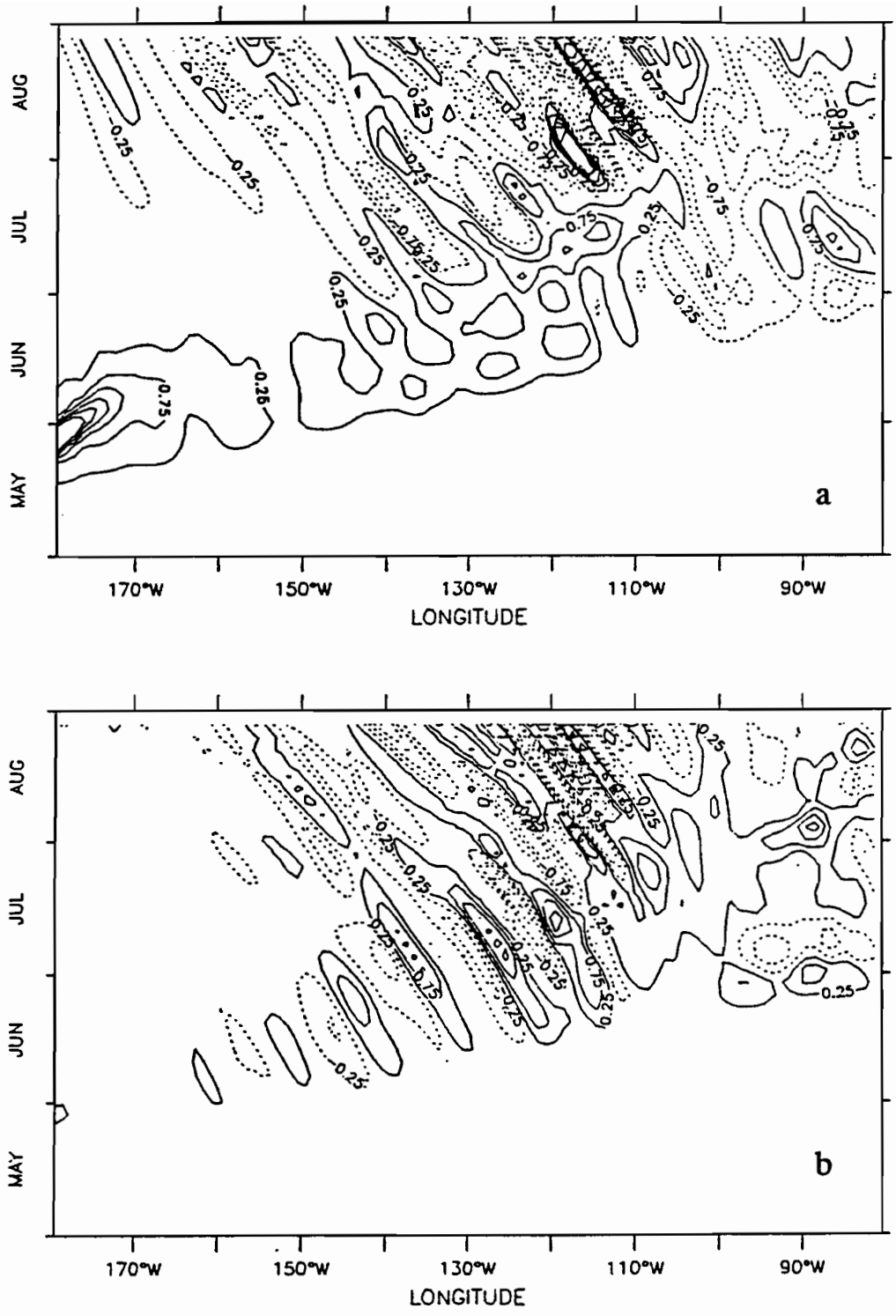

Figure 4.15 Time-longitude contours of anomalous surface (top) zonal and (bottom) meridional heat advection for experiment B16. The contour interval is 0.5 °C month^{-1} from -3.75 to 3.75 °C month^{-1}.

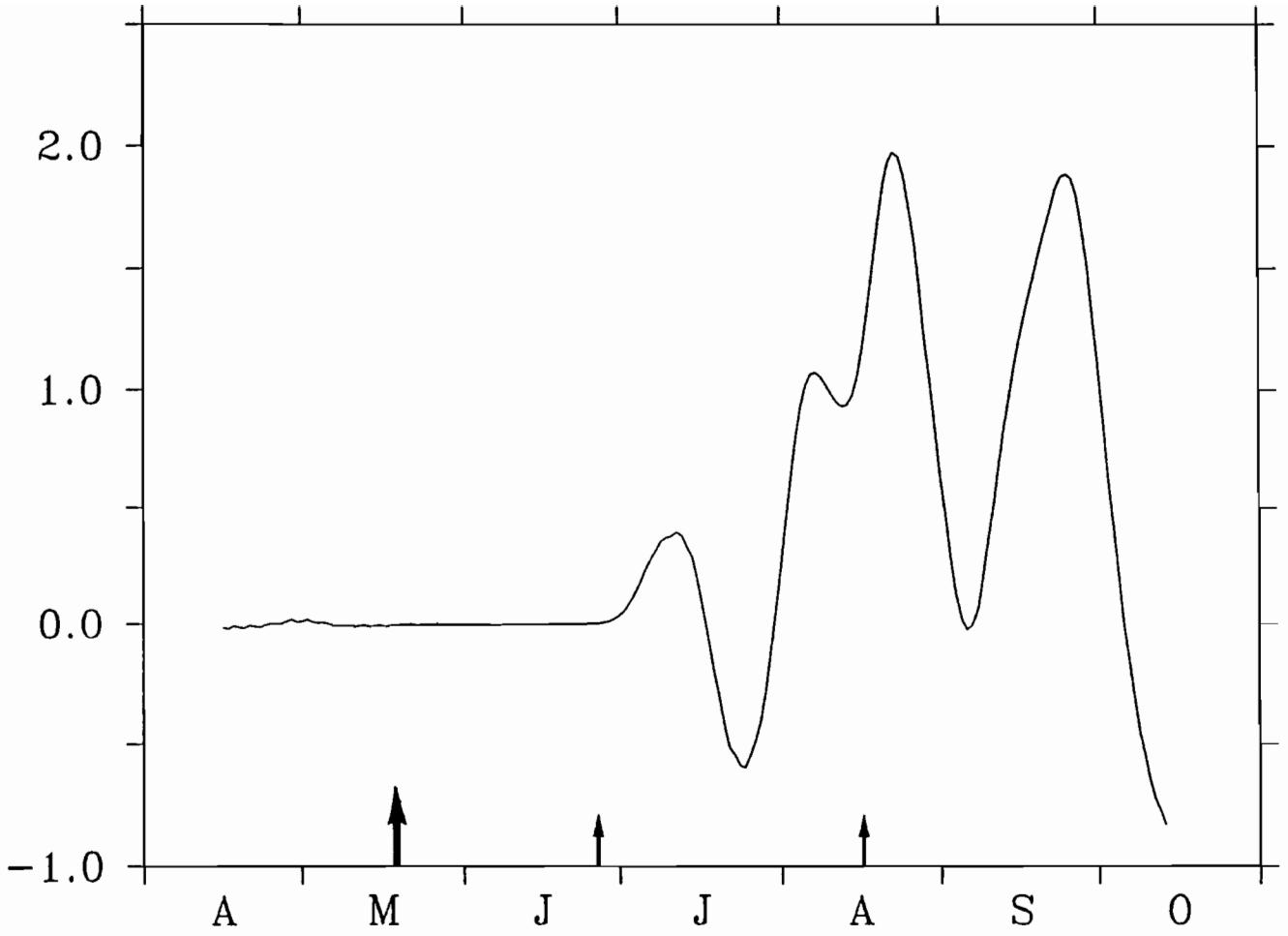

Figure 4.16. Model temperature anomaly at Paita (0°S, 81.5°W) in experiment B16. The arrow in mid-May indicates the peak of the wind burst in the western Pacific. The arrows in July and August indicate the expected arrival of the first and second baroclinic Kelvin pulses.

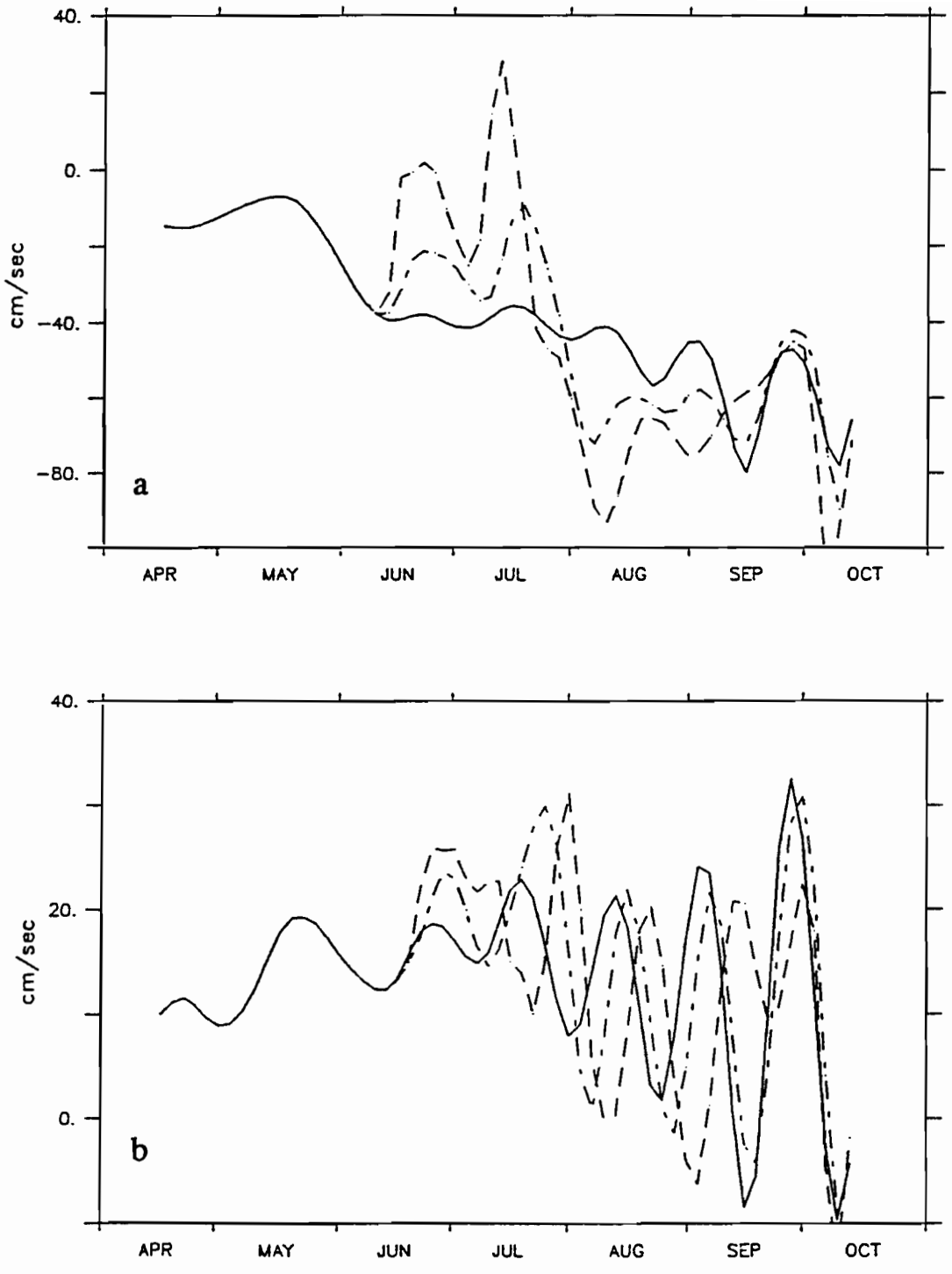

Figure 4.17 Surface (top) zonal and (bottom) meridional velocity at 0°N, 110°W for climatology (solid line), experiment B31 (dashed line) and B16 (dotted-dashed line).

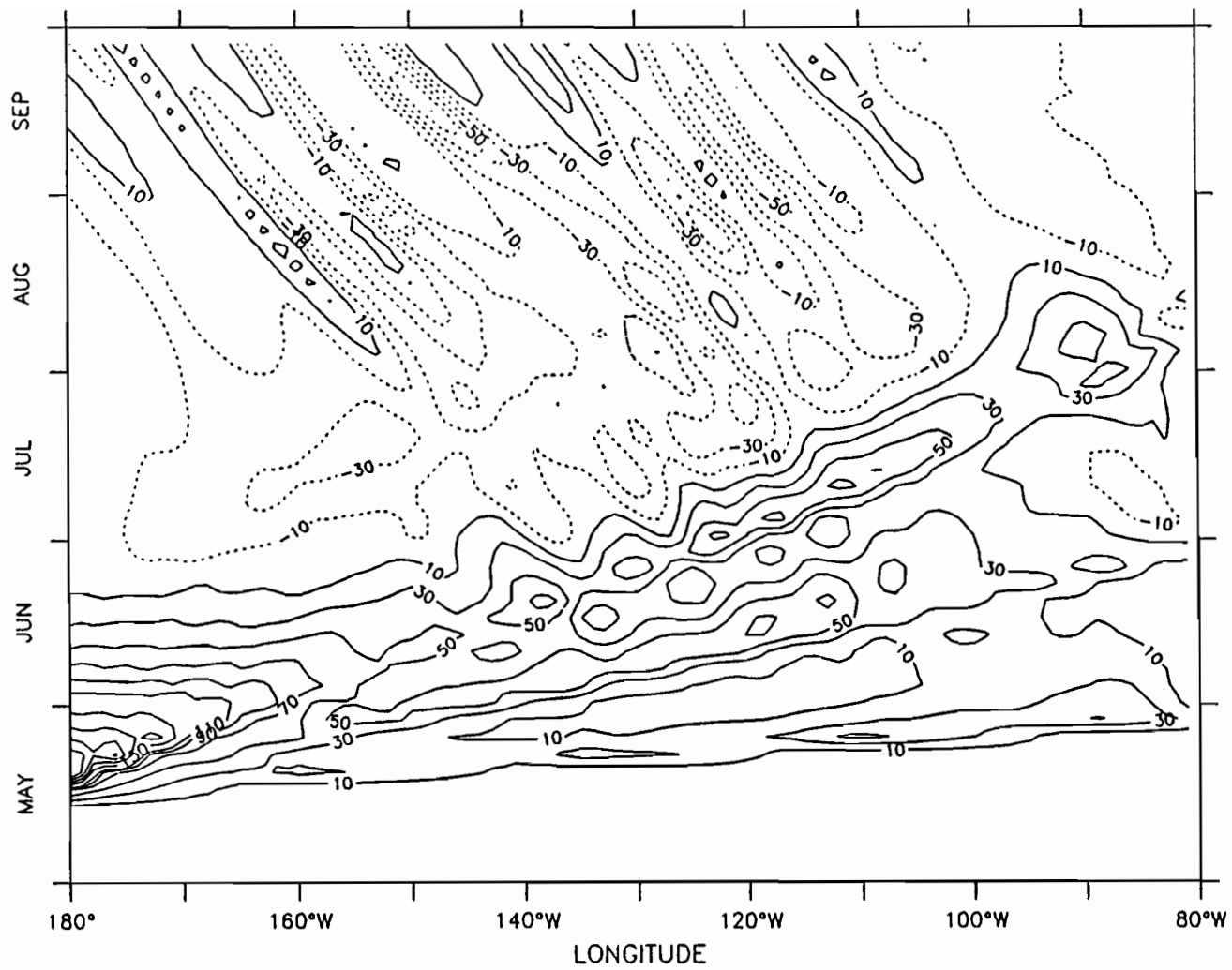

Figure 4.18. A time-longitude contour of the surface zonal velocity anomaly from the model experiment with a propagating wind patch (B33). The wind patch travels at 10 m sec^{-1}.

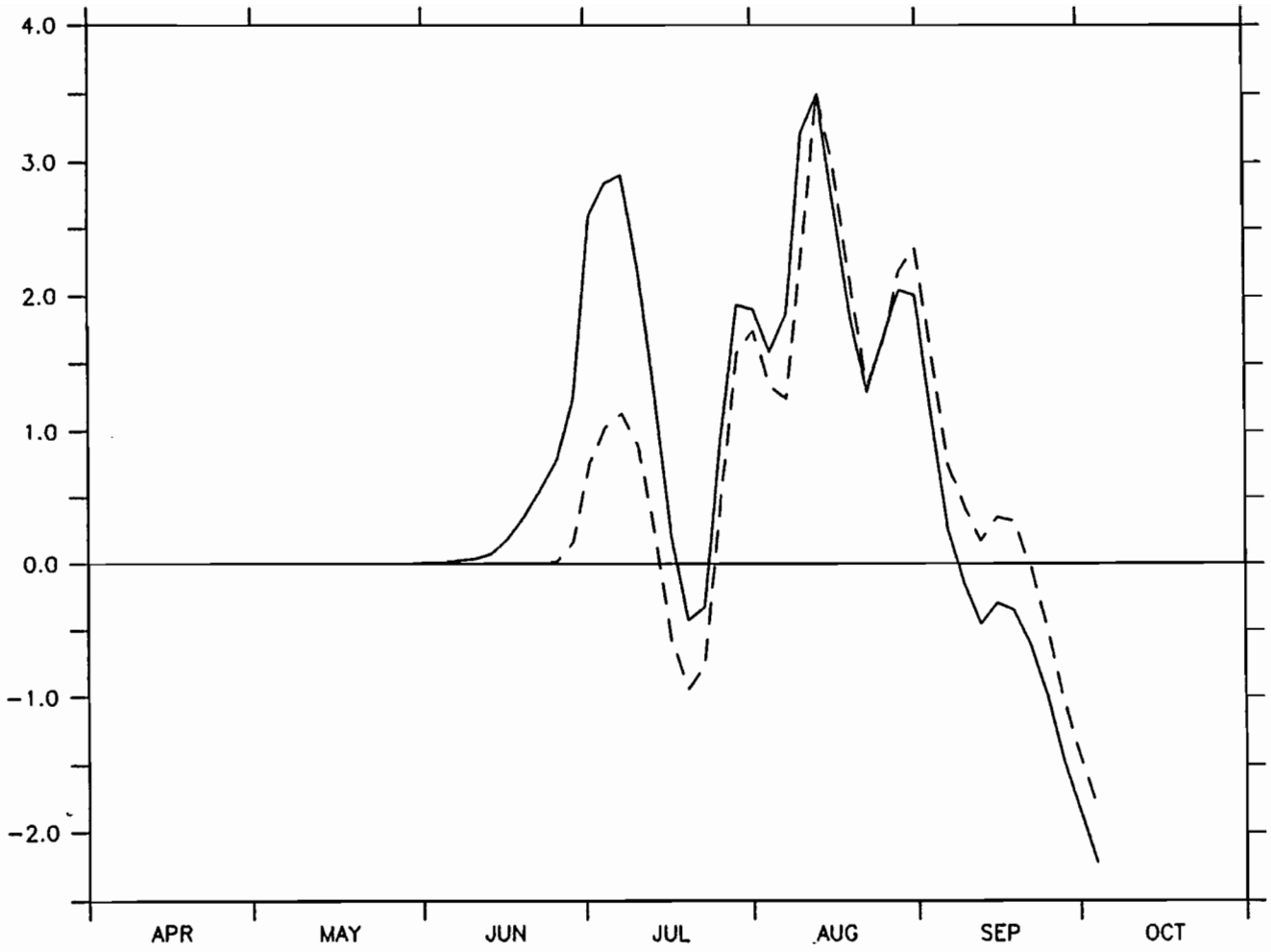

Figure 4.19. A plot of the model temperature anomaly at 0°N, 81.5°W for the propagating wind patch experiment B33 (solid line). The temperature anomaly from the stationary wind forcing of 4 dynes cm^{-2} (experiment B31) is shown as a dashed line.

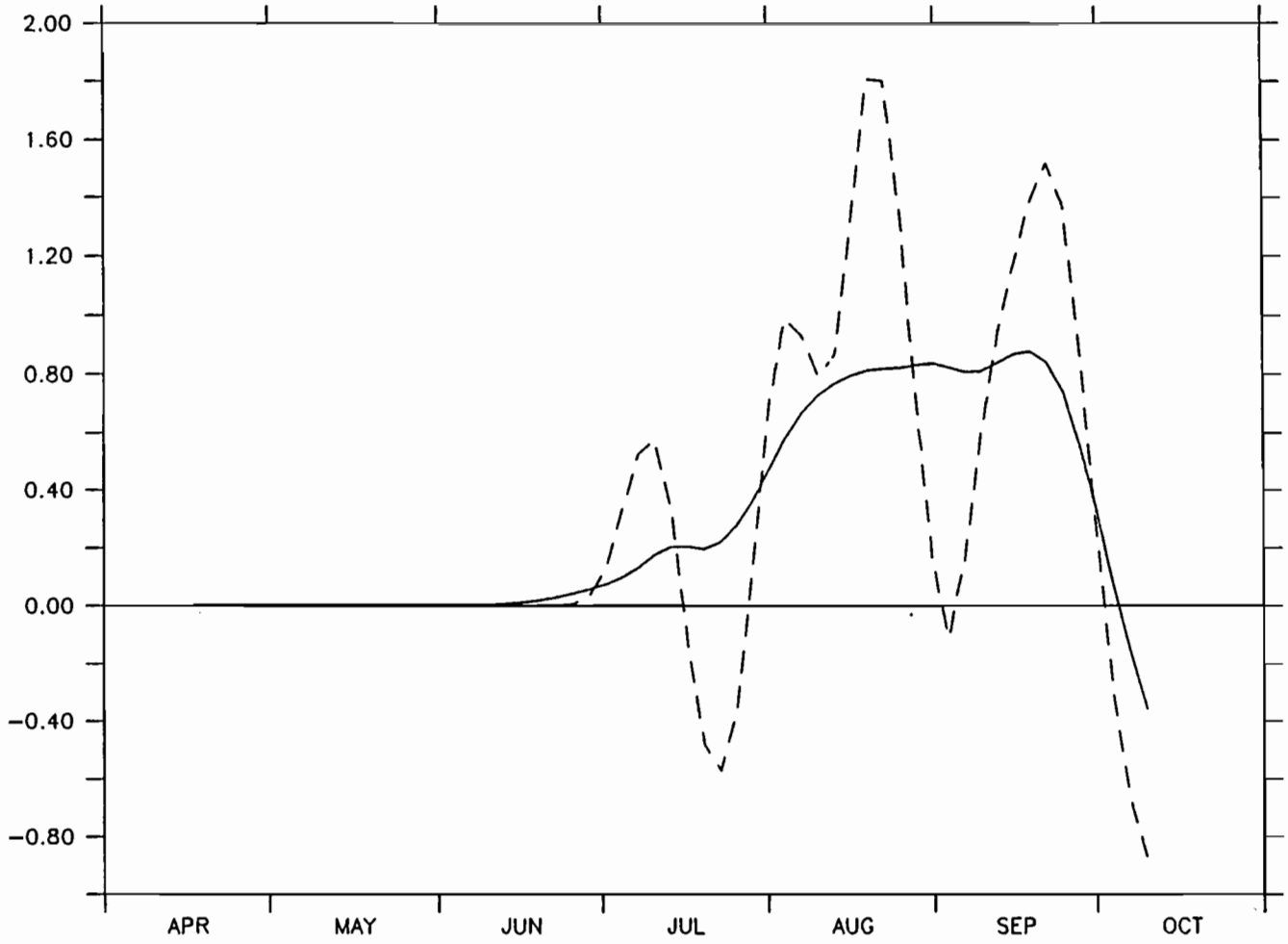

Figure 4.20. The temperature anomaly at 0°N, 81.5°W for the monthly averaged wind burst (experiment B29: solid line) and the 10-day wind burst of 2 dynes cm^{-2} experiment B16: dashed line).

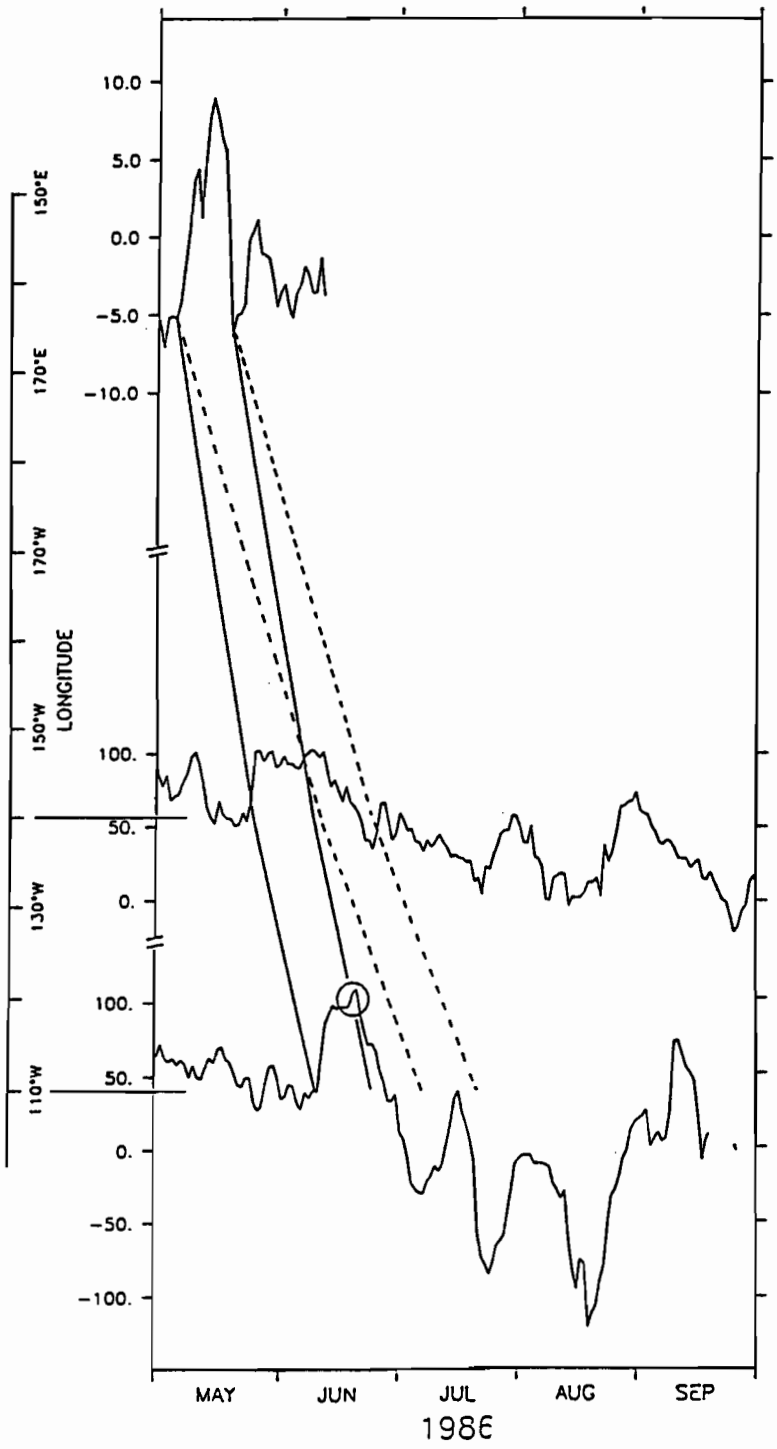

Figure 4.21 Time series of wind (top) and surface zonal currents at 140°W (middle) and 110°W (bottom). The solid lines define the expected width of the first baroclinic mode response and dashed lines the second mode response.

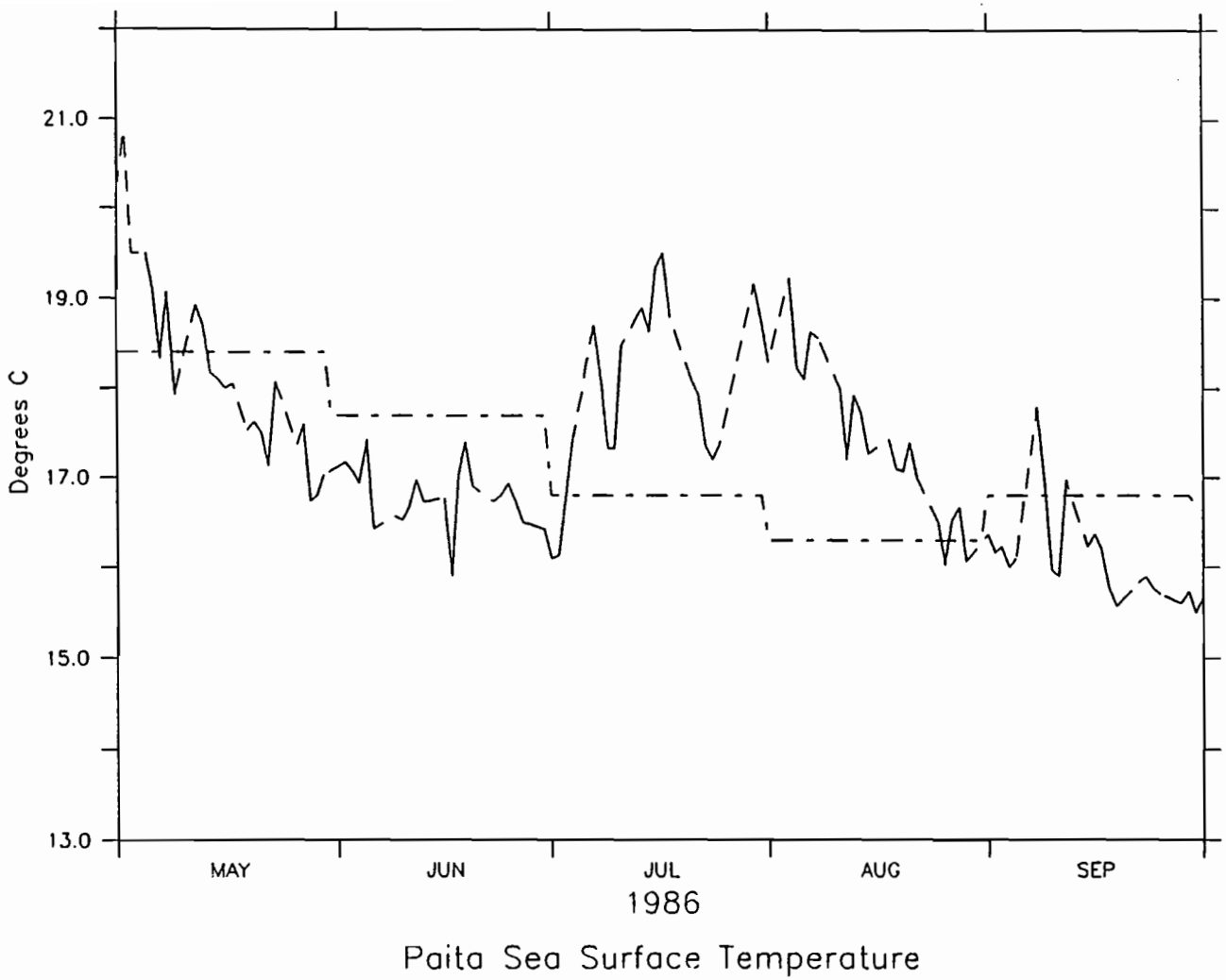

Figure 4.22. The sea surface temperature at Paita, South America for May through September 1986. Where the line is dashed, missing observations have been filled in by linear interpolation. The dashed-dotted line is monthly climatology.

5. SUMMARY AND DISCUSSION

The remote oceanic response to a single episode of intense westerly wind stress in the western Pacific is investigated using a combination of linear theory and experiments with an ocean general circulation model. Episodes of westerly wind are potentially important in evolution of ENSO as a coupling mechanism between ocean and atmosphere. In this report the oceanic response is isolated from the coupled problem by specifying surface wind forcing.

Episodes of westerly wind are an integral part of wind variability at island stations near the equator in the western Pacific. The number and intensity of wind events increases prior to and during ENSO years. There is a seasonal pattern to westerly winds, with more activity south of the equator during the austral cyclone season and more activity north of the equator during the boreal cyclone season. Poleward of 5° there is little difference in power spectra between ENSO and non-ENSO years, indicating that anomalous forcing is largely constrained to the equatorial waveguide.

The spatial and temporal characteristics of episodes of westerly wind are determined using daily averaged surface wind observations taken from islands in the western Pacific. The structure of wind anomalies varies both seasonally and interannually, so a typical wind event is described instead of finding the actual average wind event. The typical wind event is idealized as Gaussian in time with a width at half-maximum of ten days. The peak zonal wind stress anomaly is 2.0 dynes cm^{-2} (approximately 10 m sec^{-1}). The wind anomaly is Gaussian meridionally, centered at the equator, and with a width at half-maximum of 3° of latitude. Zonal structure is a top-hat function with a width of 20° of longitude centered at 160°E.

Linear theory predicts that the typical westerly wind burst excites a train of Kelvin pulses which emanate from the forcing region. Because the phase speed of Kelvin pulses varies inversely with baroclinic mode number, Kelvin pulses separate as they propagate eastward. For density stratification typical of the western Pacific, the surface zonal velocity of the first and second baroclinic modes are of comparable amplitude, at 32 cm sec^{-1} and 24 cm sec^{-1} respectively. As Kelvin pulses propagate into the equatorial cold tongue with its negative zonal temperature gradient, they advect warm water to the east. Because the velocity perturbation associated with Kelvin pulses is always to the east, there is a net warming. The amount of anomalous warming caused by Kelvin pulses is proportional to the seasonally variable zonal temperature gradient. Using a gradient of 1°C in 10° of longitude at 110°W for the month of June (Reynolds, 1982), the first baroclinic mode Kelvin pulse yields a warming of about 0.4°C. Linear theory predicts a comparable warming from the second baroclinic mode.

The effects of including a realistic shoaling thermocline can be estimated by making a WKB approximation. Because the characteristic width of the Kelvin pulse is small compared to the length over which the thermocline shoals, the approximation is appropriate. By conserving the flux of energy as the waves propagate from the western to the eastern Pacific, an expression

for the change in the surface zonal current of the Kelvin pulse is obtained. Using stratification typical of the western and eastern Pacific, the expression predicts that the first vertical mode will have smaller zonal surface currents in the eastern Pacific than in the western Pacific. In contrast, surface zonal currents of the second baroclinic mode are greater in the eastern Pacific than in the western Pacific. Conservation of energy flux predicts that surface currents of the second baroclinic mode double relative to the surface currents of the first baroclinic mode.

The change in stratification from west to east causes a redistribution of energy in the vertical, decreasing surface zonal velocity and increasing bottom zonal velocity of the first baroclinic mode. Higher baroclinic modes, which are sensitive to changes in stratification near the surface, experience the opposite effect. A similar mechanism may explain Gill's (1982) observation that changes in thermal structure during the 1972-73 ENSO were dominated by the first baroclinic mode in the western Pacific, yet changes in the eastern Pacific required a dominant second baroclinic mode.

Two sets of experiments were then conducted using an ocean general circulation model forced by a typical episode of westerly wind. In the first set of experiments the model was initialized with no background currents. These experiments allow an examination of evolution of Kelvin pulses in the absence of mean flow or other sources of natural oceanic variability. When the wind anomaly is weak, model results match predictions of linear theory. When the wind anomaly is strong (greater than 2 dynes cm^{-2}), low baroclinic modes have amplitudes that are greater than predicted by linear theory. Correspondingly, high baroclinic modes have amplitudes that are less than those predicted by linear theory.

When the wind anomaly is strong there is vigorous mixing in the forcing region which affects Kelvin pulses in two ways. First, the deeper mixed layer yields a slower phase speed of the pulses within the forcing region, so that they are subject to forcing for a longer period of time. This effect is more pronounced for low vertical modes that have large phase speeds than for the third and higher vertical modes (see Fig. 3.3). Second, the change in vertical structure alters projection of forcing onto vertical modes. A deeper thermocline tends to enhance low vertical modes at the expense of high vertical modes. Also, as waves become larger, shear increases. Since friction in the model is parameterized to be proportional to vertical shear, larger amplitude waves will experience greater frictional damping. Because high vertical modes have much more shear than low vertical modes, they will tend to be damped out more rapidly than the low vertical modes.

In one experiment (B24), the second baroclinic mode Kelvin wave evolved into a train of solitary waves, with properties consistent with a soliton packet. A soliton requires a balance between dispersion and advection, and since Kelvin waves are non-dispersive, solitons ordinarily cannot occur. Background meridional shear, however, can provide dispersion to allow solitons (Boyd, 1984). The second baroclinic mode propagates coincidentally with the first baroclinic

mode for over 40° of longitude. It is possible that the first baroclinic mode provides shear to allow the second baroclinic mode to evolve into a solitary wave train.

In the second set of experiments, the wind anomaly is imposed on top of climatological winds. In these experiments the ocean contains an equatorial undercurrent, a shoaling thermocline and 20-30 day period instability waves. Within the equatorial waveguide the Kelvin wave response is obscured by the presence of instability waves. Kelvin pulses modify existing instability waves: amplitude of the waves increase and the phase changes. Modified instability waves induce changes in sea surface temperature that can be as large as the SST change induced by zonal advection associated with Kelvin pulses.

The phase speed of the model first baroclinic mode Kelvin pulse with a surface zonal velocity of 50 cm sec^{-1} is about 14% above linear phase speed. Observations of first mode Kelvin pulses indicate that they travel 10-20% faster than linear phase speed (Knox and Halpern, 1982; McPhaden *et al.*, 1988). The increase in phase speed has been described as either Doppler shifting by the equatorial undercurrent (McPhaden *et al.*, 1986) or as nonlinear self advection (Ripa, 1984). Six of the wind burst experiments are relevant to the question of which process accounts for the phase speed increase in the model. In the four experiments conducted in the absence of mean flow, a phase speed increase was found with increasing Kelvin pulse amplitude. The phase speed increase is a few percent for small amplitude pulses to nearly 50 percent in the case which formed solitons. Nonlinear self-advection adequately accounts for phase speed increases. Because there are no background currents in these experiments, there can be no Doppler shifting by the Equatorial Undercurrent. Two experiments were conducted with identical background currents and forcing conditions, except that the amplitude of the wind burst was doubled in the second experiment. The phase speed of the second baroclinic mode in both cases is larger than predicted by linear theory. For the second baroclinic mode the phase speed in the more strongly forced case is larger by 10% than the phase speed in the more weakly forced case (see Fig. 4.17). Doppler shifting cannot account for phase speed discrepancies between waves of different amplitudes. The modeling work indicates that nonlinear self-advection makes an important contribution to the phase speed increase of model Kelvin pulses. The phase speed increase is consistent with observations.

At the coast of South America anomalous warming is much greater than in the equatorial waveguide. A single ten-day episode of westerly wind in the western Pacific causes a sea surface temperature anomaly of up to 2°C for a period exceeding 45 days at the coast of South America. Warming at the coast of South America is primarily associated with the second baroclinic mode. Linear theory predicts that although the first and second modes have comparable surface zonal current amplitudes in the western Pacific, because of changes in thermal structure across the Pacific, the second baroclinic mode has larger surface zonal current amplitude in the eastern Pacific. Observations of Gill (1982) and Lukas (1984) show strong

second baroclinic mode structure in the eastern Pacific. A model of sea level variability during the 1982-83 El Niño requires equal contributions from the first and second baroclinic modes in the eastern Pacific (Busalacchi and Cane, 1985). Linear theory predicts that second mode currents are twice as strong as first mode currents in this model. One and a half layer models, which include only one baroclinic mode, obviously cannot represent warming at the coast of South America due to the second mode. The modeling work here indicates that timing and duration of warming is significantly different from that expected in a one and a half layer model.

The timing, duration and magnitude of the model warming agree well with observations of sea surface temperature at Paita, South America following the strong wind event in May 1986. Paita data show a warm anomaly of 3° to 4°C starting in the beginning of June and lasting through the end of August. Temperature data indicate there were two periods of warming (Fig. 4.22), consistent with the interpretation of having two energetic baroclinic modes.

In the composite El Niño of Rasmusson and Carpenter (1982) warming is between 2° and 3°C at the coast of South America. Because a single episode of westerly wind results in warming that lasts for almost two months, a series of four westerly wind bursts at intervals of two months could plausibly account for the duration and magnitude of warming observed at the coast of South America during El Niño.

A propagating wind patch enhances the first vertical mode and thus makes the model sea surface temperature anomaly at the coast of South America more similar to Paita temperature observations. Because the wind anomaly propagates jointly with the first baroclinic mode for a longer period of time than the higher baroclinic modes, the first baroclinic mode is affected most by the propagating wind patch. The propagating patch has little effect on the second and higher baroclinic modes.

When the wind anomaly is incorporated into monthly averaged winds, oceanic SST response at the coast of South America is nearly the monthly average of the oceanic response to a short duration wind anomaly. However, the peak of the warm anomaly is nearly twice as large as for the month averaged burst. Mechanisms that are sensitive to sea surface temperature, such as atmospheric convection, will respond differently in the two cases.

In this report, the effect of westerly wind bursts on the tropical Pacific has been examined from the uncoupled oceanic perspective. An atmospheric perturbation is specified in the wind forcing field; no feedback exists to alter atmospheric forcing as a result of oceanic changes. Because of the ocean model heat flux parameterization, the oceanic state will necessarily relax back to the pre-disturbed state.

Because warming along the equatorial waveguide is weak and is followed by a period of cooling, it is not clear how an altered ocean state results in increased westerly wind activity. Such a mechanism would be required to fully couple the ocean and the atmosphere, with

westerly wind bursts as primary coupling agent. This does not preclude the possibility that episodes of westerly wind play an important role in development of El Niño.

A study of a model coupled ocean-atmosphere system has been performed by Latif *et al.* (1988). In that study they forced a coupled and an uncoupled model by a very large westerly wind burst. The forcing region extended from 130°E to 180°, from 10°S to 10°N and lasted for an entire month. The magnitude of the wind anomaly is 2 dynes cm^{-2}. In the uncoupled model run the western Pacific response of zonal currents and temperature is quite strong. However, there is little response in the eastern Pacific. This is perhaps due to large friction coefficients used in the ocean model. Their horizontal friction coefficient is 1.0×10^8 cm^2 sec^{-1} and vertical friction coefficient is a constant 15 cm^2 sec^{-1} (Latif, 1987). Strong viscosity probably prevents Kelvin wave radiation into the eastern Pacific, mitigating coastal response to westerly wind bursts.

In coupled runs the atmosphere responds to altered sea surface temperature. In these experiments the central Pacific maintains a warm anomaly of 2° to 3°C for over ten months. There is almost no warm anomaly in the eastern Pacific; in fact there appears to be a cool anomaly at 90°W for much of the coupled run (Latif *et al.*, 1988; Fig. 11b). Again, it is possible that friction damps the remote response too quickly to propagate into the eastern Pacific. Oddly, the warm anomaly in the central Pacific is stationary, in contrast to model simulations of the 1982-83 El Niño (Harrison *et al.*, 1989) which show an eastward propagation of the anomalous warm region. It is notable that the warm anomaly in the coupled run is between 180 and 150°W: a region where zonal temperature gradients in the model are unrealistically large. Observations indicate that during January there is a 1.5°C temperature difference between 180 and 150°W. In the uncoupled model, the temperature difference between 180 and 150°W is 3.5°C, more than double the observed temperature gradient.

Furthermore, the coupled model uses a flux-correction method, that forces model sea surface temperature and wind stress back to the uncoupled state. The flux-correction method introduces artificial sources and sinks of heat and wind stress at the air-sea interface (Latif *et al.*, 1988).

The role of westerly wind bursts in evolution of ENSO can be fully understood only in context of the coupled ocean-atmosphere system. In this report, only the oceanic response to anomalous wind stress is examined. There is growing interest in processes which couple ocean and atmosphere in the western Pacific. These studies will undoubtedly shed light on coupling between ocean and occurrence of intense westerly episodes. Further coupled ocean-atmosphere general circulation models should be done, with new momentum and heat exchange parameterizations.

6. ACKNOWLEDGMENTS

I thank my advisor, D.E. Harrison, for suggesting an interesting problem and supporting my research efforts. I am especially grateful for his thoughtful guidance. I thank my dissertation committee: L. Rothstein and E. Sarachik who served on the reading committee and P. Quay and M. Wallace who served on the supervisory committee. I am indebted to H. Mofjeld and D. Moore for many helpful discussions. In the course of the research I generated more than 2 trillion numbers. The analysis of these numbers was made possible by the expert programming skills of J. Davison, S. Hankin and M. Verschell of the TMAP group of NOAA/PMEL. I would like to thank my father, for his constant support, advice and enthusiasm. And to Rachel, for her love.

7. REFERENCES

Anthes, R.A. (1982): Tropical cyclones: their evolution, structure and effects. *Am. Meteorol. Soc., 19*(41), 204 pp.

Arakawa, A. (1988): Finite-difference methods in climate models. In *Physically-Based Modelling and Simulation of Climate and Climatic Change*, M.E. Schlesinger (ed.), Kluwer Academic Publishers, Dordrecht.

Berlage, H.P. (1966): The Southern Oscillation and world weather. Koninklijk Nederlands Meteorlogisch Institut, Mededelingen en Verhandelingen No. 88, 152 pp.

Boyd, J.P. (1980): The nonlinear equatorial Kelvin wave. *J. Phys. Oceanogr., 10*, 1-11.

Boyd, J.P. (1984): Equatorial solitary waves, Part 4. Kelvin solitons in a shear flow. *Dynamics Atmos. and Oceans, 8*, 173-184.

Bjerknes, J. (1969): A possible response of the atmospheric Hadley circulation to equatorial anomalies of ocean temperature. *Tellus, 18*, 820-829.

Bryan, K., and M.D. Cox (1967): A numerical investigation of the ocean general circulation. *Tellus, 19*, 54-80.

Bryan, K. and M.D. Cox (1972): An approximate equation of state for numerical models of ocean circulation. *J. Phys. Oceanogr., 2*, 510-514.

Busalacchi, A.J. and J.J. O'Brien (1981): Interannual variability of the Equatorial Pacific in the 1960's. *J. Geophys. Res., 86*, 10,901-10,907.

Busalacchi, A.J. and M.A. Cane (1985): Hindcasts of sea level variations during the 1982-83 El Niño. *J. Phys. Oceanogr., 15*, 213-221.

Busalacchi, A.J., and M.A. Cane (1988): The effect of varying stratification on low-frequency equatorial motions. *J. Phys. Oceanogr., 18*, 801-812.

Cane, M.A. and E.S. Sarachik (1976): Forced baroclinic ocean motions: I. The linear equatorial unbounded case. *J. Mar. Res., 34*, 629-665.

Cane, M.A. and E.S. Sarachik (1981): The response of a baroclinic equatorial ocean to periodic forcing. The linear equatorial periodic case. *J. Mar. Res., 39*, 651-693.

Cane, M.E. (1984): Modeling sea level during El Niño. *J. Phys. Oceanogr., 14*, 1864-1874.

Cane, M.E., and S.E. Zebiak (1985): A theory for El Niño and the Southern Oscillation. *Science, 228*, 1085-1087.

Clarke, A.J. (1983). The reflection of equatorial waves from oceanic boundaries. *J. Phys. Ocean., 13*, 1193-1207.

Colin, C., C. Henin, P. Hisard and C. Oudot (1971): Le Courant de Cromwell dans le Pacifique central en fevrier. *Cah. ORSTOM Ser. Oceanogr., 7*, 167-186.

Cox, M.D. (1980): Generation and propagation of 30-day waves in a numerical model of the Pacific. *J. Phys. Oceanogr., 10*, 1168-1186.

Cox, M.D. (1984): A primitive equation, 3-dimensional model of the ocean. GFDL Ocean Group Tech. Rep. No. 1, GFDL/NOAA.

Eriksen, C.C., M.B. Blumenthal, S.P. Hayes and P. Ripa (1983): Wind-generated equatorial Kelvin waves observed across the Pacific ocean. *J. Phys. Oceanogr., 13*, 1622-1640.

Eriksen, C.C. (1988): On wind forcing and observed oceanic wave number spectra. *J. Geophys. Res., 93*, 4985-4992.

Fjeldstad, J.E. (1933): Interne Wellen. *Geofys. Publ. Kasjoner, 10*(6), 53 pp.

Gill, A.E. and A.J. Clarke (1974): Wind-induced upwelling, coastal currents and sea-level changes. *Deep-Sea Res., 21*, 325-345.

Gill, A.E. (1982): Atmosphere-Ocean Dynamics. Academic Press, Inter. Geophys. Series, W.L. Donn, (ed.), *30*, 662 pp.

Gill, A.E. (1982): Changes in thermal structure of the equatorial Pacific during the 1972 El Niño as revealed by bathythermograph observations. *J. Phys. Oceanogr., 12*, 1373-1387.

Gill, A.E. (1983): An estimate of sea-level and surface-current anomalies during the 1972 El Niño and consequent thermal effects. *J. Phys. Oceanogr., 13*, 586-606.

Gill, A.E. and B.A. King (1985): The effect of a shoaling thermocline on equatorially-trapped Kelvin waves. Dynamical Climatology, DCTN 27, 28 pp.

Harrison, D.E., and P.S. Schopf (1984): Kelvin wave-induced advection and the onset of SST warming in El Niño events. *Mon. Wea. Rev., 112*, 923-933.

Harrison, D.E., and B.S. Giese (1988): Remote westerly wind forcing of the eastern equatorial Pacific; some model results. *Geophys. Res. Lett., 15*, 804-807.

Harrison, D.E. (1987): Monthly mean island surface winds in the central tropical Pacific and El Niño events. *Mon. Wea. Rev., 115*(12), 3133-3145.

Harrison, D.E. , W.S. Kessler and B.S. Giese (1989): Ocean circulation model hindcasts for the 1982-83 El Niño: Thermal variability along the ship of opportunity tracks. Accepted to *J. Phys. Oceanogr.*

Harrison, D.E., and D.S. Luther (1989): Surface winds from tropical Pacific islands—climatological statistics. Accepted to *J. Climate.*

Hayes, S.P., and D. Halpern (1984): Correlation of current and sea level in the eastern equatorial Pacific. *J. Phys. Oceanogr., 14*, 811-824.

Hildebrand, F.B. (1976): *Advanced Calculus for Applications*. Prentice-Hall, New Jersey, 702 pp.

Hughes, R.L. (1981): The influence of thermocline slope on equatorial thermocline displacement. *Dynamics Atmos. and Oceans, 5*, 147-157.

Hurlburt, H.E., J.C. Kindle and J.J. O'Brien (1976): A numerical study of the onset of El Niño. *J. Phys. Oceanogr., 6*, 621-631.

Keen, R.A. (1982): The role of cross-equatorial tropical cyclone pairs in the Southern Oscillation. *Mon. Wea. Rev., 110*, 1405-1416.

Kerr, I.S. (1976): Tropical storms and hurricanes in the southwest Pacific. New Zealand Meteorological Service, Pub. 148, 114 pp.

Knox, R.A. and D. Halpern (1982): Long range Kelvin wave propagation of transport variations in Pacific Ocean equatorial currents. *J. Mar. Res., 40* supplement, 329-339.

Knox, R.A. (1987): Equatorial ocean response to impulsive wind. In: *Further Progress in Equatorial Oceanography*, E.J. Katz and J.M. Witte (eds.), Nova University Press, Florida.

Latif, M. (1988): Tropical ocean circulation experiments. *J. Phys. Oceanogr., 17*, 246-263.

Latif, M., J. Biercamp and H. von Storch (1988): The response of a coupled ocean-atmosphere general circulation model to wind bursts. *J. Atmos. Sci., 45*, 964-979.

Legeckis, R. (1977): Long waves in the eastern equatorial Pacific Ocean: A view from a geostationary satellite. *Science, 197*, 1179-1181.

Levitus, S. (1982): Climatological atlas of the world ocean. NOAA Professional Paper 13, U.S. Dept. of Commerce.

Lighthill, M.J. (1969): Dynamic response of the Indian Ocean to onset of the southwest monsoon. *Phil. Trans. Roy. Soc., A265*, 45-92.

Lukas, R., S. Hayes and K Wyrtki (1984): Equatorial sea level response during the 1982-83 El Niño. *J. Geophys. Res., 89*, 10,425-10,430.

Luther, D.S., D.E. Harrison, and R.A. Knox (1983): Zonal winds in the Central Equatorial Pacific and El Niño. *Science, 222*, 327-330.

Luther, D.S. and D.E. Harrison (1984): Observing long-period fluctuations of surface winds in the Tropical Pacific: Initial results from island data. *Mon. Wea. Rev., 112*, 285-302.

Mariners Weather Log. National Oceanographic Data Center, NOAA, Washington, DC.

Matsuno, T. (1966): Quasi-geostrophic motions in the equatorial area. *J. Meteor. Soc. Japan, 44*, 25-42.

McCreary, J.P. (1976): Eastern tropical ocean response to changing wind systems–with applications to El Niño. *J. Phys. Oceanogr., 6*, 632-645.

McCreary, J.P. (1981): A linear stratified ocean model of the equatorial undercurrent. *Phil. Trans. R. Soc. London, Ser. A, 298*, 603-635.

McCreary, J.P. (1983): A model of tropical ocean-atmosphere interaction. *Mon. Wea. Rev., 111*, 370-387.

McPhaden, M.J., J.A. Proehl and L.M. Rothstein (1986): The interaction of equatorial Kelvin waves with realistically sheared zonal currents. *J. Phys. Oceanogr., 16*, 1499-1515.

McPhaden, M.H., P. Freitag, S.P. Hayes, B.A. Taft, Z. Chen and K. Wyrtki (1988): The response of the equatorial Pacific ocean to a westerly wind burst in May 1986. *J. Geophys. Res., 93*, 10,589-10,603.

Miller, L., R.E. Cheney and B.C. Douglas (1988): GEOSAT altimeter observations of Kelvin waves and the 1986-87 El Niño. *Science, 239*, 52-54.

Moore, D.W. (1968): Planetary-gravity waves in an equatorial ocean. Ph.D. thesis, Harvard University, Cambridge, Massachusetts.

Moore, D.W. and S.G.H. Philander (1977): Modelling of the tropical oceanic circulation. In *The Sea*, Vol. 6, Chapter 8, Goldberg *et al.* (eds.), New York, Interscience.

Osborne, A.R., and T.L. Burch (1980): Internal solitons in the Andaman sea. *Science, 208*, 451-460.

Pacanowski, R.C. and S.G.H. Philander (1981): Parameterization of vertical mixing in numerical models of tropical oceans. *J. Phys. Oceanogr., 11*, 1443-1451.

Peters, H., M.C. Gregg and J.M. Toole (1988): On the parameterization of equatorial turbulence. *J. Geophys. Res., 93*, 1199-1218.

Philander, S.G.H., and R.C. Pacanowski (1980): The generation of equatorial currents. *J. Geophys. Res., 85*, 1123-1136.

Philander, S.G.H. (1981): The response of Equatorial Oceans to a relaxation of the trade winds. *J. Phys. Oceanogr., 11*, 176-189.

Philander, S.G.H., and R.C. Pacanowski (1981): Response of equatorial oceans to periodic forcing. *J. Geophys. Res., 86*, 1903-1916.

Philander, S.G.H., and A.D. Seigel (1985): In *Coupled Ocean-Atmosphere Models*, Nihoul, J. (ed.), Vol. 303, Amsterdam, Elsevier.

Philander, S.G.H., W.J. Hurlin and R.C. Pacanowski (1986): Properties of long equatorial waves in models of the seasonal cycle in the tropical Atlantic and Pacific Oceans. *J. Geophys. Res, 91*, 14,207-14,211.

Pullen, P.E., R.L. Bernstein and D. Halpern (1987): Equatorial long-wave characteristics determined from satellite sea surface temperature and in situ data. *J. Geophys. Res., 92*, 742-748.

Quinn, W.H. , D.O. Zopf, K.S. Short, and R.T.W. Kuo Yang (1978): Historical trends and statistics of the southern oscillation, El Niño, and Indonesian droughts. *Fish. Bull., 76*(3), 663-678.

Rasmusson, E.M., and T.H. Carpenter (1982): Variations in tropical sea surface temperature and surface wind fields associated with the Southern Oscillation/El Niño. *Mon. Wea. Rev., 110*, 354-384.

Reynolds, R.W. (1982): A monthly averaged climatology of sea surface temperatures. NOAA Tech. Report, NWS 31, 35 pp.

Revell, C.G., and S.W. Goulter (1986): South Pacific tropical cyclones and the Southern Oscillation. *Mon. Wea. Rev., 114*, 1138-1145.

Ripa, P. (1982): Nonlinear wave-wave interactions in a one-layer reduced-gravity model on the equatorial ρ plane. *J. Phys. Oceanogr., 12*, 97-111.

Ripa, P. (1984): Nonlinear effects in the propagation of Kelvin pulses across the Pacific Ocean. *Advances in Nonlinear Waves*, Vol. II, L. Debnath (ed.), Pitman, 43-55.

Rothstein, L.M. (1984): A model of the equatorial sea surface temperature field and associated circulation dynamics. *J. Phys. Oceanogr., 14*, 1875-1892.

Rothstein, L.M., M.J. McPhaden, and J.A. Proehl (1988): Wind forced wave-mean flow interactions in the equatorial waveguide. Part I: The Kelvin wave. *J. Phys. Oceanogr., 18*, 1435-1447.

Sadler, J.C., and B. Kilonsky (1983): Meteorological events during the evolution of positive SST anomalies in the equatorial Pacific in 1982. *Trop. Ocean-Atmos. Newsl., 16*, 3-4, Univ. of Wash., Seattle.

Semtner, A.J. (1974): An oceanic general circulation model with bottom topography. Num. Simul. Wea. and Clim., Tech. Rep. 9, Dept. of Met., UCLA.

Schopf, P.S. and D.E. Harrison (1983): On equatorial wave and El Niño. I: Influence of initial states on wave-induced currents and warming. *J. Phys. Oceanogr., 13*, 936-948.

Walker, G.T. (1924): Correlation in seasonal variations of weather IX. Mem. Indian Meteor. Dept., 24, Part 9, 275-332.

Walker, G.T., and E.W. Blis (1932): World weather V. *Mem. Roy Meteor. Soc., 4*(36), 53-84.

Weickmann, K.M., S.J.S. Khalsa and E.J. Steiner (1989): The dynamics and thermodynamics of a 30-60 day tropical oscillation. Submitted.

Wyrtki, K. (1975): El Niño, the dynamic response of the equatorial Pacific ocean to atmospheric forcing. *J. Phys. Oceanogr., 9*, 572-584.

Appendix A: Vertical and Meridional Normal Modes

The primitive equation of momentum for a parcel of water is

$$\frac{D\vec{u}}{Dt} + 2\vec{\Omega} \times \vec{u} = -\frac{1}{\rho} \nabla p - \vec{g} + \upsilon \nabla^2 \vec{u} + \vec{Q}(x,y,z,t) \tag{A.1}$$

where $\vec{u}$ is the velocity vector, $\vec{\Omega}$ is the rotation rate of the earth, ρ is the density of water, p is pressure, $\vec{g}$ is the acceleration due to gravity, υ is a coefficient of frictional dissipation and $\vec{Q}$ can be either surface wind or thermal buoyancy forcing term. The full equations of motion for oceanic flow do not in general permit analytic solutions, and only by making several assumptions about flow near the equator can solutions be readily obtained. These assumptions, their limitations and resulting solutions are discussed in great detail in the literature (Lighthill, 1969; Cane and Sarachik, 1976; Moore and Philander, 1977; Cane and Sarachik, 1981; McCreary, 1981).

Near the equator effects of rotation are small and can be approximated by a linear function of distance from the equator ($f = \beta y$). This is the "β-plane" approximation; a good description is given by Gill (1982). This approximation is the same as $\sin\theta = \theta$ which incurs an error of 0.12% at $\theta = 5°$. The vanishing of the Coriolis force at the equator allows a set of solutions to the equations of motion that are trapped at the equator, creating a waveguide. The vertical Coriolis term ($w \cos\theta$) is scaled by the aspect ratio H/L, where H is the ocean depth and L is an appropriate length scale. Using a mean depth of 4000 m and a length scale of 2×10^5 m, the aspect ratio is 2×10^{-2}. Therefore the vertical Coriolis term is ignored.

By making standard assumptions that the flow is hydrostatic, Boussinesq and meridionally geostrophic, the long-wave inviscid equations linearized about a state of rest forced by a body force wind become

$$u_t - \beta y v + p_x = F(x,y,z,t) \tag{A.2a}$$
$$\beta y u + p_y = G(x,y,z,t) \tag{A.2b}$$
$$u_x + v_y + w_z = 0 \tag{A.2c}$$
$$p_z = -\rho g \tag{A.2d}$$
$$N^2 w = -g \rho_t \tag{A.2e}$$

N is the rest state buoyancy frequency, and is given by

$$N^2 = -\frac{g}{\rho} \frac{d\bar{\rho}}{dz} . \tag{A.3}$$

The background density field is given by $\bar{\rho}$. Time dependent forcing by wind stress will excite waves governed by Equations A.2a-A.2e.

Solution of Equations A.2a-e require five boundary conditions or initial conditions. The ocean floor is assumed to be flat and rigid, so that the vertical velocity at the bottom is zero. Setting vertical velocity of the ocean surface to zero (the rigid-lid assumption) eliminates barotropic waves and allows only internal waves. Internal modes are vertically standing waves and so there is no vertical propagation of energy for each individual mode. Exclusion of barotropic waves is not severe; its phase speed is about 200 m sec^{-1} and thus crosses the Pacific in about 24 hours. Thus, the barotropic time scale is too short to be important in oceanic response to forcing on one-week time scales. Furthermore, since the characteristic meridional scale of the barotropic mode is on the order of thousands of kilometers, it cannot be considered equatorially trapped. Density stratification, and hence N, is specified and does not vary as a function of time, latitude or longitude. Surface wind stress acts as a body force over a mixed layer, h_{mix}.

The assumption that nonlinear terms in the equations of motion are small, except for the possibility of vertical advection of a background stratification, allows a separation of horizontal variability from vertical variability (Fjeldstad, 1933). This separation ignores longitudinal changes of vertical structure which are characteristic of the equatorial Pacific. Then variables in Equations A.2a-A.2e can be written as

$$u(x,y,z,t) = u(x,t)\,\psi(z)\,D(y) \tag{A.4a}$$

$$v(x,y,z,t) = v(x,t)\,\psi(z)\,D(y) \tag{A.4b}$$

$$p(x,y,z,t) = p(x,t)\,\psi(z)\,D(y) \tag{A.4c}$$

$$w(x,y,z,t) = w(x,t)\,D(y)\int_0^z \psi(z)\,dz \tag{A.4d}$$

$$\rho(x,y,z,t) = \rho(x,t)\,D(y)\,\psi_z(z) \tag{A.4e}$$

where ψ expresses vertical structure and D meridional structure of the perturbed state.

By substituting A.4c and A.4d into A.2d and A.2e and solving for a single equation in ψ gives a second order differential equation of form

$$\frac{d}{dz}\,\frac{1}{N^2}\,\frac{d\psi_n}{dz} + \frac{1}{c_n^2}\,\psi_n = 0\,. \tag{A.5}$$

With two boundary conditions Equation A.5 represents a Sturm-Liouville equation, with separation constant c_n. Solutions to Equation A.5 are a set of orthogonal eigenfunctions or standing vertical modes where the separation constant is identified as the phase speed of each vertical mode n. Using a boundary condition of no vertical velocity at the ocean floor (z = H) and surface (z = 0) translates into

$$\frac{d\psi_n}{dz} = 0 . \qquad (A.6)$$

For simple forms of N the above equation can be solved analytically. In the special case where N is a constant the eigenvalue problem is analogous to finding harmonics of a piano wire. The wire, fixed at both ends, has a displacement maximum in the center of the wire as its fundamental mode. Eigenvectors for this case are standing cosines, with a half integral number of wavelengths between fixed points.

A more realistic N profile is shown in Fig. 3.1. This density stratification is typical of the eastern Pacific, with the thermocline near the surface. In this stratification, the maximum value of N is 10 cycles per hour at a depth of 20 m. Eigenvectors for this more complex stratification must be found numerically. Structure functions of zonal velocity for the lowest four vertical modes are also presented in Fig. 3.1, normalized such that the value at the surface is unity. Each mode, n, has n zero crossings; each zero crossing corresponds to a maximum in vertical displacement. The profile of vertical velocity is the depth integral of these structure functions (see Equation A.4d), with value zero at surface and bottom.

Lighthill (1969) used normal modes as a basis set to represent how wind stress is transmitted into the ocean. The critical assumptions are that wind stress acts as a body force over a surface mixed layer (h_{mix}) and that the body force can be written for the zonal wind in separable form as

$$F = \frac{\tau(t)}{\rho_0 h_{mix}} X(x)\ Y(y)\ Z(z) . \qquad (A.7a)$$

In the mixed layer, momentum is envisioned to mix rapidly in the vertical, so that velocity is nearly constant throughout the layer. The presumed vertical distribution of the body force (Z(z)) is then expanded as the sum of vertical eigenfunctions

$$Z(z) = \Sigma\, Z_n \psi_n(z) \qquad (A.7b)$$

where Z_n is the depth-independent amplitude of each mode n. Amplitude coefficients represent how much of the total forcing will be distributed in each vertical mode. By knowing structure functions and the vertical distribution of wind stress, Z_n can be found as

$$Z_n = \frac{\int_0^H \psi_n Z(z)\ dz}{\int_0^H \psi_n^2\ dz} \qquad (A.8)$$

(Hildebrand, 1976). Since Z(z) has value unity throughout the mixed layer and is zero elsewhere, Z_n becomes

$$Z_n = \frac{\int_0^{h_{mix}} \psi_n \, dz}{\int_0^H \psi_n^2 \, dz} \tag{A.9}$$

where the numerator is integrated from surface to the base of the mixed layer, h_{mix}. Since the structure function is approximately 1 in the mixed layer, the numerator integrates to h_{mix}, making Z_n proportional to mixed layer depth.

Combining Equations A.1a through A.1c results in the horizontal equation. It is convenient to employ two auxiliary variables q and r, such that $q = p/c + u$ and $r = p/c - u$ (Gill and Clarke, 1974). Introducing these auxiliary variables into the equations of motion A.2a-A.2c and isolating the zonal component of wind forcing for study yields:

$$q_t + cq_x + cv_y - \beta yv + F_n(x,y,t)\, Z_n \tag{A.10a}$$

and

$$r_t - cr_x + cv_y + \beta yv = -F_n(x,y,t)\, Z_n \, . \tag{A.10b}$$

Dropping the subscript n for vertical mode, the auxiliary variables can be expressed in terms of parabolic cylinder functions, D_m, as

$$q = \Sigma\, q_m(x,t)\, D_m(y) \tag{A.11a}$$

$$r = \Sigma\, r_m(x,t)\, D_m(y) \, . \tag{A.11b}$$

Parabolic cylinder functions have the useful property that they raise and lower the order of D (Gill and Clarke, 1974), giving

$$\frac{d}{dy} D_m + \frac{1}{2} y D_m = m D_{m-1} \tag{A.12a}$$

$$\frac{d}{dy} D_m - \frac{1}{2} y D_m = -D_{m+1} \, . \tag{A.12b}$$

Substituting A.11a and A.11b into the horizontal structure equations (A.10a and A.10b) and utilizing the raising and lowering properties of A.12a and A.12b results in the equation

$$(q_{m+1})_t + (q_{m+1})_x - v = F_{m+1} \ . \tag{A.13}$$

Equation A.13 yields an infinite number of meridional modes, m. In the long wave limit assumed above, m greater than one corresponds to westward propagating Rossby waves. In the special case when $m = -1$, Equation A.13 has form

$$(q_0)_t + (q_0)_x + F_0 \tag{A.14}$$

which has exponential decay away from the equator. This is the equatorial Kelvin wave, counterpart of the coastal Kelvin wave. The Kelvin wave has no meridional particle velocity or meridional phase speed. Using the definition of q and Equation A.14, meridional structure of the equatorial Kelvin wave can be found as

$$u(y) = e^{-y^2/2R_0^2} \tag{A.15}$$

where the quantity $R_o = (\beta/c_n)^{-1/2}$ is the Rossby radius of deformation, a scale of Kelvin wave width. Faster low vertical modes will be broader than more slowly propagating high vertical modes. Thus, meridional structure is linked to vertical structure through phase speed c_n.

Because different vertical modes have different meridional structure, projection of wind forcing depends not only on meridional structure of the wind but also on vertical mode number. Using the meridional structure functions as a basis set, meridional structure of zonal wind forcing Y(y) can be expressed as

$$Y(y) = \Sigma\, Y_m D_m(y) \ . \tag{A.16}$$

Using Kelvin structure function in Equation A.18 for any vertical mode n, the meridional projection coefficient, Y_n becomes

$$Y_n = \frac{\int_{-\infty}^{\infty} e^{-\beta y^2/2c_n}\, Y(y)\, dy}{\int_{-\infty}^{\infty} e^{-\beta y^2/c_n}\, dy} \tag{A.17}$$

where Y(y) is an arbitrary meridional structure of zonal wind.

Equations A.7b and A.16 specify the equatorial wave response to arbitrary forcing. When the forcing is specified Equations A.8 and A.17 determine the wave projection of the forcing onto any Kelvin vertical mode n.

GPO 673-002/92036